ANALYSIS AND DESIGN OF A HIGH FREQUENCY INDUCTION-HEATING SYSTEM

by

Irshad Khan

Thesis submitted to the
Department of Electrical and Electronic Engineering,
University of Cape Town,
in fulfillment of the requirements for the degree of
MASTER OF SCIENCE
February 2003

DECLARATION

The thesis is submitted for the fulfillment of the requirements for the degree of Master of Science in Electrical Engineering at the University of Cape Town. It has not been submitted before for any degree at this or any other university. The author confirms that this thesis is based on his own work.

I. Khan

04 February 2003

ACKNOWLEDGEMENTS

I thank my creator and my parents for giving me the strength to achieve this qualification. I would also like to thank my beloved wife Rhoda for her sincere, devoted encouragement, support and understanding throughout this project. A big thank you goes out to my brothers Azeem and Zaheed whose support and encouragement has always inspired me to do my best.

A big thank you to the following:

- National Research Foundation (NRF) for their financial support in this project
- Prof. J Tapson, my Thesis Supervisor, to whom I will always be grateful to, for his sound advice, guidance and confidence in my ability
- A big thank you to my devoted research students, Shaun Harwin and Edson Naylor, who assisted with the construction, measurements and testing of the prototype system
- Thank you is also due to, Prof B Mortimer, Mr A. J. Campbell and the Center for Instrumentation Research for their support throughout this project
- Colleagues: Mr Trevor Lind, Dr Ian de Vries and Dr Jevon Davies

SYNOPSIS

Advances in power electronic semiconductor technology are making high frequency converters for induction heating more feasible at power levels up to 50kW.

This research presents the development and analysis of a solid-state induction-heating system, operating directly off single-phase mains frequency, which enables optimum and efficient operation over a frequency range of 80kHz to 200kHz. The system essentially comprises a DC-DC converter configured as a controlled current source, which feeds a load resonant DC-AC inverter, driving a parallel resonant load circuit. The load circuit comprises an induction-heating coil and a reactive power compensating capacitor. The systems active switching elements comprise power MOSFET's but can be extended to almost any other controlled power devices such as IGBT's, BJT's, SCR's, GTO's or SIT's.

An automatic frequency control system ensures that the DC-AC inverter drives the load at its resonant frequency, thereby achieving zero voltage switching of the power semiconductors. This operating mode always ensures maximum power transfer to the load as well as maximum operating efficiency of the DC-AC inverter. Driving the load at resonance presents an essentially resistive load to the DC-DC converter, thereby reducing the losses associated with a reactive load. A compact circuit layout combined with this optimum mode of operation eliminates the need for any snubber circuit components in both the DC-DC and DC-AC converters at this power level.

An overview into various applications and technologies of induction-heating is presented in this research. A detailed analysis of the induction-heating coil and work-piece are presented in order to aid the design of the load circuit. The induction-heating technology overview presents various induction-heating power sources, discussing the configurations of various topologies. A brief mathematical analysis is used to describe the operation of power electronic converters employed in the induction-heating system developed for this research.

The parallel resonant induction-heating load circuit is characterised mathematically, allowing for the determination of the optimum operating conditions. This is followed by a simulation analysis, which is used to gain insight into the problem of frequency control. The frequency control system is modeled and the steady-state error response evaluated under different input conditions.

Experimental results on the system implemented, based on operating waveforms and efficiency measurements of the solid-state induction-heating system are presented along with recommendations for future work. The implemented power source was tested at a maximum power of 2.3kW at 151kHz. A system efficiency of 86% at 1.3kW was measured when operating at 138kHz. This design however, provides for scaling to power levels up to 50kW. The induction-heating system's frequency tracking capability is evaluated by heating a steel work-piece through its Curie transition temperature. The induction-heating system is used to heat a 26mm x 35mm stainless-steel billet (work-piece) to 1200°C in 130 seconds using the calculated power of 1.35kW.

TABLE OF CONTENTS

CHAPTER 1

INTRODUCTION

Induction-heating is an important enabling technology in the manufacturing industry. With its vast range of applications extending from heating to melting, brazing to welding and cap sealing to bonding, it is often the key to adding value to a particular process in industry. This is realised by the fact that induction-heating provides a higher heating rate than any other commercial heating process available.

Induction-heating is caused by the Joule heating effect when an electrically conductive object (work-piece) is placed in an alternating magnetic field. In its simplest form the output of an induction heater consists of a water-cooled copper tube coil carrying an alternating current, surrounding the metallic work-piece, which is to be heated. The power source is used to produce the alternating current, which sets up the magnetic field in the coil.

The advent of solid state power sources for induction heating has enabled conversion efficiencies of up to 93 % due to low switching losses and good high frequency coupling [1]. Induction heating at high frequency increases the coil to work-piece coupling efficiency, thereby reducing the power required for a particular application. The savings in power required considerably reduces the cost and size of the induction heating equipment, making high frequency solid state systems the current and future technologies for induction heating. Solid-state power sources used to drive induction-heating loads are usually very efficient, provided the load is driven at its natural resonant frequency [2]. This facilitates zero voltage (ZVS) switching of the converter, resulting in reduced power losses in the semiconductor switches [3], [2]. Another advantage of driving a load at resonance is to enable an input power factor close to unity, thereby reducing the KVA rating of the power source [3]. These parameters enable high conversion efficiencies due to reduced switching losses in the power source [3],[4],[5].

The induction-heating load forms part of a resonant tank circuit with a quality factor (Q) ranging from 3 to 50, which is dependent on the coil geometry, coupling coefficient, frequency, and properties of work-piece being heated such as resistivity and magnetic permeability. The temperature and loading effect on the induction heating coil facilitates the variation of the properties mentioned above which tend to alter the load characteristics presented to the power source. A fixed frequency power source will therefore not be able to provide maximum power transfer to the load and will also have to supply the reactive power demanded by the load if operation at resonance is not maintained. This operating mode (off resonance) constitutes a load mismatch and solid-state power sources develop severe switching losses when operated in this mode [6]. Semiconductor devices in the power source are usually over-rated with special matching circuits designed in order to cope with this situation, but it does not eliminate the problem.

In the present work, a frequency control system is implemented that would automatically search for and operate at the natural load resonant frequency, and continuously track this resonant frequency during the heating cycle. This is accomplished by monitoring the load phase angle and altering the inverter operating frequency accordingly. This system is referred to as the automatic frequency control system (AFC) or the resonant locked loop control circuit (RLL) [7], [8].

Power control to the load is accomplished by varying the current fed to the inverting stage (DC-AC) of the induction heating system [3], [9]. Power control is realised by the implementation of a DC-DC buck converter topology configured as a constant current source. This converter operates at 72kHz and supplies the regulated DC power to the inverter. The necessary protection mechanisms are provided by the power control stage, which allows the inverter to operate independently with its automatic frequency control system. Separating the inverter and power control stages results in a robust and relatively simple design, which does not require sophisticated protection and control circuitry [1]. These benefits therefore allow the induction heating system to be utilised for a wide range of heating applications.

CHAPTER 2

THEORY AND CONTROL OF INDUCTION HEATING

2.1 BACKGROUND

Electromagnetic Induction, the basis of all induction heating was first discovered by the "father" of Induction, Michael Faraday, in 1832. With his induced emf theory he proved that currents could be induced in a closed secondary circuit as a result of varying the current in a neighboring primary circuit. The essential feature was a change in the magnetic flux linkage within the closed secondary circuit, produced by an alternating current in the primary. In 1927, almost a century later, the first medium frequency induction furnace was developed by the Electric Furnace Company (EFCO) and since then, the number and size of heating installations have grown steadily [10].

2.2 INDUCTION HEATING PRINCIPLES

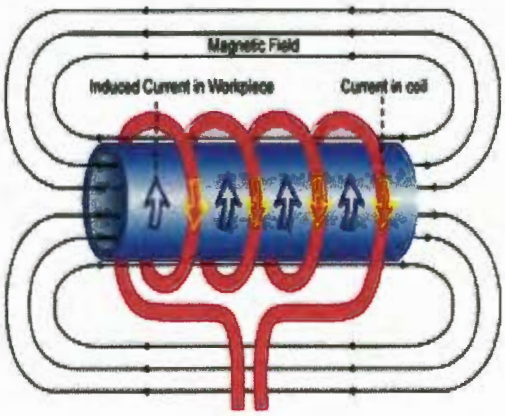

Figure 2.1: Principle of induction heating showing coil current and induced eddy currents, which are responsible for the heat generated in the work-piece. The red conductor represents the induction coil, which sets up the magnetic field and is usually manufactured from copper [12].

Induction heating utilizes three main effects: electromagnetic induction, skin effect and heat transfer. The heating is caused by the Joule heating effect when an electrically conductive object called the work-piece, is placed in an alternating magnetic field [11]. This alternating magnetic field is set up in the water-cooled work coil. The induction heating coil and work-piece can be visualized as a transformer with primary turns (work-coil) and a short-circuited secondary turn (work-piece) [10].

When alternating current flows in the primary, voltages are induced in the secondary which cause currents to flow in it, and these currents tend to cancel the flux that produced them, according to Lenz's law. The frequency of these induced eddy currents in the work-piece is determined by the frequency of the power source. These eddy currents are induced into a peripheral layer of the work-piece known as the skin-depth (δ) or penetration depth which is characteristic of current flow at high frequency due to the skin effect. The penetration of the current, due to the skin effect is therefore dependent on the frequency and properties of the material being heated, i.e., resistivity and relative permeability. The depth of heating and thus the power density will therefore also be affected by these parameters [11].

2.3 APPLICATIONS

Induction heating provides a method of generating heat within the work-piece. This allows very high temperatures (in excess of 2000°C) to be achieved. Because the application of the magnetic field is instantaneous, very fast heating rates enable induction heaters to have short cycle times (several seconds). Induction processes fit well into automated production methods and provide repeatable consistency in the heated work-piece. By varying the frequency of the alternating magnetic field in the coil, various heating patterns can be achieved. Typical installations vary from 50Hz (mains frequency) for heating and melting to 450 kHz (radio frequency) for surface heating [10].

2.3.1 Through Heating

Figure 2.2: Through heating of a steel work-piece using a saddle coil [12].

Induction heating provides a convenient method for bulk-heating metals. It replaces large conventional furnaces, which have the disadvantage of long start-up and shutdown times. Induction heaters are relatively small in size compared to other

furnace types, and are immediately available for use. Heating times are usually short - a few minutes, except when a large thermal mass is being heated. Because induction heating takes place within one skin depth, the heat reaches the rest of the billet or slab by thermal conduction. By not trying to confine the heating to the surface in through heating, lower frequencies can be used. Supply frequency (50 / 60 Hz) is an attractive option, as no frequency conversion is needed; however medium frequencies (1kHz to 25kHz) are also extensively used and are becoming increasingly popular.

Typical through heating is used for forging, forming and annealing. Aluminium and other non-ferrous metals heated for extrusion are power-intensive applications, with throughputs in tones per hour. Typical induction heating systems for these applications have power consumptions ranging from hundreds of kilowatts to several megawatts [11].

2.3.2 Surface Heating

Figure 2.3:.Surface heating by induction followed by a quench cycle [12].

Small heating depths and high power densities are achieved by using high frequency. Heat can be concentrated in a localised region within the work-piece. This region can have its metallurgical nature changed without affecting the rest of the material. The result is a shallow hardened region with a less-brittle core, combining the virtues of surface wear resistance with general strength, as well as virtually no distortion during the hardening. Because induction hardening heats a localised region to a high temperature without affecting the rest of the material, it saves energy (compared to through heating) and allows selective hardening. Because of the high power densities achieved by high frequency, surface heating cycles are typically less than one second (0.3 to 0.5s for 0.45% carbon steel). This is followed by a quenching cycle, which helps the metal to retain its hardened properties. Operating frequencies vary from 3kHz to 450kHz with installations approaching hundreds of kilowatts (depending on

the application) for surface heating by induction [11]. A typical application of surface heating would be for hardening of tool tips, saw blades and engine parts (crank shafts) for the automobile industry.

2.3.3 Induction Melting

Figure 2.4: Precious metal melting by induction.

No basic differences exist between through heating and melting by induction. Induction melting when compared to other forms of melting however offers the following advantages:

- Fast melting – size for size, induction furnaces have a better production output than any other furnace types;
- Improved working conditions – there are no excessive heat losses from the furnace and no smoke, dirt or ashes;
- Automatic stirring produced by the eddy currents in the molten metal – this is an advantage for alloying purposes since the stirring helps to absorb the materials and to produce a homogenous melt;
- The furnace provides safer working conditions by eliminating the danger of using open flames, and also by eliminating gas leaks;
- Special techniques, such as vacuum melting, produce alloys that can be produced in no other way.

Induction melting is used in large-scale applications for steel casting where installations rated at 2.5 MW / 500Hz, capable of casting 8 tons of steel are common. Other melting applications range from several hundred kilograms (at low frequencies) down to a few grams (at high frequency). A common application of high frequency small scale induction melting is in the precious metals industry, where small quantities of platinum (20g to 120g) can be induction melted and cast using less than 2kW at 140kHz [13].

2.3.4 Other Applications

Figure 2.5: Copper brazing by induction [12].

Figure 2.6: Induction soldering [12].

An extensive variety of other applications of induction heating also exist. They all however can be classified into the three main categories listed above. These applications include:

- **Induction cooking:** A pancake coil is used to induce eddy currents into the base of a steel or cast iron cooking vessel or pot. This technique offers many advantages over the conventional types (gas burners, radiant coil and solid disk type radiant element cookers) of cooking, such as greater electrical efficiency, improved safety and faster control over the power delivered [14], [15], [16]. Frequencies around 15kHz to 25kHz are usually used for this application at power levels ranging from 500W to 10 kW [17].

- **Soldering and brazing:** An induction coil induces eddy currents, which heat the interface between two metals to be joined. Induction provides fast-localized heating and control, which prevent oxidation and distortion of the joined parts. This technique utilises both through heating and surface heating, depending on the size of the work-piece and the location of the joint [11]. Typical frequencies used for soldering and brazing range from 3kHz to 450kHz at various power levels. Applications include soldering or brazing of large copper or steel tubes, and lead solder reflow heating on printed circuit boards used in the electronics industry [12].

- **Paint drying and curing:** A metallic surface is induction heated to accelerate the drying process of a paint coat or the curing of a bonding agent. This is usually

conducted at frequencies ranging from 50kHz to 450kHz at various power levels [18].

- **Bonding:** Metal is heated and bonded to glass or plastic for various applications. A typical application is where the edges of the metal grid of an audio speaker cover are induction heated and pressed into the plastic border where they bond to form one piece [18].

- **Cap sealing:** Thin aluminium and steel foils are induction heated to about 100°C, which melts the resin between the foil and the opened top of the container, which is being sealed. This bond forms an airtight seal and is used throughout the packaging industry. Typical installations use low power (1kW – 8 kW) at frequencies ranging from 30kHz and 450kHz. The short heating times achieved by induction in this application, makes it well suited for high volume production runs [19],[20].

- **Fluid heating:** Metallic vessels heated by induction can be used to heat liquid in contact with them. Because the heat is applied instantaneously and the surface area of the heated vessel can be large this method offers a unique advantage (by increasing the contact area between the water and vessel) over the conventional forms of heating [21], [22]. These operations range from 50Hz to 70kHz at power levels of 8kW to 150kW.

- **Tube welding:** Induction heating combined with mechanical pressure, is extensively used in the manufacture and joining of tubes. The ends of tubes are brought together and heated to welding temperature and axial pressure on the tube forms the weld. Installations for tube welding range from several kilowatt up to 500kW operating at frequencies between 100kHz and 500kHz [23].

2.4 SKIN EFFECT

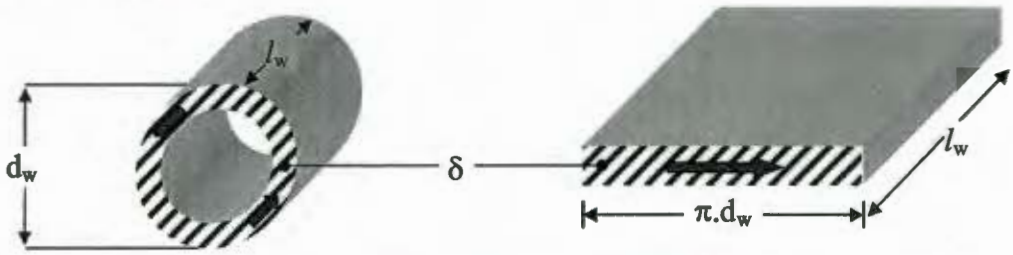

Figure 2.7: Skin depth (δ) in work-piece illustrating the concentration of eddy currents near the surface. This section is converted to the equivalent sleeve as shown, which is used to calculate the resistance of the work-piece. δ is the depth, d_w and l_w are the work-piece diameter and length respectively.

The tendency of alternating current to concentrate itself in a peripheral layer (near the surface) of an electrical conductor is one of the factors that make induction heating possible. The skin depth (δ) where the eddy current concentration occurs is given by:

$$\delta = \sqrt{\frac{\rho}{\mu_o \mu_r \pi f}} \qquad \textbf{2. 1}$$

Where:

δ = penetration depth

ρ = resistivity of work-piece

f = frequency of eddy currents

μ_o = permeability of free space

μ_r = relative permeability of the work-piece

The skin depth is roughly where the current density has fallen to about one third its surface value. The current density falls off from the surface to the center of the work-piece and the rate of decrease is higher at higher frequencies [10]. The skin depth δ is illustrated in figure 2.7. It should be noted that the induction-heating coil too is subjected to skin effects (δ_c). The skin depth δ is also dependent on two properties of the work-piece namely, resistivity and relative permeability [24].

The resistivity of most metals changes with temperature according to the relationship,

$$\rho_\theta = \rho_1 [1 + \alpha_{20} (\theta - \theta_1)] \qquad 2.2$$

Where:

ρ_θ = The resistivity at any temperature θ,

α_{20} = the temperature coefficient of resistance at a temperature of 20°C,

ρ_1 = the resistivity at temperature θ_1

The coil is water-cooled in order to keep its resistivity constant by reducing the heat generated due to skin effect in the coil and the heat radiated from the work-piece. An additional loss is associated with magnetic materials such as steel namely, hysteresis loss.

2.4.1 HYSTERESIS LOSS

Hysteresis loss is defined as the intermolecular friction when the material is magnetized first in one direction and then in the other. The molecules may be regarded as small magnets, which turn around with each reversal of direction of the magnetic field [24]. The effect of relative permeability can be ignored when heating non-magnetic materials such as copper, aluminium, gold, silver, platinum, etc which eliminates hysteresis losses. The heating of Ferro-magnetic materials (steel and iron) however, poses a special problem because of the phase change at the Curie point. Above the Curie temperature (780°C for steel) the material loses its magnetic properties when its relative permeability reduces to unity. This results in a large increase in skin depth in the work-piece, which substantially reduces the power density at the applied frequency, resulting in a lower heating rate [25].

2.5 INDUCTION HEATING LOAD

The work-piece is usually situated inside a cylindrical coil. A minimum clearance (air-gap) between the work-piece (d_w) and coil (d_c) is maintained to provide mechanical clearance, electrical and thermal insulation. The physical structure of the coil and work-piece is shown in figure 2.8.

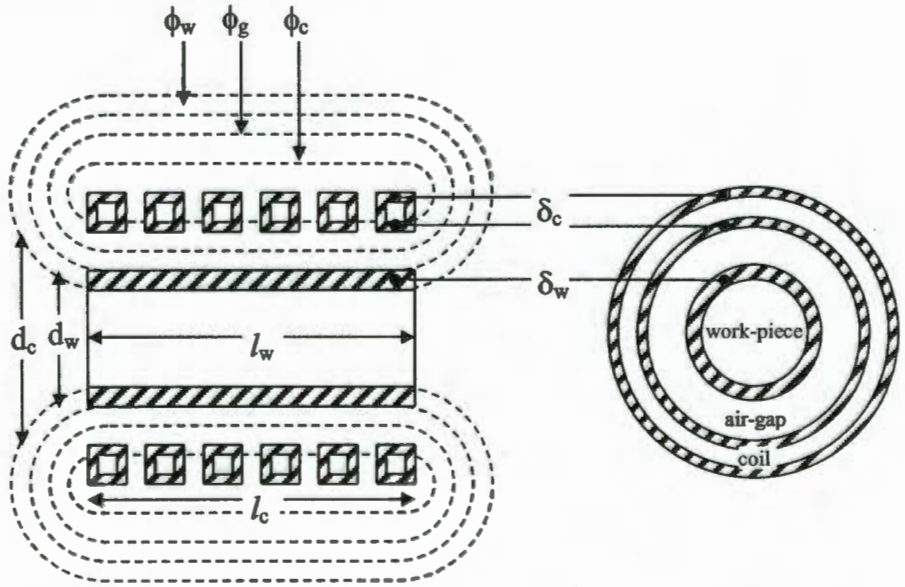

Figure 2.8: Physical structure of the coil and work-piece (using Baker's model) **[11]** illustrating the concentration of eddy currents near the surfaces. Three components of flux exist namely, the coil flux (ϕ_c) linking the coil turns, the flux in the air-gap (ϕ_g) and the flux linking the work-piece (ϕ_w). The work-piece is shown as being hollow because skin effect results in the eddy current concentration at the work-piece surface and is given by δ_w. The same effect can be seen within the induction-heating coil.

The coil and work-piece can be modeled as a loosely coupled transformer as shown in figure 2.9 [26]. The coil is the primary with N turns and the work-piece is a single turn short-circuit secondary winding. The induction-heating coil is a magnetic field source, which sets up a flux used to induce a voltage into the work-piece. This flux is divided into three components namely, the coil flux (ϕ_c) which passes through the coil surface, the flux in the air gap (ϕ_g) and the flux linking the work-piece (ϕ_w). If it is assumed that all the paths share a common magnetic field intensity, the three components of the total flux ($\phi_w + \phi_c + \phi_g$) can be used to derive the electrical equivalent circuit of the induction-heating load shown in figure 2.10 [11]. The shunt magnetising reactance X_{mag} is assumed to be very large compared to the other circuit reactances and is therefore omitted in figure 2.10. The equations for this model

assume close coupling between the coil and work-piece and are only valid for single layered coils.

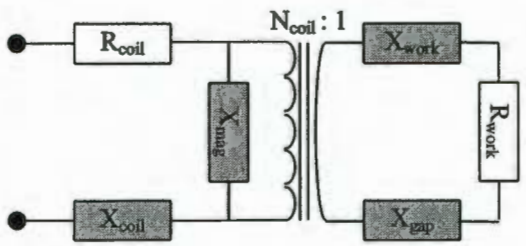

Figure 2.9: Transformer model of induction-heating load. The coil is the primary of the transformer with N turns. The work-piece acts as a single turn short-circuit secondary winding with impedance R_{work} and X_{work}. The air-gap between the coil and work-piece is modeled as a reactance due to its flux component ϕg.

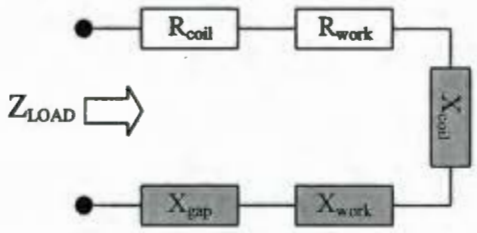

Figure 2.10: Equivalent circuit of induction heating load reflected to the terminals of the coil. This model assumes that all paths share a common magnetic field, which implies close coupling between coil and work-piece.

For the conditions stated, this model can be used to calculate the parameters of the induction-heating load. The impedance of the induction-heating load presented to the terminals of the coil is given by equation 2.3.

$$Z_{LOAD} = (R_{work} + R_{coil}) + j(X_{coil} + X_{work} + X_{gap}) \quad [\Omega] \qquad \textbf{2.3}$$

The reactances in the load dominate the impedance. This presents an inductive load to the power source driving it. Depending on the application, the air gap varies according to the physical dimensions of the coil and work-piece. An increase in air-gap therefore increases X_{gap}, making the load more inductive. Using Baker's model, the equivalent circuit parameters of figure 2.10 can be calculated as follows [11]:

$$R_{work} = K(\mu_r p A_{work}) \qquad \textbf{2.4}$$

$$R_{coil} = X_{coil} = K\left(\frac{k_r \pi d_{coil} \delta_{coil}}{2}\right) \qquad \textbf{2.5}$$

$$X_{gap} = K(A_{gap}) \qquad \textbf{2.6}$$

$$X_{work} = K(\mu_r q A_{work}) \qquad \textbf{2.7}$$

$$\text{where} \quad K = \frac{2\pi f \mu_o N^2}{l_{coil}}; \quad p = \frac{2}{\left(1.23 + \frac{d_{work}}{\delta_{work}}\right)}; \quad q = \frac{2}{\frac{d_{work}}{\delta_{work}}} \qquad \textbf{2.8}$$

Where:

A_{work} and A_{gap} are the cross sectional areas of the work-piece and air-gap respectively,

d_{work} and d_{coil} are the diameters of the work-piece and coil respectively,

l_{coil} is the axial length of the induction coil and

k_r is the coil correction factor which accounts for inter-turn spacing.

Coupling efficiency is a measure of the amount of power transferred between the coil and work-piece. The efficiency of coupling in this case is dependent on the resistance of the coil and that of the work-piece and is given by eq. 2.9.

$$\eta = \frac{R_{work}}{R_{work} + R_{coil}} \qquad \textbf{2.9}$$

Practical factors affecting coupling efficiency include:

- Geometry of work-piece, which improves for a tightly packed, solid work-piece and decreases for a loosely packed work-piece due to leakage flux.
- Geometry of the heating coil, which improves for a closely wound coil around the work-piece. Other factors also concerned with geometry are the length of the coil and the number of coil turns.
- The material used for the heating coil. The higher the coils electrical conductivity, the lower the I^2R losses in the coil, hence the more power transferred to the work-piece.

Equation 2.9 gives a broad-brush idea of what controls the coupling efficiency [27]. If for example one considers a load material with high resistivity and permeability such as steel, an efficiency approaching 100% can be achieved, but copper with a low resistivity, has an efficiency of about 50%. The efficiency increases during the heating cycle due to fact that the resistivity of the work-piece increases with temperature.

2.5.1 EDDY CURRENT EFFECTS

Inductance is defined as the flux linkage of a coil per ampere of its current and is given by [28]:

$$L = \frac{\lambda}{I} \quad [H] \qquad \textbf{2. 10}$$

$$\lambda = N \times \Phi \qquad \textbf{2. 11}$$

Where:

λ is flux linkage per coil turn,

N is the number of coil turns,

ϕ is the flux produced in the coil due to the flow of current

From equation 2.10 the approximate inductance of an infinitely long air cored solenoid (where the field inside is uniform and axially directed) is found to be[29]:

$$L = \mu_o N^2 \frac{A}{l} \quad [H] \qquad \textbf{2. 12}$$

However air cored solenoid coils of infinite length are not practical and the inductance of a coil of finite length can be found using the Wheeler formula [30]:

$$L \cong \frac{10\pi\mu_o N^2 a^2}{9a + 10l} \quad [H] \qquad \textbf{2. 13}$$

Where:

N is the number of coil turns,

a is the inner coil radius,

l is the axial coil length.

The inductance value can be found to an accuracy of less than 1% if the coil length (l) is larger than 0.8 times the inner coil radius (a) [30].

The formulae used above are only valid for air-cored coils and do not account for the skin effect in the work-piece, which tends to change the coil inductance when loaded. This change in inductance is relatively difficult to approximate empirically and usually involves finite element analysis. For the purposes of this research, the no-load coil inductance will be used as the design guideline, and will be compensated for experimentally once the load circuit has been constructed.

2.6 CHOICE OF FREQUENCY

Frequency is a very important parameter in induction-heating because it is the primary control over the depth of current penetration and therefore the depth of heating. Frequency is also important in the design of induction-heating power supplies because the power components must be rated to operate at the specified frequency. Due to reduced switching losses at elevated switching frequencies (up to 1MHz), enhancement-mode power MOSFETs have become an important component in high frequency power sources for induction heating [1].

For effective induction heating, the critical frequency of the alternating magnetic field in the work-coil is of paramount importance and is given by:
Where:

$$f_c = \frac{6.45\ \rho}{\mu\ d^{\ 2}} \qquad \textbf{2.14}$$

f_c = critical frequency

ρ = the electrical resistivity of the work-piece (Ωm)

d = the diameter of the work-piece (m)

μ = the permeability of the work-piece (Hm^{-1})

Equation 2.14 is defined as the critical frequency below which, a loss of heating would occur due to field cancellation in the work-piece. The critical frequency is calculated at a ratio of work-piece diameter to penetration depth (d/δ) > 4.5. Where a free choice of frequency exists, it should be chosen greater than or equal to f_c [11].

2.6.1 Advantages of high frequency operation

High frequency induction heating has the following advantages:

- The concentration of skin depths at high frequency produces a high loss per unit area (high power density) in the work-piece surface, ensuring faster heating rates than can be achieved at lower frequencies.
- Poorly or loosely coupled loads can still be heated effectively since the ratio between the work-piece diameter and penetration depth (d/δ) is relatively large ($\pm 40:1$) [10].
- High frequency is also an advantage since power switching above 20kHz is above the audible range so no discomforting switching noise is presented to the user.

2.6.2 Disadvantages of high frequency operation

High frequency operation however has the following disadvantages:

- Switching losses in power semiconductors increase sharply with frequency and special techniques (Zero-Voltage and Zero-Current Switching) need to be employed in order to minimize this problem.
- Power MOSFET's and IGBT's require more power from the gate drive circuitry when operated at high frequencies. This increases the need for paralleling and heat sinking of the gate drive circuitry in order to function at these elevated frequencies.
- Compact physical layout of the power electronic circuitry becomes difficult to achieve since the effects of parasitic elements become more prominent at higher operating frequencies and special power filtering circuitry need to be employed in order to achieve optimum inverter performance[31].

2.7 RESONANCE

In order to compensate for the poor coil power factor, a resonant capacitance (C_t) is used to supply the reactive power (VAR's) demanded by the coil. This reduces the required ratings of the power source, since it only has to supply the real power demanded by the load. Loads are resonated by either placing a capacitance in series or in parallel with the coil. L_t and R_t represent the work-piece and coil parameters reflected to the terminals of the power source. The load circuit for this research formed part of a parallel resonant tank circuit as shown in figure 2.11.

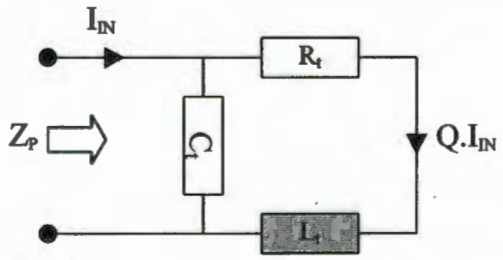

Figure 2. 11: Induction heating load circuit with a parallel resonant capacitor. This circuit is usually driven by a constant current source.

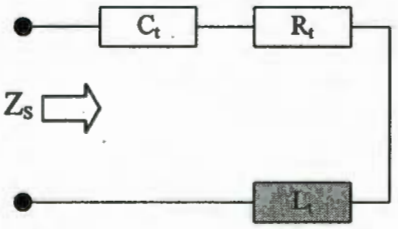

Figure 2. 12: Induction heating load circuit with a series resonant capacitor. This circuit is usually driven by a constant voltage source.

A square waveform contains high frequency harmonic components, which see a low impedance for the current, with a parallel resonant circuit and a low impedance for the voltage with a series resonant circuit. The power source is therefore generally determined by the resonant configuration used, being either a voltage source for series resonance or a current source for parallel resonance. The frequency at which maximum response occurs (maximum V or I) is defined as the natural resonant frequency of the load ω_o which is given by:

$$\omega_o = \frac{1}{\sqrt{L_t C_t}} \quad [rad/\sec] \qquad \textbf{2. 15}$$

Where:

ω_o = resonant frequency in rad/sec

L_t = inductance of the load in Henries

C_t = capacitance of the load in Farads

The frequency ω is defined as the operating frequency. At resonance, $\omega = \omega_o$ and the phase angle of the impedance is zero. The frequency response characteristic of a parallel resonant circuit is shown below:

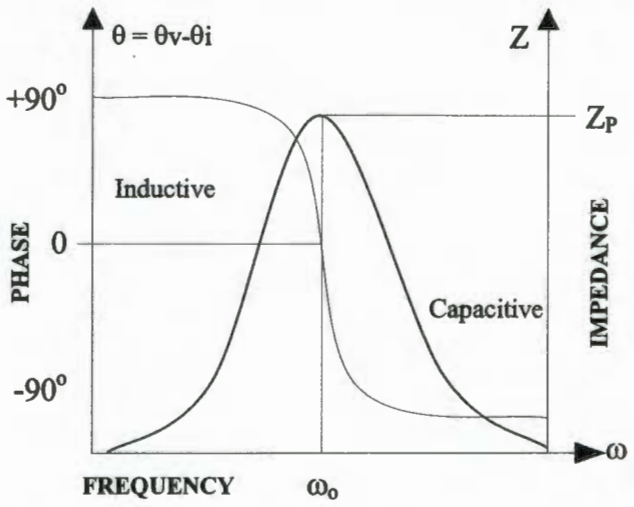

Figure 2. 13: Frequency response of a parallel resonant circuit. At frequencies below resonance, the circuit's impedance falls due to a decrease in inductive reactance resulting in a lagging phase of the driving current. At frequencies above resonance, the circuit's impedance falls due to a decrease in the capacitive reactance, resulting in a leading phase of the driving current.

At frequencies below resonance the inductor impedance is lower than the capacitor impedance, and hence presents a lagging power factor to the source. At frequencies above resonance, the capacitor impedance is lower and presents a leading power factor to the source. At the resonant frequency (ω_o), both the voltage and current are in phase and the input power factor to the tank circuit is therefore unity. Most resonant converters for induction heating applications operate by driving the load circuit at its resonant frequency. The latter has the advantage of providing reduced switching losses and thereby achieving a high operating efficiency in the power source [1], [2], [3] [4], [9]. A load resonant converter topology will therefore be employed in this research.

The ratio between the stored energy (in the reactive elements) and the dissipated energy (in the real elements) per cycle in a resonant circuit is called the quality factor (Q) and is given by:

$$Q = 2\pi \frac{\max imum\ stored\ energy}{total\ energy\ lost\ per\ period} \qquad \textbf{2. 16}$$

$$Q = \frac{\omega L_t}{R_t} \qquad \textbf{2. 17}$$

This unitless quantity is also a measure of the selectivity of the circuit, which provides the information about its bandwidth. The oscillating coil current is Q times the input current I_{IN} supplied to the tank circuit. This is favorable in induction heating because the high oscillating coil current produces a strong magnetic field needed for efficient induction heating. It is also evident that the Q acts as an impedance transformer, which helps to optimally match the load to the power source [32].

2.8 INDUCTION HEATING POWER SUPPLY

Induction heating power sources are frequency converters that convert utility line frequency (50Hz) power to the desired single-phase power at the frequency required by the induction-heating process. The rectifier portion of the power supply converts the single-phase or three-phase line frequency input to DC, and the inverter portion changes the DC to single-phase high frequency (100kHz) AC. This is illustrated in figure 2.14:

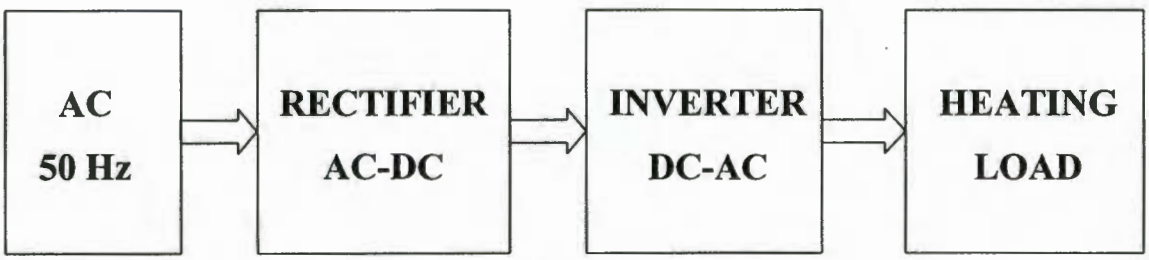

Figure 2. 14: Layout of the high frequency power source showing the converter, inverter and heating

Inverter circuits use solid-state switching devices such as thyristors (SCR's) and transistors. For high power and lower frequencies, large thyristors are commonly used. For low power or frequencies above 25kHz, transistors are used because of their ability to be turned on and off very fast with low switching losses. Vacuum tube oscillators have been used extensively for many years at frequencies above 300kHz. However, tube oscillators have a low conversion efficiency of 55 to 60% compared to 85 to 93% for inverters using transistors. Power vacuum tubes have a limited life of typically 2000 to 4000 hours and are therefore a costly maintenance item. The high voltage (over 10000 volts) required for tube operation is more dangerous than the 1000 volts or less present in typical transistorised inverters.

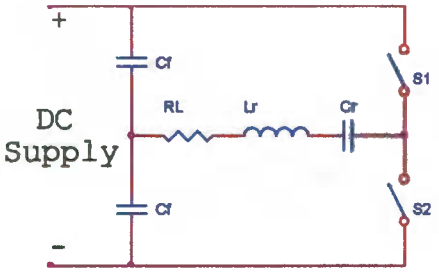

Figure 2. 15: Half-bridge voltage-fed inverter topology

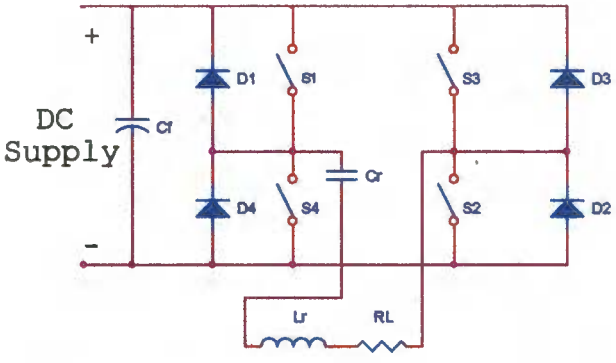

Figure 2. 16: Full-bridge voltage-fed inverter topology

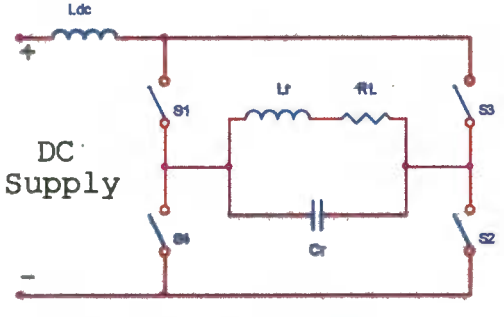

Figure 2. 17: Current-fed full-bridge inverter topology

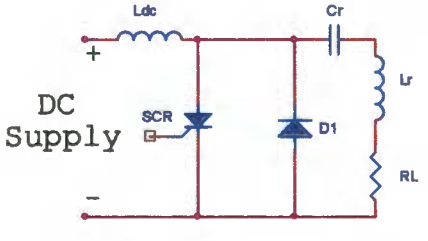

Figure 2. 18: Current-fed chopper or quarter bridge

These negative features of tube oscillators have brought about a dramatic move toward use of transistorized power supplies in heat-treating applications that require a frequency of less than 1MHz [3]. Induction heating power supplies utilize various techniques to produce the high frequency alternating current. Various topologies include:

- Half-bridge voltage-fed inverter topology (Figure 2.15)
- Full-bridge voltage-fed inverter topology (Figure 2.16)
- Current-fed full-bridge inverter topology (Figure 2.17)
- Current-fed chopper or quarter bridge (Figure 2.18)

The switch implementations (S1, S2, etc.) can be any power semiconductor such as IGBT, MOSFET, BJT, SIT or SCR. Inverter topologies are classified into two main categories namely, voltage-fed and current-fed. The application of a particular topology (voltage or current fed) is determined by the resonant load configuration (series or parallel resonant) and frequency.

A series resonant load requires a voltage-fed inverter and parallel resonant load, a current fed inverter. The quarter bridge inverter topology (figure 2.18) is an exception where a series resonant load is driven by a current source topology (characteristic of the DC bus inductor). Bridge inverter topologies (fig. 2.15 to 2.18) usually employ SCR's as the active switching elements at frequencies below 10kHz and at power levels up to 1.5MW. Operation of SCR converters above 10kHz is limited by the long turn-off time required for the SCR's to commutate. IGBT's are commonly used in bridge inverter circuits from frequencies above 10kHz at power levels of up to several hundred kW [3], [23]. IGBT's also have turn-off time limitations, which restrict their use to operating frequencies below 50kHz. New high-speed technologies are making IGBT driven power sources at 150kHz possible [19]. Power MOSFET's however, are employed in bridge topologies at frequencies from 50kHz to over 1MHz at power levels of up to 100kW.

2.9 POWER CONTROL

Power control is required in order achieve a desired heating pattern, or to maintain a desired billet (work-piece) temperature. This is achieved by varying the DC voltage supplied to the inverter. The power control system in most induction heating power sources must therefore be variable from as little as 10% to 100% of the available power. Various types of power control systems include:

2.9.1 Controlled Rectifiers

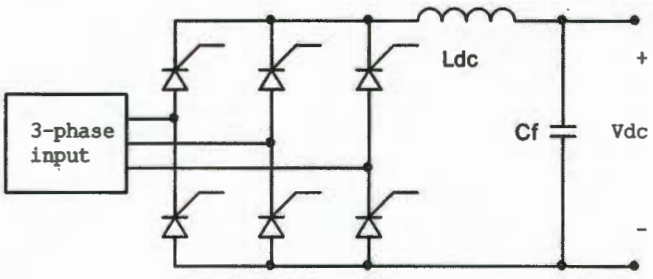

Figure 2.19: Controlled rectifier used for power control stage of induction heating power source. The output power is controlled by varying the firing angles of the SCR's with respect to the supply phase. The rectified output is then filtered to form the DC supply for the inverting stage.

Controlled rectifiers are used to vary the DC output voltage supplied to the inverter stage of the power source. This supply can be configured as a constant voltage source or constant current source depending on the load circuit configuration. The controlled rectifier power control stage is commonly used in induction heating power sources ranging from 50kW up to 1.5MW for forging and tube welding applications [2], [33], [34], [35]. Power control from 0 to 100% is achieved by varying the thyristor firing angle ($\propto$) of the bridge rectifier from 120° to 0°. The firing angle control also provides a soft-start and protection feature to the inverter, in the event of load faults or line transients.

At low power levels the firing angle control produces increased harmonic distortion of the line current drawn, which in turn worsens the input power factor of the system. The controlled rectifier is employed as the front-end stage for all bridge inverters

(half, full or quarter bridge) operating at frequencies ranging from 50Hz to over 1MHz.

2.9.2 DC-DC Converters

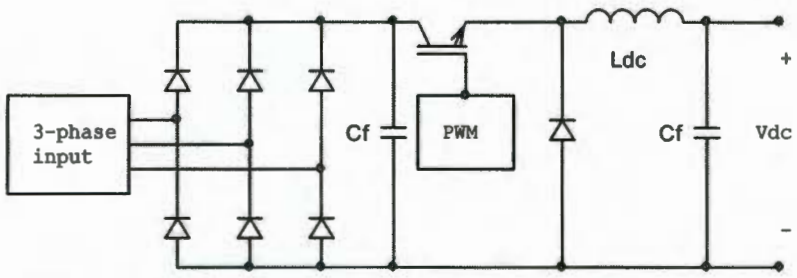

Figure 2.20: DC-DC step down buck converter employed as the power control stage of an induction heating power source. The output power is controlled by varying the duty cycle of the IGBT. Cf forms a low impedance path for the high frequency switching currents drawn by the inverter.

A system which reduces the problems associated with harmonic distortion and input power factor, utilizes a DC-DC converter as the power control stage [36], [37]. This converter can be configured as either a constant voltage or current source and operates at frequencies between 1kHz and 100kHz. The configuration shown is a step down chopper (commonly used in DC drives), and provides an output voltage variable from zero to approximately the maximum available input voltage by varying the duty cycle of the switch.

The high converter operating frequency substantially reduces the size of the filtering components, and also allows for effective high speed protection required when feeding a high frequency inverter. The active switching element is usually an IGBT but can be any forced commutated power semiconductor switch. These converters are employed as the front end stage for bridge inverters at power levels from under 1kW to 100kW and are commonly used to feed inverters operating at frequencies above 50kHz.

2.9.3 Uncontrolled Rectifiers

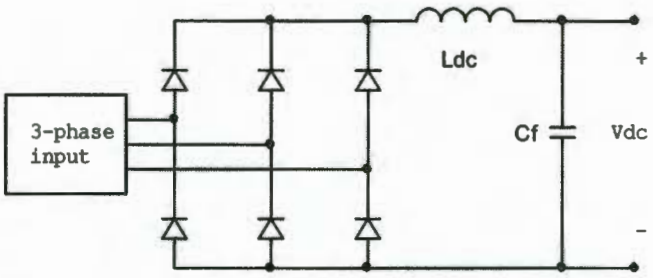

Figure 2.21: Uncontrolled rectifier used to feed Swept Frequency inverters or PWM inverters. These inverter topologies perform both frequency and power control in the inverter stage of the induction heating power source

Uncontrolled rectifiers feed stages in which the inverter performs both frequency and power control. This type of inverter is classified into two categories namely, PWM inverters, and swept frequency inverters. The PWM inverter achieves power control by varying the duty cycle of the inverter switches from 0 to less than 50% [38], [39].

The swept frequency inverter achieves power control by varying the inverter driving frequency away from the load resonant frequency. This is accomplished by using a series resonant load which has a characteristic increasing impedance when operated away from resonance, thereby drawing less power from the uncontrolled rectifier [40].

SCR converters are often of the swept frequency type operating below the natural resonant frequency of a series compensated load. Power control from 10% to 100% is achieved by swept frequency means and the capacitively reactive nature of the load below resonance is used to commutate the SCR's, thereby simplifying the control and drive electronics required for this converter [10], [41].

2.10 FREQUENCY CONTROL

The quest for increased operating efficiency has led to the evolution of the load resonant inverter. This type of inverter operates at the natural resonant frequency of the induction heating load at all times and yields conversion efficiencies of greater than 95% [11], [25]. Driving the load at its natural resonant frequency facilitates zero voltage or zero current switching, considerably reducing the switching losses usually associated with switch-mode operation.

Load resonant converters allow for higher inverter switching frequencies to be achieved efficiently and also enable lower power rated switches to be employed due to the reduction in switching power losses. Due to the dynamic nature of induction heating loads, a considerable change in natural resonant frequency of the load circuit can occur during the heating cycle. Unlike RF valves, solid-state switches cannot tolerate mismatched load circuits very well at high frequencies (because of excessive power dissipation in the semiconductors), making these supplies unstable and inefficient under these conditions [6]. Driving a mismatched load brings about the conduction of the integral body diode within the MOSFET. This results in a conduction power loss as well as a reverse recovery loss when the load current is commutated from one half cycle to the next at high frequency. In order for the inverter to maintain efficient operation at resonance, the inverter must now have the ability to search, find and continuously track the load resonant frequency during operation. This added feature has led to a new field of study in induction-heating control strategies. The most common form of frequency control available is based on phase locked loop techniques. The next section presents a brief overview of frequency control using this technology.

2.10.1 Phase-Locked Loops

A phase-locked loop is a circuit which synchronizes the signal from an oscillator with a second input signal, called the reference, so that they operate at the same frequency with a fixed phase relationship between the two [42]. Phase-locked loops are often used because they provide filtering for the phase or frequency of a signal that is similar to that which is provided to voltage or current waveforms by ordinary electronic filters.

Phase locked loops find wide application in the areas such as communications, wireless systems, digital circuits, etc. The first description of phase locked loops was published by de Bellescize in 1932 on work involving the synchronous reception of radio signals [42].

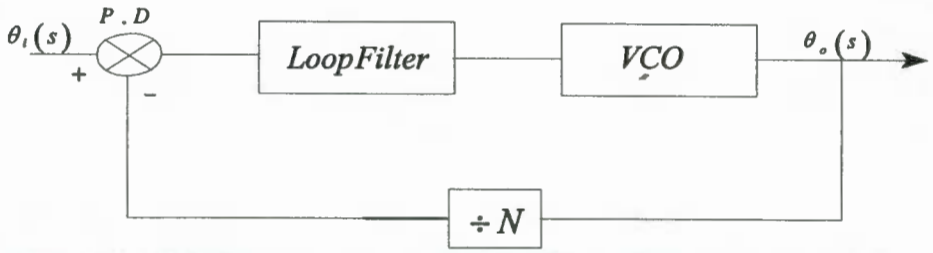

Figure 2.22: Block diagram of basic PLL configuration showing all its basic components showing the phase detector provides information regarding the phase-difference between the two input signals. The loop filter produces a DC voltage proportional to the phase-difference, and drives the VCO, which produces a frequency output within its operating range. Often the VCO operates at a frequency higher than the input signal frequency. The VCO output frequency can then be divided down in the feedback loop before it reaches the phase-detector.

2.10.2 Loop Fundamentals

The basic loop consists of a phase detector (P.D), a loop filter and a voltage-controlled oscillator (VCO). With the input signal to the loop expressed in the frequency domain, having a phase of $\theta_i(s)$ and an output of $\theta_o(s)$ as shown in figure 2.22.

2.10.3 Phase Detector

The ideal phase detector output voltage is proportional to the phase difference between its inputs, i.e:

$$Vd = Kd\,(\phi_i - \phi_o) \qquad \textbf{2. 18}$$

where Kd is the phase detector gain factor with dimensions of volts per radian (V/rad). Many different types of phase detectors exist, all performing essentially the function of multiplication in a typical PLL system. For the purposes of this project only the triangular type phase detector will be discussed:

2.10.3.1 Triangular phase detectors

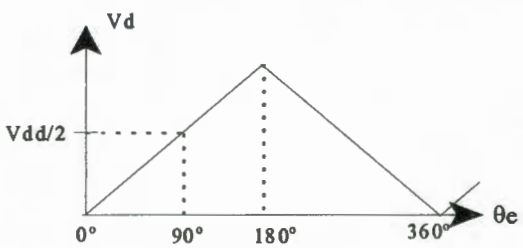

Figure 2. 23: XOR phase detector characteristic showing optimum operating point at 90°.

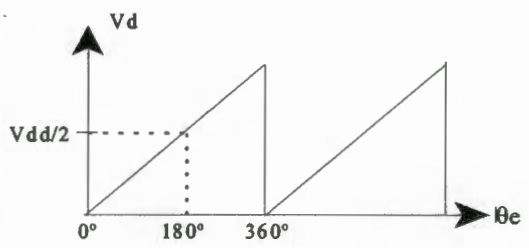

Figure 2. 24: R-S latch phase detector characteristic showing optimum operating point at 180°.

Unlike sinusoidal characteristic phase detectors, linearity in triangular P.D.'s are near perfect for phase angles as large as 90°. A triangular characteristic is realized by driving the inputs to a multiplier with square waves. This operation gives the P.D. an exclusive-OR characteristic [43]. Digital phase detectors are realized when using an XOR gate or an edge-triggered R-S flip-flop. These form part of the triangular family of P.D.'s but have a slightly different output characteristic as shown in figures 2.23 and 2.24.

2.10.3.2 XOR phase detector

Operation from a single supply and a close examination of the XOR truth table yields the digital P.D. characteristic. Is should be observed that preferred operation of this device would be when the two input signals are phase shifted by 90°. This puts the P.D in the center of its linear region and ensures accurate lock operation over the range $0 < \phi < 180°$.

The XOR gate being a digital device is relatively immune to switching and input signal noise. The trade-off however, is that the input signal range is limited to a 50 % duty cycle in order to ensure correct operation of this device.

2.10.3.3 R-S latch

The extended operating range of ($0 < \phi < 360°$) for the R-S latch makes it an attractive option for a P.D. This device is not duty-cycle limited like the XOR but has its disadvantages. Being an edge-triggered device makes it susceptible to noise effects and therefore the two input signals must be of a quality that will trigger the flip-flop reliably [42]. Also the input signal-to-noise ratio must be high, and this type of detector is of no value if a signal must be recovered from a larger noise. This type of phase detector often requires matched filters at the input in order to allow reliable operation [44].

2.10.4 Loop Filter

The output of the phase detector is filtered by the loop filter, which provides a phase error voltage to drive the VCO to keep the loop in lock. Since the P.D. and the VCO designs are usually inflexible, the design of the loop filter provides more flexibility in controlling the PLL characteristics [45], [46]. The desired PLL response will determine the loop-order. The loop-order required therefore dictates the loop filter type. Loop filters are generally of two types, namely passive and active.

2.10.4.1 Passive loop filter

Passive loop filters are of the low pass type or of the phase-lead-lag type. For simple phase-locked applications requiring low loop gain, marginal phase-accuracy and transient loop stability, passive loop filters provide a quick and easy solution.

2.10.4.2 Active loop filter

For a passive loop filter the maximum dc gain achievable is 1. An active loop filter provides dc loop gains that are essentially infinite and provide better tracking performance. Many types of active loop filter configurations (such as the integrator, integrator and lead, lead-lag filter) are available in references [42], [45], [46]. The final loop filter configuration used for this research will be discussed briefly.

2.10.4.3 Integrator plus lead filter

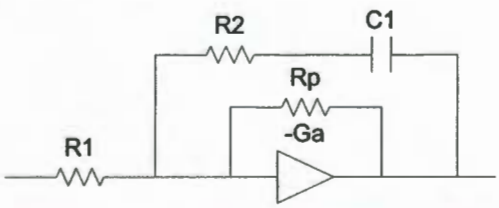

Figure 2. 25: Simplified representation of an active integrator and lead loop filter showing an op-amp configuration and the passive components, which determine the loop parameters.

The integrator plus lead filter forms a basic PI controller as shown in figure 2.25. The prime purpose of introducing an integral term into the controller is to remove any steady state phase error. At high frequency the ac gain (proportional term Kp) is formed by R2/R1. It will be illustrated later that for the purposes of this research the ac amplifier is actually used as an attenuator to the high frequency ripple, providing a jitter free signal to the VCO. The dc gain of the filter is usually infinite as mentioned before. In many applications involving high order loops however, it is always desirable to control the dc loop gain to prevent instability. Rp/R1 controls the dc gain component of the loop filter and therefore also indirectly controls the entire loop gain.

Design of a PLL requires the ability to be able to control the natural loop frequency (ω_n), damping factor (ζ) and dc loop gain (K). Passive loop filters such as the single pole low-pass and the two-pole low pass filter do not allow for the control of ω_n, ζ and K independently. The control of K ensures good tracking as mentioned before but with a high gain loop (large K) also comes wide bandwidth. Therefore, narrow bandwidth and good tracking are usually incompatible in first order loops. If it is necessary to have large gain and small bandwidth, the loop will be badly under damped (low ζ) and transient response will be poor (low loop bandwidth). The active integrator plus lead filter having two independent time constants ($\tau 1$ and $\tau 2$), draws on the concept of tachometer feedback which allows for the independent control of natural frequency (transient response), damping factor (overshoot) as well as the dc gain (good tracking).

2.10.5 Voltage Controlled Oscillator

The voltage-controlled oscillator provides an output frequency, which is controlled by the filtered error voltage it receives from the loop filter. Since frequency is the derivative of phase, the VCO operation may be described as:

$$\frac{d\phi_o}{dt} = K_o V_{in} \qquad \textbf{2. 19}$$

$$\begin{aligned} \textit{where } K_o &= \textit{VCO gain} \\ V_{in} &= \textit{VCO input voltage} \\ \phi_o &= \textit{VCO output phase} \end{aligned}$$

It is therefore apparent that the phase of the VCO output will be proportional to the integral of the input voltage V_{in}. The VCO should be operated within its linear range to ensure a constant loop-gain parameter (K_o). For the purposes of this research, a linear relationship between input control voltage and output frequency is assumed and is given by:

$$k_o = \frac{\Delta f_o}{\Delta V_o} \qquad \textbf{2. 20}$$

The VCO's employed in the frequency control system for this research were derived from two 4046 PLL integrated circuits.

CHAPTER 3

DESIGN OF THE INDUCTION HEATING SYSTEM

The induction heating power supply is designed by first determining the application, specimen to be heated (work-piece properties), and the power required to reach the target temperature. The next step is to design the coil in order to couple the necessary energy as efficiently as possible to the work-piece. This is followed by load circuit calculations, which are required to optimally match the coil and work-piece to the high frequency power source. The induction heating power supply simulation and design is then undertaken in order to understand the operation thereof and also to validate the solution implemented in chapter 4.

3.1 HEATING LOAD (BILLET)

A 26mm diameter stainless steel work-piece having the dimensions shown in appendix 1A is to be heated to 1200°C. The billet is to be heated in approximately 145 seconds before being extruded into a different shape. A graphical method for calculating the power required to do this work is used by Tudbury *et al* [24]. Using this method, it is shown in appendix 1A that the power required to heat the stainless-steel billet to 1200°C in approximately 145 seconds is 1.085 kW.

3.2 COIL DESIGN

The next step involves the design of the heating coil needed to couple the necessary power from the power source to the work-piece. An air-gap of 5mm between the work-piece and coil is chosen for both thermal insulation and mechanical clearance. 1/8 inch annealed copper tubing was used for the 9-turn induction-heating coil. The length of the coil was 35mm (same as work-piece) with an inner diameter of 36mm. Using the Baker model [11] from Chapter 2 (section 2.5) to calculate the coil inductance was found to yield incorrect results. This was because of the assumption that the coil resistance is equal to its reactance (equation 2.5) and the calculation of X_{gap} (equation 2.6), which assume an infinitely long solenoid coil with a uniform field along its axial length. This is not the case for the current application, and the Baker model merely gives a guideline as to which factors are to be considered during coil

design. The Wheeler formula (equation 2.13) however, yielded the best result for the calculation of the unloaded coil inductance, and was in agreement with measured values of constructed coils. From the dimensions provided above, the calculated inductance of the coil using the Wheeler formula from equation 2.13 (as shown is appendix 1B) was 2.1uH.

3.3 ELECTRICAL EQUIVALENT CIRCUIT

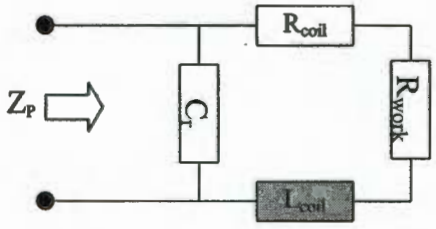

Figure 3. 1: Induction heating load circuit parameters designed for this research. The coil inductance was calculated using the Wheeler formula. The coil and work-piece resistance was calculated using Baker's model.

The electrical equivalent circuit is derived using Baker's model [11] which yields the work-piece resistance (R_{work}) of 111.3mΩ, coil resistance (R_{coil}) of 29.2mΩ and coupling efficiency of 83.4% as shown in appendix 1B. The power needed at the coil terminals is 1.3kW at 140kHz. The quality factor of this tank circuit was calculated to be approximately 12.8. A resonant capacitor (C_r) of 630nF was required to resonate the tank circuit at 140kHz. The tank circuit impedance at resonance (Z_p) is 23.16Ω. At an output current of $10A_{RMS}$ the inverter will deliver 1.56kW to the tank circuit. This is within the specification of the designed value required of 1.3kW.

The calculated value of coil inductance does not account for the loading effect of the work-piece. This effect will tend to reduce the coil inductance and alter the tank circuit characteristics. Once constructed, the necessary alteration was made to compensate for this effect, as it was difficult to quantify with simple calculations. The procedure followed thus gives the designer a generalised approach to the design of the induction heating load circuit.

3.4 RESONANT TANK CAPACITOR

The resonant capacitor exchanges oscillating energy with the induction-heating coil in the tank circuit. The kVAR rating of the tank capacitor at 140kHz is 28.7kVAR. The RMS current rating of the tank capacitor must be greater than $128A_{RMS}$. A capacitor bank using high current low ESR metalised polypropylene capacitors was implemented. The capacitor bank consisted of five 150nF / 600Vac capacitors connected in parallel. The impedance of the tank circuit at resonance is dependant on the Q and the resonant capacitance used. These two parameters influence the operating frequency, and in turn, help the user to design for an optimum impedance matching to the power source. The parallel resonant tank circuit by virtue of its quality factor, acts as a loss less impedance matching transformer.

3.5 DC-AC INVERTER TOPOLOGY

The merits of employing a parallel resonant load circuit have been discussed. The parallel resonant induction heating load is current supportive and as mentioned before would require a constant current source drive. An H-Bridge current-source inverter was therefore employed as the high frequency power source. This is determined by whether the DC bus is terminated by a large filter capacitance or inductance immediately before the inverting stage of the induction heating power supply.

3.5.1 Inverter Topology

The prototype inverter employed a current-fed load resonant topology. This topology provides the following benefits over the series resonant bridge implementations:

- A current-fed topology can drive a parallel resonant load directly with or without a matching transformer. The square waveform current fed to the load has high-frequency components, which see a low impedance flowing into a parallel resonant circuit.
- Driving a parallel resonant load directly (without coupling from a series tuned circuit) ensures that the load only has one resonant frequency. This factor

simplifies the frequency control system implementation and allows for a wider frequency tracking range.

- The current-fed inverter achieves inherent short-circuit protection provided by a smoothing choke connected between the inverter and power control system which restrict the rate of rise of current in the event of a fault. Coil short-circuits are common in certain induction heating applications.
- Due to the robust nature of this topology, it requires simple control and protection circuitry.
- High voltage capacitors are not required.
- Power semiconductor switches conduct only the active current of the load.
- For a parallel resonant topology, operation with an unloaded coil is possible (due to maximum impedance at no load), which is inherent in this circuit topology [1].

The H-Bridge Current-Fed inverter topology is shown in figure 3.1. Power MOSFET's are employed as the active switching elements due to their high-speed characteristics. Blocking diodes D1 to D4 prevent the MOSFET's anti-parallel diodes from conducting. Due to their slow switching speeds (860ns) the antiparallel diodes, if allowed to conduct, would suffer reverse recovery losses and degrade the efficiency of the power source. Anti-parallel diode reverse recovery often leads to diode failure, which causes total MOSFET destruction. Under normal operation when switched at zero voltage, these diodes would not conduct. The blocking diodes, however serve as protection, in the event of the loss of zero voltage switching occurring in the inverter for whatever reason. The addition of the blocking diodes does not have a major impact on efficiency, and at high powers it can be considered to have negligible effect on efficiency whilst improving the reliability and robustness of this inverter topology.

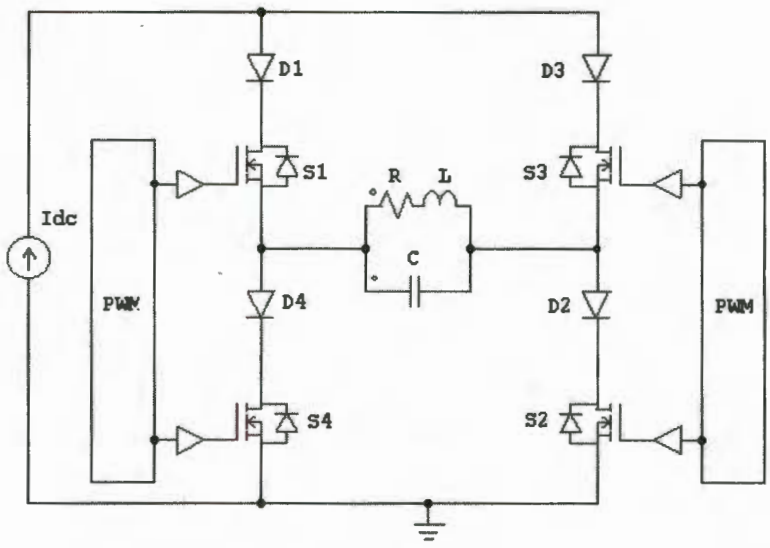

Figure 3. 2: Current-fed inverter configuration showing the application of power MOSFET's as the active switching elements. The induction-heating load is modeled by the RL combination with its resonant capacitor bank C. Fast recovery diodes D1 to D4 prevent the antiparallel diodes in the MOSFET's from conducting.

The AC output is produced by switching pairs S1, S2 and S3, S4 alternatively every half cycle of the resonant frequency. The firing signals are produced by the PWM circuitry, which receives a master clock signal from the frequency control circuitry. The resonant load circuit requires that the inverter functions like a DC current source presenting a high impedance to the switching frequency currents. The current source is usually accomplished by placing a large reactor in the DC bus. In order to present a very large impedance to the high frequency currents, the DC bus reactor should have a reactance of at least ten times the load impedance at the inverter operating frequency [47], [48]. For an inverter operating frequency of 100kHz, a DC reactor inductance of approximately 716 uH is required.

The inverter switches create a square wave of current that passes through the parallel resonant load. This square wave current contains high frequency harmonics and can be expressed by the following Fourier series [49]:

$$i_o(t) = \sum_{n=1}^{\infty} bn \sin\left(\frac{2\pi n}{T}\right)t \quad [A] \qquad \textbf{3. 1}$$

where:

$$bn = \frac{2I_{DC}}{n\pi}\left[\cos\frac{2\pi n}{T}\frac{t_{DB}}{2} - \cos\frac{2\pi n}{T}\left(\frac{T - t_{DB}}{2}\right)\right] \qquad \textbf{3. 2}$$

The overlap commutation period between the positive and negative half-cycle of the inverter output current is given by t_{DB} which is very small in relation to the period (T) and is assumed to be negligible in this case, in order to simplify the analysis. When the inverter operating frequency ω is equal to the load resonant frequency ω_o, the load impedance looks purely resistive to the fundamental component of the inverter output current i_o. Higher harmonics in the square wave are subjected to a much lower impedance (due to selectivity of the load), making the load voltage nearly sinusoidal and in phase with i_o.

The fundamental RMS component of the square wave current i_o fed to the load is given by:

$$i_{o1(rms)} = \frac{4I_{DC}}{\sqrt{2}\,\pi} \quad [A] \qquad \textbf{3. 3}$$

The magnitude of the load impedance is frequency dependant and has a maximum value at parallel resonance. This load circuit impedance can be expressed in terms of the circuit Q and inverter operating frequency (ω) and is given by:

$$Z_p(\omega) = Q_o R \left(\frac{Q_o - j\frac{\omega}{\omega_o}\left[Q_o^2 \frac{\omega^2}{\omega_o^2} + 1 - Q_o^2 \right]}{\frac{\omega^2}{\omega_o^2} + Q_o^2 \left[\frac{\omega^2}{\omega_o^2} - 1 \right]^2} \right) \quad [\Omega] \qquad \textbf{3.4}$$

$$If: \; Q_o = \frac{\omega_o L}{R} = \frac{1}{\omega_o RC}$$

where:

ω = inverter driving frequency,

ω_o = natural resonant frequency of the load,

Q_o = quality factor of the resonant load.

The inverter RMS output voltage impressed across the tank circuit is therefore given by:

$$v_{o(rms)} = \frac{4I_{DC}}{\sqrt{2}\pi} \cdot \frac{Q_o^2 R}{\frac{\omega^2}{\omega_o^2} + Q_o^2 \left[\frac{\omega^2}{\omega_o^2} - 1 \right]^2} \quad [V] \qquad \textbf{3.5}$$

It can be noted that the RMS load voltage is a maximum at the frequency $\omega = \omega_o$. This frequency corresponds to the point of maximum impedance of the load circuit at resonance. The output power developed in the tank circuit is therefore given by:

$$P_{out} = \frac{8I_{DC}^2}{\pi^2} \cdot \frac{Q_o^2 R}{\frac{\omega^2}{\omega_o^2} + Q_o^2 \left[\frac{\omega^2}{\omega_o^2} - 1 \right]^2} \quad [W] \qquad \textbf{3.6}$$

3.5.2 Inverter Gate Drive Circuitry

A power MOSFET is switched into saturation by applying a gate control signal of approximately 12V with respect to its source terminal. The MOSFET gate input presents a capacitive load to the gate drive and the switching speed of the MOSFET is approximated by the time taken to deliver the necessary charge to the MOSFET gate. This time is given by Coulomb's law, which allows for the calculation of the power needed to drive the MOSFET [48]:

$$Q_{gate} = I_{driver} \cdot t_{sw} \quad [C] \qquad 3.7$$

and

$$P_{gate} = Q_{gate} \cdot V_{driver} \cdot f_{switch} \quad [W] \qquad 3.8$$

where:

Q_{gate} = gate charge required by the MOSEFET,

I_{driver} and V_{driver} = current and voltage supplied by the driver,

t_{sw} = MOSFET switching time and

f_{switch} = operating frequency of the gate drive circuit.

Bridge inverter configurations require the switching control signals to be conveyed to the high-side switches. The switching signals can be conveyed in numerous ways some of which include:

- Opto-coupled drive with separated supplies
- Electronic charge-pump configurations
- Isolated gate drive via pulse transformers.

The opto-coupler drive was not considered for this application since the gate drive circuit for an H-Bridge inverter configuration would require 3 separate floating auxiliary power supplies, which would add to the cost and complexity of the gate drive solution. The electronic charge-pump configuration was not considered, since it does not provide isolation between the control electronics and power electronic circuitry. Another reason for not employing this solution was because the charge-pump circuitry cannot withstand reverse voltages of greater than 10V across its output

stage, which is common in this converter configuration under tracking from one resonant-mode to another. The negative voltage across the MOSFET is caused by the inverter series blocking diodes, which prevent the MOSFET's integral body diode from conducting under reverse voltage conditions. The optimum solution for the inverter gate drive circuit was realised by employing an isolated pulse transformer gate drive configuration as shown below.

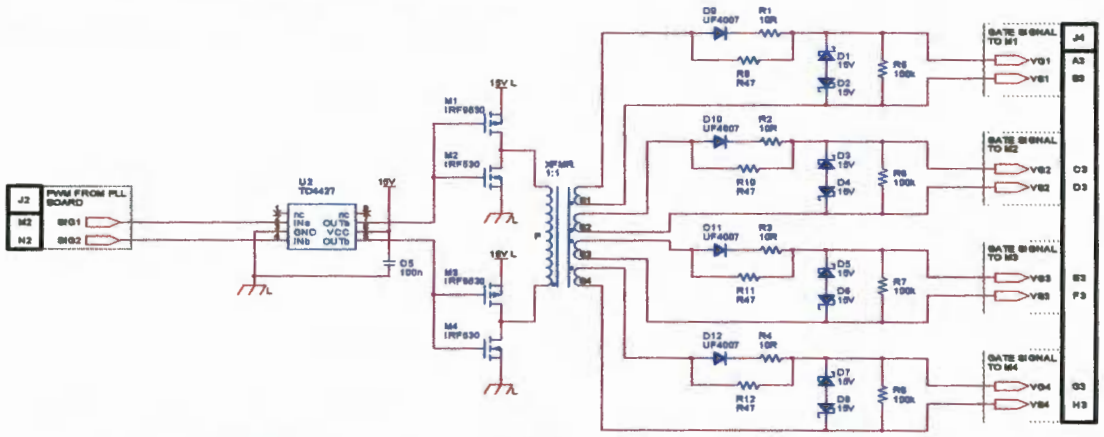

Figure 3. 3: Isolated high frequency pulse transformer gate drive circuitry. An ETD 29 Ferrite transformer was used to convey drive power to the MOSFET switches in the H-Bridge inverter stage. A MOSFET implemented totem pole configuration was employed on the pulse transformer primary winding and eliminated the need for a center-tapped winding.

The switching control signals are received from the PLL control circuit and are amplified via the totem pole stage and used to drive the pulse transformer primary winding of the ETD 29 Ferrite core. The gate drive circuit is essentially a series RLC resonant circuit consisting of resistance (output driver resistance + connecting lead resistance + gate resistance), inductance (transformer secondary leakage inductance + connecting lead inductance) and the MOSFET gate capacitance. The operation of this gate drive circuit configuration produces uncontrolled over voltages at the MOSFET gate terminal, which can cause semiconductor failure if it exceeds the maximum allowable gate voltage of ±20V. The resistor diode networks on the transformer secondary winding in figure 3.3 were configured experimentally in order to provide optimum switching times, provide damping on the gate (to eliminate voltage overshoot), as well as control the overlap time between the switching of the diagonal legs in the inverter bridge. The back-to-back zener diodes perform a bi-directional over voltage clamping function and regulate the voltage applied to the MOSFET gates.

3.6 ASPECTS OF FREQUENCY CONTROL

3.6.1 Motivation for frequency control

The dynamic behavior of the resonant load circuit is of major interest to all fields of induction heating. The load changes its characteristics (resonant frequency and quality factor due to a change in resistivity and inductance) under different loading conditions as well as during the heating cycle. With an increase in temperature, these operating conditions will eventually present a mismatched load to the power source if driven at a fixed frequency. Driving the load away from its natural resonant frequency results in a reduction of real power transfer to the load, and also an increased kVA demand from the power supply. Presenting a reactive load to the solid-state DC-AC inverter poses special problems. Firstly, a loss of zero voltage switching increases the inverter switching losses and reduces the overall system efficiency. Secondly, an inductively reactive load (driven below resonance) generates over voltage transients across the switches at turn-off [50] facilitating the need for snubber circuits and reducing system efficiency. A capacitively reactive load (driven above resonance), results in reverse recovery losses in the active switching elements of the DC-AC inverter. This mismatched condition can cause failure of the inverter switches and has a negative effect on its reliability.

An automatic frequency control system, which seeks, and continuously tracks the load resonance at all times, is therefore a key factor in enabling the successful and efficient implementation of this power source.

3.6.2 Loading effect

The unloaded induction-heating coil resonates with the tank capacitor at a frequency defined by equation 2.10. The inductance of the coil is given by:

$$L = \frac{N\phi}{i}[H] \qquad \textbf{3. 9}$$

$$E = N\frac{d\phi}{dt}[V] \qquad \textbf{3. 10}$$

From Faraday's induced emf equation (equation 3.10) it can be shown that the flux per meter width in the coil is given by [11]:

$$\phi = \frac{\mu H_s}{\alpha\sqrt{2}}\sin\left(\omega t - \frac{\pi}{4}\right)[wb] \qquad \textbf{3. 11}$$

$$\alpha = \frac{1}{\delta} = \sqrt{\frac{\mu\omega}{2\rho}} \qquad \textbf{3. 12}$$

When a high conductivity work-piece (e.g. copper) is placed inside the coil, the induced eddy currents in the work-piece create an opposing magnetic field to that of the coil, resulting in a decrease in coil flux and hence, decreased inductance as compared to its no-load value. The above explanation assumes that the work-piece is non-magnetic having a relative permeability of 1. When a magnetic work-piece is placed in the coil, its relative permeability reduces the skin depth (δ), which causes in an increase in flux (ϕ), resulting in a corresponding increase in coil inductance given by equations 3.9, 3.11 and 3.12. The relative permeability of a magnetic work-piece remains constant until at the Curie-temperature, where its reduces sharply to unity as the material loses its magnetic properties (when heated throughout). This effect therefore results in a rapid decrease in inductance to a value determined by the resistivity effect on the coil. The relative permeability of a magnetic material, for example mild steel, can be as high as several hundred at room temperature. The effect of resistivity for most work-pieces results in a small change in flux (in comparison to the permeability effect) when loaded into the coil. The effect of permeability therefore offsets the change in flux caused by the resistivity, resulting in an overall increase in inductance when a work-piece is placed inside the coil. When non-magnetic materials such as stainless steel, copper, aluminium, etc are placed in the coil, this results in a corresponding decrease in inductance as mentioned before, since the effect of permeability is not applicable in this case. These effects will be verified experimentally in chapter 4.

These changes in inductance result in a shift of the resonant frequency of the load circuit, creating the need for frequency control in order to achieve maximum power transfer and optimum inverter switching at all times.

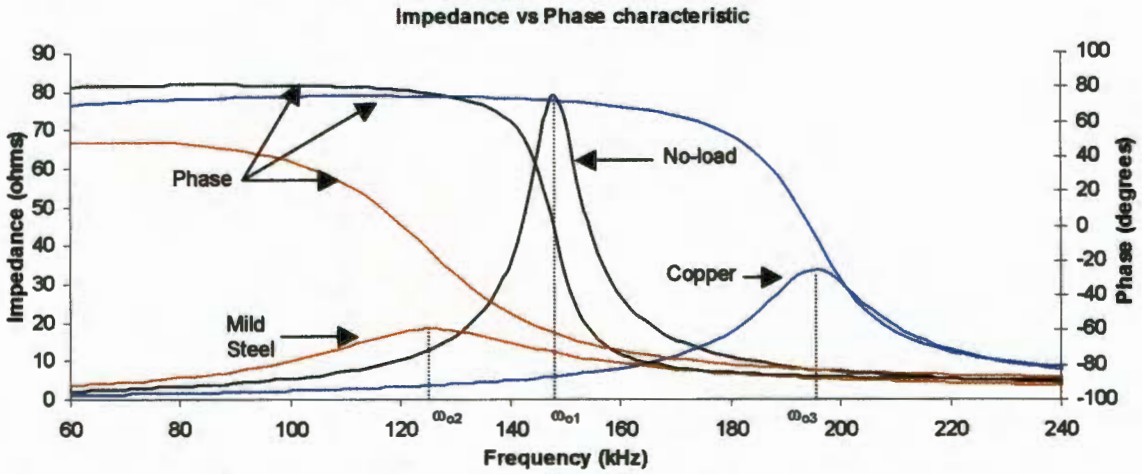

Figure 3. 4: Resonant frequency characteristics under different loading conditions. When the coil is loaded as shown, a change in load inductance results in a shift in resonant frequency. The characteristics of the work-piece (permeability and conductivity) also alter the quality factor and the bandwidth of the tank circuit.

To verify this theory experimental measurements were conducted using the model shown in figure 3.1. The procedure for determining these parameters is given in appendix A3. Three load conditions were investigated, namely: coil unloaded, copper work-piece (non-magnetic), and steel work-piece (magnetic) [51]. It can be seen in figure 3.4 that the results for the three loading conditions are in agreement with the equations 3.9 to 3.12. The load resonant frequencies are given by ω_{o1} (unloaded coil), ω_{o2} (steel work-piece) and ω_{o3} (copper work-piece) respectively. These are the optimum operating points, which correspond to the zero phase angle of the tank circuit impedance. When a high conductivity work-piece is placed inside the coil, a reduction in coil inductance (as explained above) results in an increase in resonant frequency above the unloaded value. A magnetic material such as mild steel (with a high relative permeability) increases the coil inductance when loaded, and results in a corresponding decrease in the resonant frequency below its no-load value.

3.6.3 Requirements of frequency control

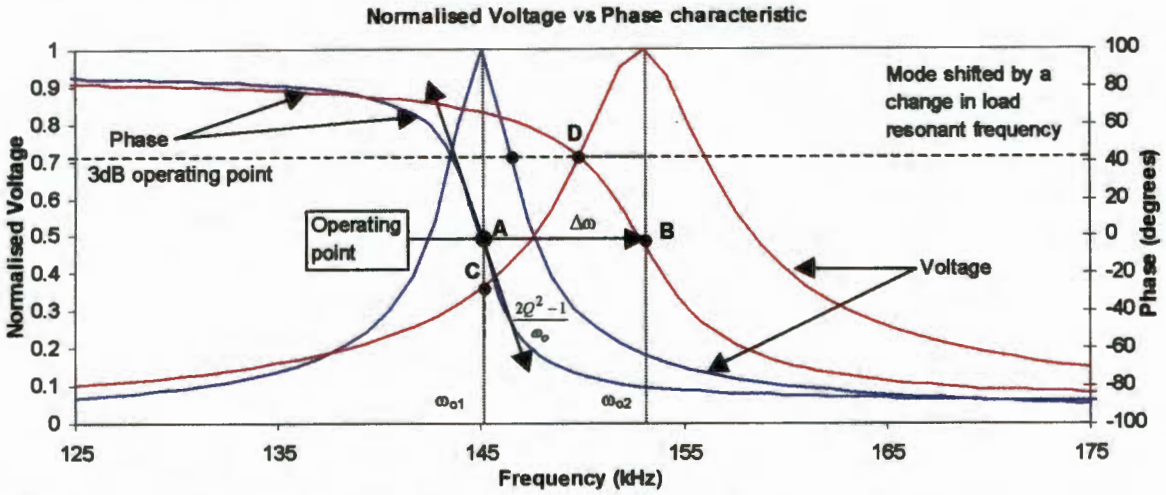

Figure 3. 5: Normalised tank circuit voltage and phase as a function of frequency. The frequency control system should be able to track the resonant frequency of the load by continuously operating at the zero phase point of the load circuit under different loading conditions. The unloaded coil operates at point A, corresponding to a resonant frequency of 145kHz. A stainless-steel work-piece is then placed inside the coil, shifting the resonant mode of the tank circuit with a new operating point at B (153kHz). Without automatic frequency control, the load would still be operated at point C (145kHz) resulting in a significant reduction in power transfer since the load is being operated far below its 3dB (half power) point at D.

It is apparent that different loading alters all the parameters of the load circuit (Q, R, ω_o and Zp) as shown in Figure 3.4. In figure 3.5 the frequencies ω_{o1} and ω_{o2} correspond to the resonant frequencies for two conditions namely, no-load and stainless steel. These are noted as the frequencies at which maximum response occurs (maximum impedance and maximum load voltage) for a parallel resonant load circuit. Load resonance (for a Q of >10) is also determined as the frequency at which the driving voltage and current are in phase [32]. With current as the reference vector ($I\angle 0°$), this is given by the zero degree points on the voltage phase plots (A and B) in figure 3.5 above. Operating at these points imply that optimum real power transfer to the load is taking place and zero voltage switching of the power source is being achieved.

The system initially operates at no-load corresponding to the load resonant frequency ω_{o1} and operating point A (figure 3.5). With no frequency control present, when a stainless steel load is placed inside the coil, the load characteristic would be altered and the optimum operating point now would be point B corresponding to frequency ω_{o2} (figure 3.5). However since there is no frequency control, the power source will still be driving the load at ω_{o1} corresponding to operating point C (Figure 3.5). This

mode of operation would be far from optimum since the 3dB operating point of the new load characteristic lies at operating point D, which corresponds to the half power point of the load. Operation below point D (3dB point) would result in a significant reduction in power transfer (< 50%). It is therefore required that an automatic frequency control system be able to track the zero phase operating points (A and B) of this dynamic load. Since the control system finds and tracks load resonance, it can be termed the resonance-locked loop (RLL) [51], [52].

3.6.4 **Resonance-locking methodology**

The implementation of the resonance locked loop required the control of two distinct variables whose phase relationship was a function of the applied frequency of the power source. A simplified schematic of the current fed inverter (power source) is shown in figure 3.6.

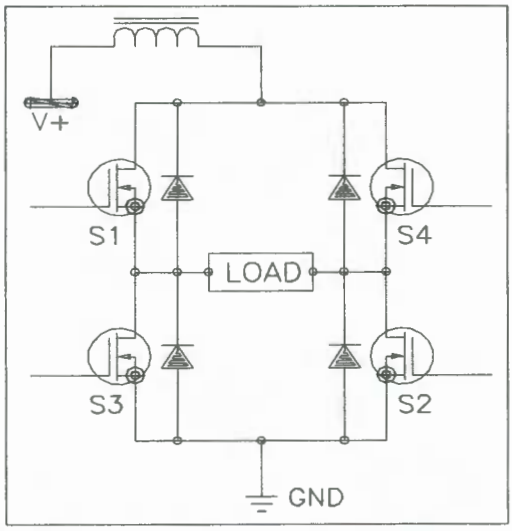

Figure 3.6: Basic current-fed inverter configuration employing power MOSFET's. Gate driver circuits and series blocking diodes have been omitted for simplicity.

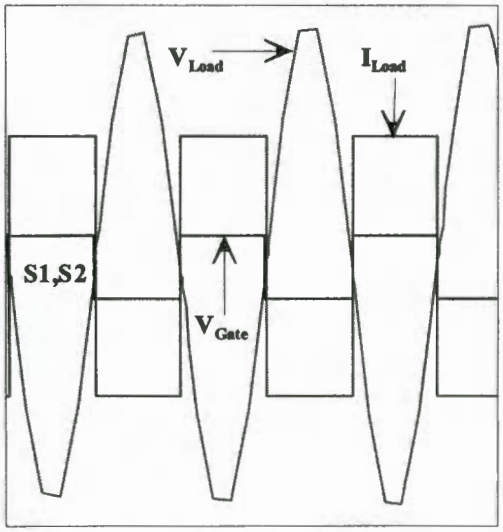

Figure 3. 7: Ideal waveforms of the driving voltage and current to the load circuit. It is apparent that the gate control signal (VGATE) is an approximate phase representative of the driving current. Horizontal axis represent time and vertical axis represent magnitude.

The induction-heating load can be characterised by the equivalent circuit shown in figure 3.1. The load circuit is current supportive and is modeled with an ideal current source which warrants the use of the iron core reactor in the inverter DC bus. The switching elements in the inverter drive the load at a frequency determined by the switching rate of the control signals fed to the gate of the power MOSFET's.

Switches S1, S2 and S3, S4 operate alternatively each to produce one half cycle of the RF power presented to the load terminals. Simulation results of the equivalent load circuit driven at resonance are shown in figure 3.7. V_{Load} is the driving voltage across the tank circuit and I_{Load} is the driving current through the load produced by the closure of switches S1, S2 and S3, S4 respectively.

Due to the principal of forced commutation it is evident in figure 3.7 that the control voltage to the power MOSFET (V_{gate}), is an actual phase representative of the driving current through the load. This concept is treated in the ideal sense and omits the propagation delay time taken to drive the MOSFET into the saturation mode of operation. This delay time is typically in the order of 200 – 300ns and is affected by the following factors:

- Rise and fall times of gate drive signal (Slew Rate)
- Value of gate resistor chosen for damping
- Input capacitance of the power MOSFET
- Stray inductance in the gate drive loop
- Characteristics of the load being switched by the power MOSFET (resistive or reactive)

This implies that the current representative signal Vgate will actually lead the load current in phase, resulting in lock operation at a non-zero phase angle. This phase error is corrected by a phase delay in the feedback circuitry of the loop [37].

In summary the control strategy employed utilized the following concepts:

- The inverter output voltage (V_{Load}) was transformed to logic levels (900Vp-p to 25Vp-p) [refer to completed schematic in Appendix 2D].
- The gate control signal fed to the power MOSFET is used as a phase representative of the driving current. This factor eliminates the need for current measurement and simplifies the layout of the inverter, making it compact and provides for stable operation.
- Control of the inverter is achieved by continuously locking the gating control signal (V_{gate}) to the inverter output voltage (V_{Load}) over its entire operating range.

3.6.5 Implementation of frequency control system

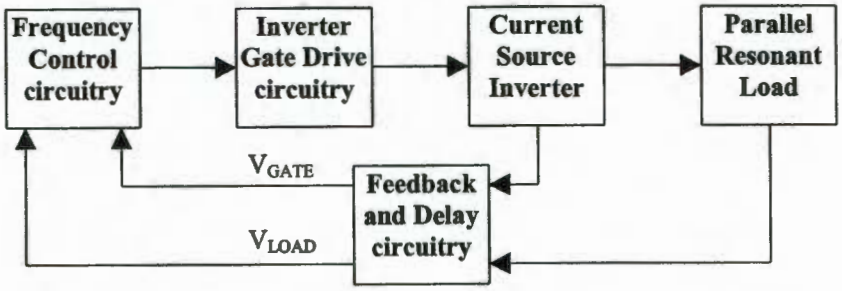

Figure 3.8: Layout of the Inverter and Frequency control System. The feedback circuitry scales the inverter output to an appropriate value while providing electrical isolation between the power and control circuitry. The delay circuitry is used to compensate for the phase shift in the current signal due to its point of measurement.

The basic layout of the high frequency power source is shown in figure 3.8. Frequency control is achieved by locking the gate control voltage (which represents the load current) to the output load voltage. The feedback circuitry consists of a step down transformer used for signal conditioning, and a zero crossing detector used to convey the phase information to the frequency control circuitry. The delay circuitry consists of a phase shifting circuit, which compensates for the phase difference between the MOSFET driving voltage V_{GATE} and the inverter output current I_{LOAD}. Using V_{GATE} as a phase representative of I_{LOAD} is advantageous because it eliminates the need for current measurement and simplifies the layout of the inverter. The frequency control circuit processes the phase information between the two input signals and generates the new driving frequency to the gate drive circuitry such that the phase-error between the two input signals V_{LOAD} and V_{GATE} is always zero.

The frequency control system is therefore able to track changes in load resonant frequency by virtue of the phase information present between V_{LOAD} and V_{GATE} over an operating frequency range extending from 80kHz to 200kHz. This will ensure that the semiconductor switches in the inverter, always experience zero voltage switching thereby maximising inverter efficiency.

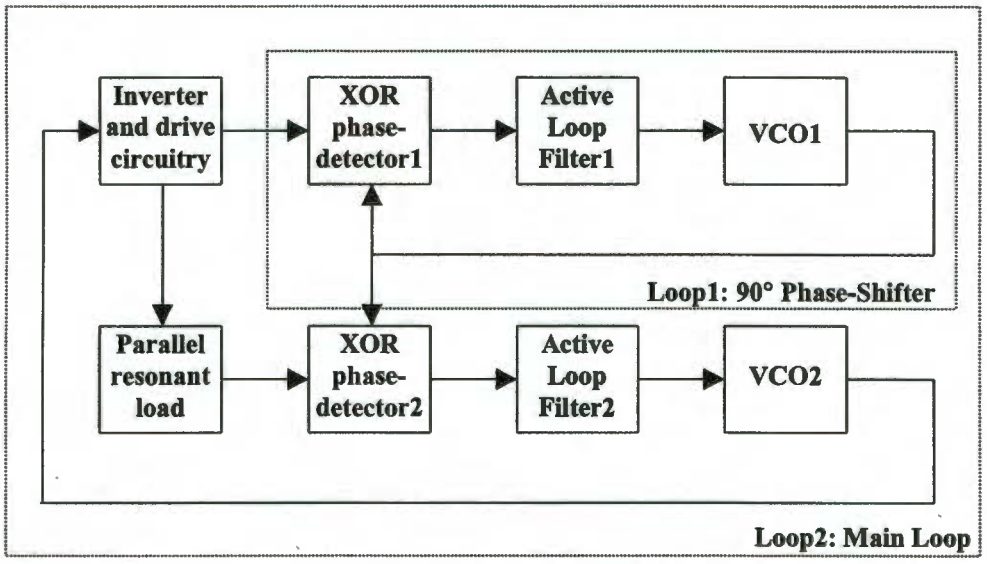

Figure 3. 9: The frequency control system comprises 2 phase locked loops with active loop filters. Loop 1 has a much faster response time than Loop 2 and is considered to be an ideal phase shifter. This assumption is used to help simplify the mathematical analysis of the frequency control system.

A simplified layout of the frequency control system implementation is shown in figure 3.9. It comprises two cascaded phase locked loops. Exclusive-OR phase detectors are employed for their high noise immunity characteristics (not being an edge-triggered device). Both loops operate as 90° phase shifters.

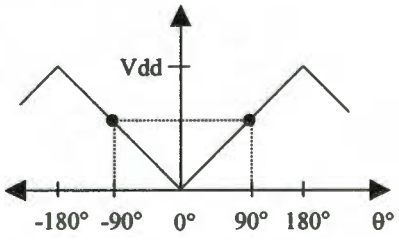

Figure 3.10: Phase characteristic of XOR PD1. The output is not monotonic over the load phase angle range (-90° to +90°).

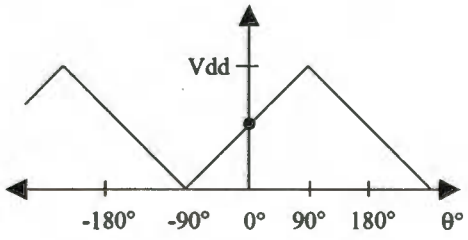

Figure 3.11: Phase characteristic of XOR PD2. When applying the 90° phase-shifted signal from loop1, the main loop PD characteristic is phase shifted by 90° and becomes monotonic.

Recalling from chapter 2, the XOR phase detector characteristic is given in figure 3.10. This reveals that although the detector has a linear phase characteristic, it is not monotonic over the entire load operating range (figure 3.10) that is from -90° to +90°. This implies that the phase detector is not able to determine the polarity (between V_{LOAD} and V_{GATE}) of the phase difference between the applied signals. For example, the average phase detector output voltage would be the same regardless of whether the load phase angle was +20° or -20°(if a change in resonance were to occur). This would result in the integrator not being able to charge in the correct direction (not

knowing whether the slope was positive or negative) and would not be able to lock V_{LOAD} and V_{GATE} in phase. The solution is to operate the phase detector in the center of its linear region thereby operating both loops as 90° phase shifters as shown in figures 3.9. With V_{GATE} processed and phase shifted by loop 1, it is fed to loop 2, which locks the phase-shifted signal (V_{GATE}) to the load voltage (V_{LOAD}). The two 90° phase shifted phase-locked loops achieves the desired phased detector characteristic shown in figure 3.11, having a linear, monotonic characteristic over the entire operating range of the load (-90° to +90°). Loop 1 acts as an ideal 90° phase-shifter independent of the operating frequency (between 80kHz and 200kHz) and has a much faster response time than loop 2. Loop 2 is the main loop, which operates with a time constant of greater than ten times that of loop 1. Setting up of the loop time constants (τ_1 and τ_2) in this manner ensures stability by placing the loop zero's far apart ($1/\tau_{LOOP1} = 1.68x10^6$ and $1/\tau_{LOOP2} = 4.54x10^3$). This ensures little interaction between the two loops and allows operation at very high DC loop gains.

3.6.6 Frequency control analysis

A conventional analysis of the induction heating load and automatic frequency control system was performed in order to provide a frequency domain model of the entire system. This analysis was required in order to characterise the system's steady-state behavior in response to certain inputs, which are likely to occur during operation.

3.6.6.1 Load analysis

The frequency response characteristics of figures 3.4 and 3.5 were derived using the electrical equivalent circuit model of figure 3.12 below. The parameters for these models were taken from actual measured values, which are derived in appendix A3.

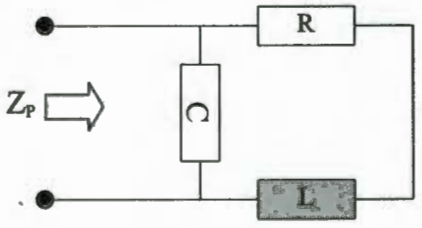

Figure 3. 12: Induction heating load circuit with a parallel resonant capacitor. This circuit is usually driven by a constant current source.

A conventional analysis of the load circuit yields the following relationships for tank voltage, V and phase, ϕ:

$$Z_p = \frac{(R + j\omega L)\left(-j\frac{1}{\omega C}\right)}{R + j\omega L - j\frac{1}{\omega C}} = \frac{R - j\left(\omega^3 L^2 C - \omega L + \omega R^2 C\right)}{\omega^2 R^2 C^2 + \left(\omega^2 LC - 1\right)^2} \qquad \textbf{3. 13}$$

For a parallel resonant system a constant current source is used. Assuming the current to be the reference vector ($I\angle 0°$), the voltage across the tank circuit is given by:

$$V = I \times Z = I \times \left[\frac{R - j\left(\omega^3 L^2 C - \omega L + \omega R^2 C\right)}{\omega^2 R^2 C^2 + \left(\omega^2 LC - 1\right)^2}\right] \qquad \textbf{3. 14}$$

$$\mathrm{Re}\{V\} = \frac{I \times R}{\omega^2 R^2 C^2 + \left(\omega^2 LC - 1\right)^2} \qquad \textbf{3. 15}$$

$$\mathrm{Im}\{V\} = \frac{I \times \left(\omega L - \omega R^2 C - \omega^3 L^2 C\right)}{\omega^2 R^2 C^2 + \left(\omega^2 LC - 1\right)^2} \qquad \textbf{3. 16}$$

$$\phi = \tan^{-1}\left[\frac{\omega L - \omega R^2 C - \omega^3 L^2 C}{R}\right] \cong \left[\frac{\omega L - \omega R^2 C - \omega^3 L^2 C}{R}\right] \qquad \textbf{3. 17}$$

Assuming a small angle approximation for the phase [52], [53], the slope of the phase at resonance can be determined through differentiation and substitution of $\omega_o = \frac{1}{\sqrt{LC}}$ as follows:

$$\left.\frac{d\phi}{d\omega}\right|_{\omega=\frac{1}{\sqrt{LC}}} = \left.\frac{L}{R} - RC - \frac{3\omega^2 L^2 C}{R}\right|_{\omega=\frac{1}{\sqrt{LC}}} \qquad \textbf{3. 18}$$

$$\frac{\Delta\phi}{\Delta\omega} = \frac{2L}{R} - RC = \frac{2Q^2 - 1}{\omega_o} \qquad \textbf{3. 19}$$

Where Q is the standard expression for the quality factor of a resonant circuit and is given by:

$$Q = \frac{\omega_o L}{R} = \frac{1}{\omega_o RC} \qquad \textbf{3. 20}$$

When the load is driven at its resonant frequency the frequency control system operates about a null point corresponding to the maximum slope of the function in equation 3.19. If we consider that a change in phase due to a change in load resonant frequency will be tracked immediately by the frequency control system, it can therefore be assumed that the differential change in phase will always be small and defined by the speed at which the frequency control system can track the disturbance (change in frequency). This assumption justifies the small angle approximation used in equation 3.19 and defines a small linear region under which the frequency control system can be analysed [53].

3.6.6.2 Linear Analysis

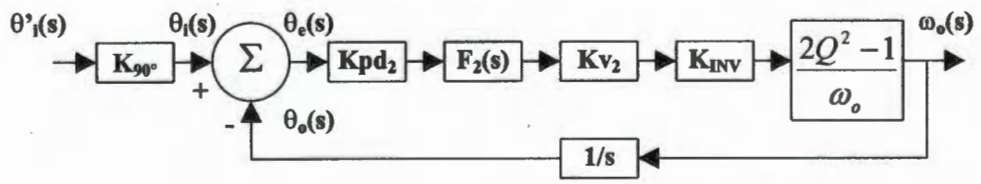

Figure 3. 13: Frequency control system loop model. The tank circuit is modeled as part of the loop as shown above. A change in resonant frequency of the tank circuit is modeled as a change in phase and is given by the system input $\theta'_i(s)$. The 90° phase-shifter loop is modeled as an ideal phase shifter (response being much faster than the main loop) and therefore does not affect the analysis.

The frequency control system can be modeled in the frequency domain using a phase model, which was adapted from the conventional phase locked analysis techniques [42], [54], [55]. As the load forms part of the control system it must be included in the model. An approximation of the load phase slope at resonance ($\Delta\phi/\Delta\omega_o$) is given by equation 3.19 and is modeled as a loop gain in figure 3.13. To simplify analysis, 90°-phase shifter loop 1 is modeled as an ideal phase shifter given by the $K_{90°}$ block in the model of figure 3.13. K_{pd2} and K_{v2} are the phase detector and VCO gains respectively. The active loop filter transfer function block is given by $F_{2(S)}$. The inverter is modeled as an ideal unity gain amplifier given by K_{INV} in the loop model of figure 3.13.

$\omega_o(s)$ represents the driving frequency of the inverter to the resonant tank circuit. ω_o represents the natural resonant frequency of the tank circuit. To evaluate the system performance with regards to phase error, it is necessary to understand the types of inputs the system is subjected to. Under normal operation with the system in lock, the inverter drives the load at its resonant frequency ω_o. From figure 3.13 the following series of equations may be expressed in Laplace form:

$$\theta_e(s) = \theta_i(s) - \theta_o(s) = \frac{\omega_o s}{\omega_o s + K_{pd2} K_{v2} K_{INV} F_2(s)(2Q^2 - 1)} \qquad \textbf{3. 21}$$

$$\frac{\theta_o(s)}{\theta_i(s)} = \frac{s\left[K_{pd2} K_{v2} K_{INV}(1+\tau_2 s)(2Q^2 - 1)\right]}{\tau_1 \omega_o s^2 + K_{pd2} K_{v2} K_{INV}(1+\tau_2 s)(2Q^2 - 1)} \qquad \textbf{3. 22}$$

With the loop operating at ω_{o1} (point A) in figure 3.5 the load phase angle is approximately zero. When a work-piece is inserted or removed from the coil, a step change in phase results. This is due to the change in inductance, which alters the load resonant frequency, and is modeled as the loop phase input $\theta_i(s)$ in figure 3.13. The phase difference between the load voltage and current (V_{LOAD} and V_{GATE}) as a result of the change in ω_o from ω_{o1} (point A) to ω_{o2} (point B) is given by $\theta_e(s)$. This phase error is processed by the loop filter and drives the VCO towards ω_{o2} (point B) where the phase displacement between the load voltage and current (V_{LOAD} and V_{GATE}) are approximately zero resulting in operation at the new load resonant frequency ω_{o2} (point B). The second type of phase input is where a magnetic work-piece is heated through its Curie temperature. This effect will be modeled as a ramp change in phase input $\theta_i(s)$. The final value theorem can be used to evaluate the system's steady-state phase error in response to a phase step is given by:

$$ess = \lim_{t\to\infty}[\theta_e(t)] = \lim_{s\to 0} s\left[\frac{\omega_o s}{\omega_o s + K_{pd2} K_{v2} K_{INV} F_2(s)(2Q^2 - 1)}\right]\frac{\theta_i}{s} = 0 \qquad \textbf{3. 23}$$

Similarly the steady-state error response (*ess*) to a ramp input is given by:

$$ess = \lim_{t\to\infty}[\theta_e(t)] = \lim_{s\to 0} s\left[\frac{\omega_o s}{\omega_o s + K_{pd2} K_{v2} K_{INV} F_2(s)(2Q^2 - 1)}\right]\frac{\theta_i}{s^2} \qquad \textbf{3. 24}$$

$$= \lim_{s\to 0}\left[\frac{\omega_o \theta_i}{\omega_o s + K_{pd2} K_{v2} K_{INV} F_2(s)(2Q^2 - 1)}\right] \cong 0 \qquad \textbf{3. 25}$$

Implementing an active loop filter $F_2(s)$ as defined in equation 3.26, with DC gain F(0) approaching infinity, results in a steady state phase error-approaching zero. The active loop filter transfer function is given by:

$$F_2(s) = \frac{(1+\tau_2 s)}{\tau_1 s} \qquad \textbf{3.26}$$

The loop parameters of both phase-locked loops were found experimentally is calculated in appendix 1C. For the loop 1, τ_1 = 4.86us, τ_2 = 5.94us. For the loop 2, τ_1 = 23.5ns, τ_2 = 8.46us. A detailed schematic representation of the frequency control circuit is provided in appendix 2D. The control system has a center frequency of 140kHz and operates from 80kHz to 200kHz.

3.7 POWER CONTROL SYSTEM

The power delivered to the load circuit is controlled by varying the dc bus current supplied to the inverter stage. The average output voltage of the converter is given by:

$$V_{out(avg)} = \frac{1}{T_{sw}}\left(\int_0^{t_{on}} V_{in(DC)}\,dt + \int_{t_{on}}^{T_{SW}} 0\,dt\right) = \frac{t_{on}}{T}\cdot V_{in(DC)} = V_{in(DC)}\cdot D \quad [V] \qquad \textbf{3.27}$$

From equation 3.27 the DC output current fed to the inverter is given by:

$$I_{DC} = \frac{V_{out(avg)}}{Z_p} = \frac{I_{in(DC)}}{D} \quad [A] \qquad \textbf{3.28}$$

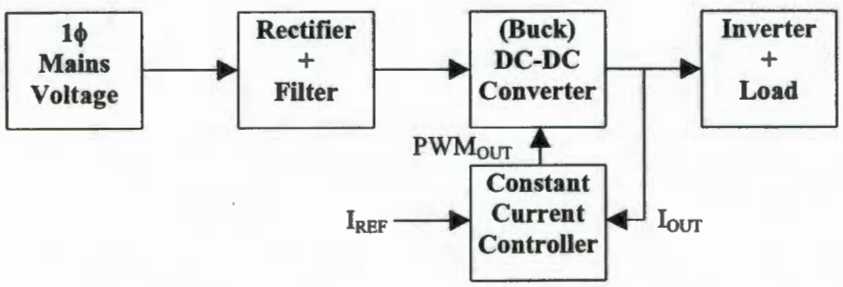

Figure 3.14: Layout of the power control system. Power is derived from an unregulated rectified DC bus, which is fed to the inverter and load through the buck regulator. The controller used closed loop feedback to maintain a constant DC output current (set by I_{REF}) by controlling the PWM duty cycle fed to the DC-DC converter.

A switch-mode buck regulator, configured as a regulated constant current-source performs this function. The DC-DC converter also provides the necessary high-speed protection in the DC bus, needed to protect the inverter stage in the event of a fault. The basic layout of the power control system is given in figure 3.14.

An unregulated and filtered DC bus derived from the single-phase mains, supplies power to the buck converter. The converter is rated at 2.5kW and operates at 72kHz supplying a regulated constant DC current of 0-10A to the inverter stage by varying the switch duty cycle in the buck converter. Due to the high operating frequency, power MOSFET's were employed as the active switching elements in the DC-DC converter. The constant current controller uses the output current as feedback to maintain closed loop control around a current reference set point. The basic current control system layout is shown below.

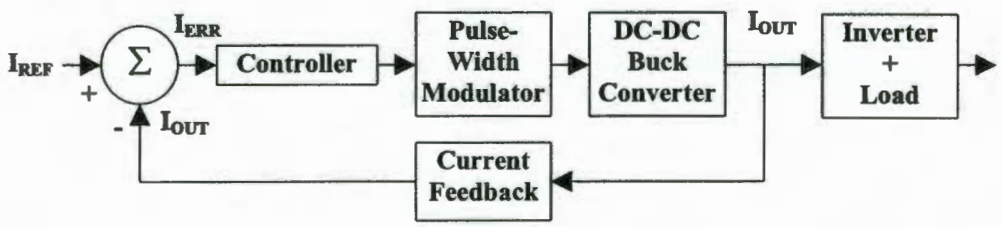

Figure 3. 15: Constant current control system model. The output current to the inverter stage is set by I_{REF}. The controller maintains this value at I_{OUT} by controlling the pulse width of the DC-DC converter. The controller essentially comprises a non-ideal op-amp based PI controller. The current feedback circuitry comprises the sensing and scaling circuitry used to provide closed loop control.

The controller maintains a constant output current by varying the switch duty cycle in order to achieve control around the set point current. The controller essentially consists of an op-amp based PI controller. The pulse width modulator generates the switch duty cycle in response to the output voltage received from the controller. The current feedback circuitry consists of the necessary sensing and signal conditioning circuits required for closed loop control. The power controller also functions as a protection system for the inverter stage, allowing the maximum current level and inverter peak switching voltage to be set independently. The PI controller parameters were found experimentally and were selected to provide both optimum transient response and tracking capability. A detailed schematic diagram of the DC-DC converter and power control circuit is provided in Appendix 2B and 2E.

3.8 SYSTEM SIMULATION

A simulation model of the high frequency power source was developed in order to better understand the operation and control of the entire system. It was also used to estimate the power semiconductor ratings. Simcad version 4.1 was used and the simulation results are described in the following section.

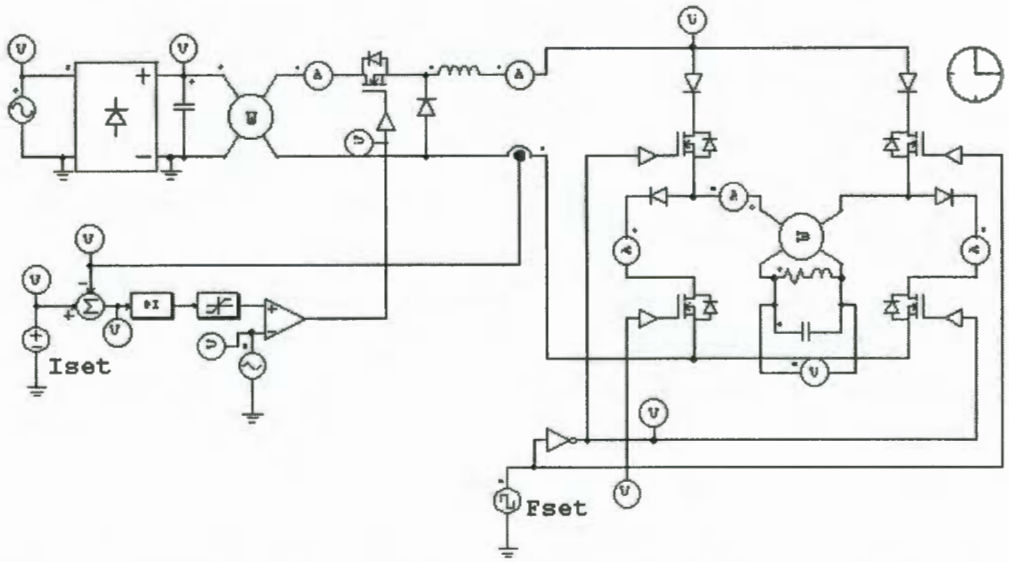

Figure 3. 16: Simulated system model showing the components of the high frequency power source.

3.8.1 DC-DC converter

The DC-DC converter is used to control the DC bus current supplied to the inverter stage. The DC current is sensed in the ground return path and fed into the constant current controller where operation around the set point current, Iset is maintained. The converter operates at 72kHz with a switch duty cycle varying from 0% to 75%. The use of high frequency plays a major advantage in power control due to the substantial reduction in inductor size (L = 1mH), which increases the speed of converter response. The converter response to a reference step of 8A is shown in the trace of figure 3.17.

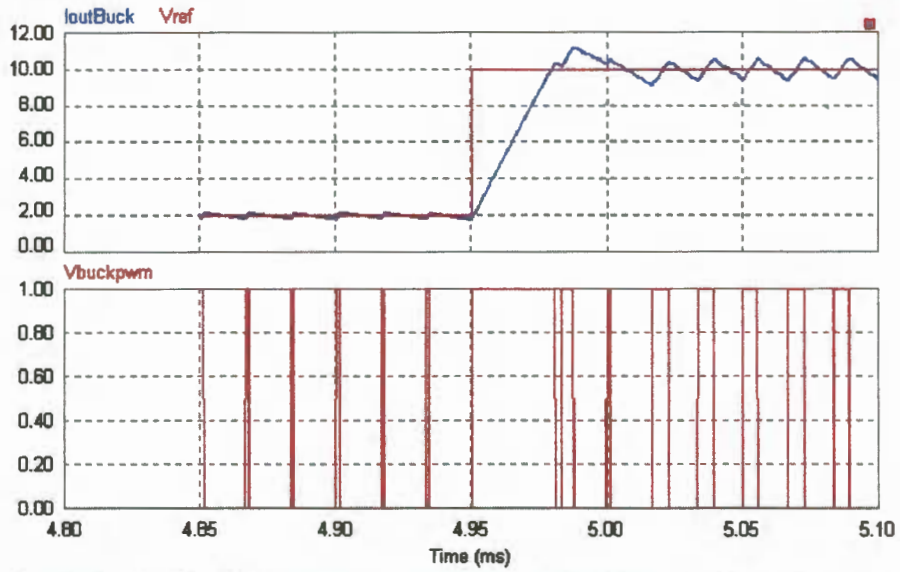

Figure 3. 17: Simulated converter response to a reference step input of 8A. The transition period from 2A to 10A is given by the load time constant.

The converter responds to a change in reference current in approximately 30us. This delay is mainly attributed to the load time constant. For the converter operating at 72kHz, the response to a reference change occurs in approximately 2 cycles of the operating frequency. The MOSFET switch current and drain-source voltage reaches a peak value of 311V and conducts close to 9A at full load. It is therefore evident that a switch voltage rating of greater than 350V and a current rating of greater than 10A is required. The buck converter employed two 500V/20A MOSFET's. The excess capacity was required to compensate for switching losses, which formed the greater part of the loss at this operating frequency. The optimum PI controller parameters were found experimentally and were chosen to provide optimum current tracking with minimal error, fast response and minimal overshoot. The loop time constants τ_1 and τ_2 were both selected to be 2.2 msec.

3.8.2 DC-AC inverter

The parallel resonant load filters the square wave DC output voltage supplied by the buck regulator and only the fundamental frequency component is applied to the resonant load. This results in the inverter switches experiencing a peak voltage in excess of 500V. From figure 3.18 it can be seen that the highest switch voltage is experienced under coil no-load conditions. This is attributed to the increase in load circuit impedance due the increase in circuit Q under no-load conditions. The peak switch voltage is approximately 570V. This application would require power MOSFET's with blocking voltage ratings in excess of 600V. Due to the local unavailability of power MOSFET's with blocking voltage ratings greater than 500V at the current rating required, these 500V power MOSFET's were utilized for this application. This was achieved by limiting the maximum DC-DC converter duty cycle, which limits the peak inverter switch voltage under no-load conditions. Power MOSFET's with RMS current ratings of greater than 7A were required for this application. The inverter comprised four 500V, 20A IRFP460 enhancement-mode power MOSFET's and four 600V, 25A fast recovery rectifier diodes (HFA25TB60).

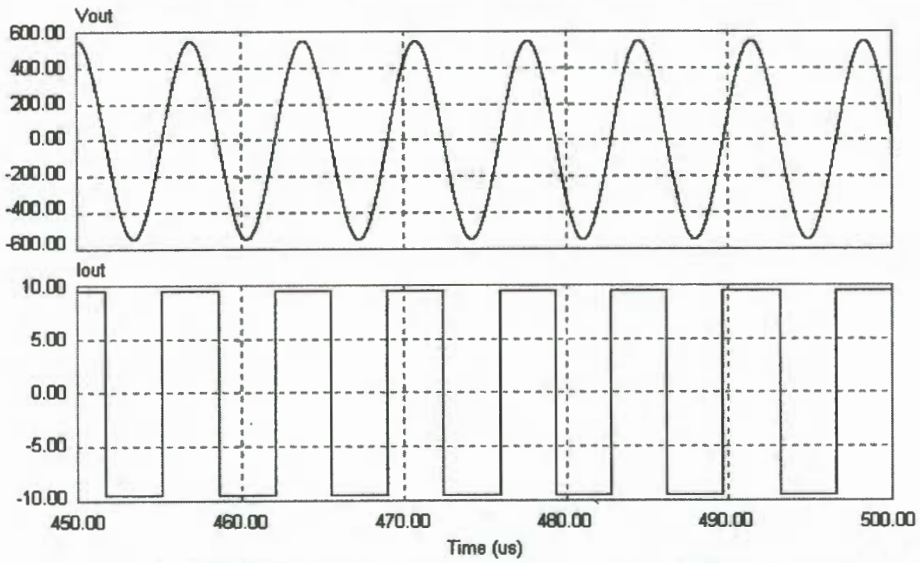

Figure 3. 18: Simulation results showing inverter output voltage and current under no-load conditions. The no-load impedance is larger due to the high circuit Q. The peak voltage across the switches is close to 500V. The inverter output current is $10A_{RMS}$ at 144kHz.

CHAPTER 4

SYSTEM IMPLEMENTATION

A 2kW 140kHz solid-state induction heater was constructed. The system consisted of a MOSFET based current-fed parallel load resonant topology. The system was operated from direct connection to the 230V single-phase supply. A DC-DC converter was employed in order to achieve power control from 0 to 100%. The next section details the implementation of the actual working prototype.

4.1 INDUCTION HEATING LOAD

Figure 4.1: Induction-heating load showing a stainless-steel work-piece, 6-turn water-cooled coil, which is connected to the inverter and capacitor bank

The induction-heating load circuit is shown in figure 4.1. The 6-turn water-cooled induction-heating coil was constructed from 3/16 inch annealed round copper tubing. A high temperature silicone based insulation covers the coil and helps to reduce the coil absorption of heat radiated from the work-piece. The stainless steel work-piece is situated inside the coil where optimum-coupling efficiency occurs. The resonant capacitor bank was constructed using eight 150nF polypropylene capacitors. This forced air-cooled capacitor bank formed a low inductance connection in parallel with the coil. The path length between the capacitor bank and the coil carries the high oscillating current needed for efficient heating. This path should always be kept as short as possible as it ensures that maximum power is coupled to the coil.

4.2 DC-AC AND DC-DC CONVERTERS

Figure 4.2: Compact layout of the DC-DC and DC-AC inverter ensures optimum performance.

A compact DC-AC and DC-DC converter construction is shown in figure 4.2. The DC-DC converter comprised two IRFP460 power MOSFETS connected in parallel, a HFA25TB60 fast recovery rectifier diode, and the charge pump driver as shown on the right half of figure 4.2. Locating the input filter capacitance physically close to the active switching element in the DC-DC converter, provides a low impedance path to the high frequency pulsed currents drawn from the DC bus. This feature combined with an optimum value of gate drive resistance has the advantage of providing fast, clean switching waveforms across the MOSFET's drain to source junction, resulting in no voltage overshoot and therefore eliminating the need for any snubber circuitry.

The MOSFET driven Current-Fed inverter employing four IRFP460's and four HFA25TB60 fast recovery rectifiers as the blocking diodes (shown in the left half of figure 4.2). Operation at load resonance facilitates zero voltage switching, eliminating the need for any snubber circuit components in the inverting stage. The inverter output current is measured by a ferrite torroidal current transformer, which is terminated into a 100Ω burden resistor. It is crucial in this inverter configuration that the lead length between the inverter output and the tank circuit be minimised. Any stray inductance in this path acts as a reactance in series with the tank circuit and will produce excessive transient voltages across the inverter switches when the square-wave output current is switched from one half cycle to another [23]. A detailed

schematic layout of the inverter and the DC-DC converter is provided in APPENDIX 2 B.

4.3 INVERTER GATE DRIVE

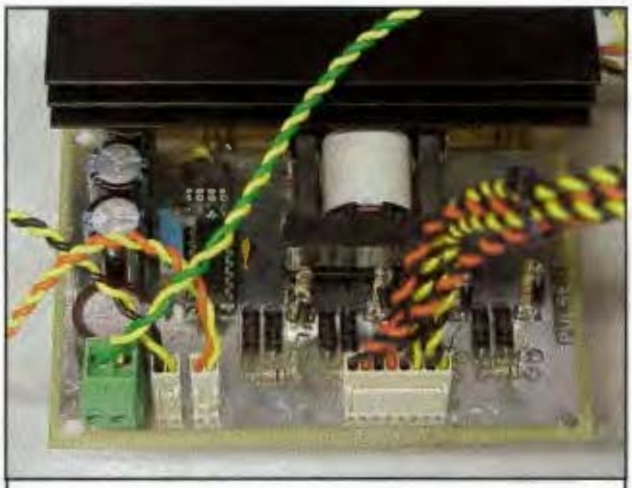

Figure 4.3: Pulse transformer based inverter gate drive circuitry.

Inverter bridge topologies require switching control signals to be delivered to two semiconductor gates referenced to ground, and independent high-side switches with reference points floating anywhere between ground and 450V. To satisfy this requirement a ferrite pulse-transformer with two primaries and four separate secondary windings was used. The turn's ratio was set to provide a ± 15V control signal at the gate of each MOSFET with reference to its source terminal. Low power complimentary MOSFET pairs were used to switch the primary windings of the pulse transformer.

A switching-aid network on the gate terminal of each MOSFET was used to control the rise and fall times of the switches so as to provide an adequate overlap period between the diagonal legs of the inverter. This process ensures that the DC bus inductor feeding the inverter is never open circuited during the commutation period from one half cycle to another [1]. Satisfying this requirement will eliminate any damaging over-voltage transients from appearing across the power MOSFET's in the inverter stage, thereby ensuring reliable operation. A detailed schematic diagram of the inverter gate-drive circuitry is provided in APPENDIX 2 C

4.4 PLL FREQUENCY CONTROL CIRCUIT

Figure 4.4: Automatic frequency control circuitry of the induction heating system. Generous grounding provided adequate shielding from the high power switching noise produced by the DC-DC converter.

Automatic frequency control was achieved by the implementing the control strategy described in chapter 3. The prototype cascaded phase-locked frequency control circuit is shown in figure 4.4.

A low-side MOSFET gate control signal (which was used to represent the inverter output current) is fed to the PLL control board where it is processed by the 90° phase-shifter inner phase-locked loop. Compensation for propagation delays in the MOSFET and drive circuitry is provided by a passive phase delay circuit on the inverter gate drive circuit. The inverter output voltage is also fed into the PLL control board where it is stepped down to a logic level through a ferrite transformer and processed by the main phase-locked loop in the control circuit. The frequency control circuit produces two complimentary clock signals at the current resonant frequency of the load circuit, which are fed to the inverter gate-drive circuitry.

Anti-lock detection circuitry was included which detects whether the loop has lost lock. In this event the control circuit will signal the DC-DC converter to trip the DC bus to the inverter, thereby protecting the inverter from destruction. The loop is brought back into lock by resetting both loop integrators. A detailed schematic layout of the cascaded phase-locked frequency control circuit is provided in APPENDIX 2 D.

4.5 POWER CONTROL CIRCUIT

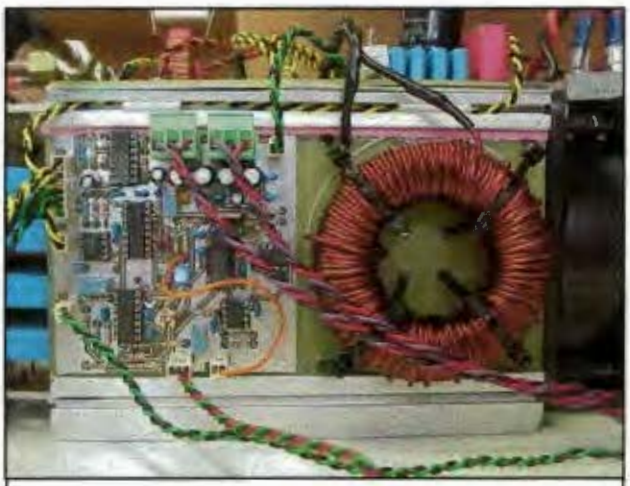

Figure 4.5: Power control circuitry for the DC-DC converter. The DC bus inductor situated on the output of the DC-DC converter is shown on the right.

Power control was realised by employing an analog PWM controller (TL494) which was configured to operate in constant-current mode. The circuit operates by controlling the DC-DC converter output current (measured by a sense resistor in the ground return path) around a user-defined set point of 0-10A. The DC-DC converter operates at 70kHz in continuous conduction-mode with a duty cycle varying between 0 and 75%. The 75% limit ensures that the peak inverter voltage never exceeds 450V thereby preventing over voltages across the power MOSFET's under no-load conditions.

Large amounts of switching noise generated by the DC-DC converter during operation was superimposed onto the current feedback signal and supply to the control circuit. This introduced instability in the form of oscillations into the constant current controller. The problem was solved by introducing a separate logic supply for the control circuitry, providing isolation in the feedback path and introducing noise filtering circuitry at the controller input. Isolation in the feedback path was achieved by employing an isolation amplifier, which was able to convey the DC information to the control circuitry for processing. A detailed schematic diagram of the power control circuitry is provided in APPENDIX 2 E.

4.6 DEVELOPED PROTOTYPE INDUCTION-HEATING SYSTEM

Figure 4.6: Layout of prototype induction furnace developed for this research project, showing the water-cooled induction coil and stainless steel work-piece connected the high frequency power source.

An overview of the prototype high frequency induction-heating system is shown in figure 4.6. The system is supplied with single-phase mains voltage and water for coil cooling. A cooling fan circulates air by blowing it across the heat sink and onto the capacitor bank where it exits at the sides, preventing the air from cooling the work-piece. An analog meter is used to indicate the current supplied to the load, which the user adjusts by means of a panel mount potentiometer. A latching circuit is used to activate or trip the DC bus when necessary. The DC bus status is indicated by means of the red (off) and green (on) LED's. A total of 3 auxiliary power supplies were employed to provide power to the control and drive electronics.

The system was tested at 2kW and the MOSFET case temperatures settled at 45°C after running for approximately 15 minutes. A compact layout in the construction of the high frequency induction heating system was the key element, which ensured the success of this implementation.

4.8 SYSTEM TESTING

Figure 4.7: Heating of a stainless steel work-piece 55 seconds after 1.9kW of power was applied.

The stainless-steel work-piece was heated using the induction-heating power source at approximately 150kHz. The power supplied to the induction heating load circuit was 1.9kW. Figure 4.7 shows the stainless-steel work-piece a period of approximately 55 seconds after the power was applied. The intensity of the heat inside the coil indicates the areas of eddy current concentration. Some of the benefits of induction heating are that not only is heat generated within the work-piece itself, but also that the heat is concentrated to a defined region within the heated work-piece. Speed, heat intensity focus and control are some of the features, which make induction heating favorable for most commercial heating applications.

CHAPTER 5

EXPERIMENTAL RESULTS

The following experimental results were used to verify and assess the performance of the high frequency induction-heating system developed for this research project. The inverter output voltage was measured using a 1:1 turns ratio ferrite transformer connected across the inverter midpoints. The inverter output current was measured using a ferrite torroidal current transformer situated at the inverter output with an output signal scale of 1V per ampere.

5.1 MEASUREMENT OF LOAD CIRCUIT PARAMETERS

In order to verify the design calculations performed in chapter 3, a method for measuring the load circuit parameters was developed. This involved driving the load circuit at low power and measuring the tank voltage, frequency and resonant capacitance. From these three measurements, the equivalent tank circuit inductance L_{total} and resistance R_{total} for both no-load and loaded (stainless-steel work-piece) conditions were found respectively.

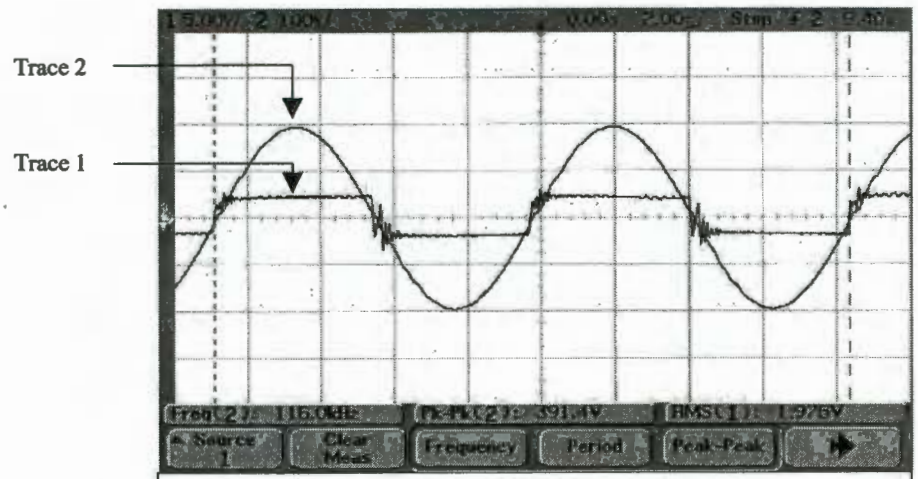

Figure 5.1: Captured trace of load circuit driven at low power (2Arms) with an unloaded coil. The inverter output current (trace 1) and voltage (trace 2) being applied to the load circuit are measured in order to determine the necessary load circuit parameters.

With a constant current of 2A RMS fed to the tank circuit, the unloaded coil is driven under closed-loop frequency control at its resonant frequency of 116kHz. The peak voltage across the tank circuit for the unloaded condition was measured to be approximately 196V peak. The tank capacitance was constructed using six 150nF polypropylene capacitors. The capacitance of this bank was measured to be 900 nF.

The same test was then conducted for the induction-heating coil loaded with a stainless-steel work-piece as shown in figure 5.2.

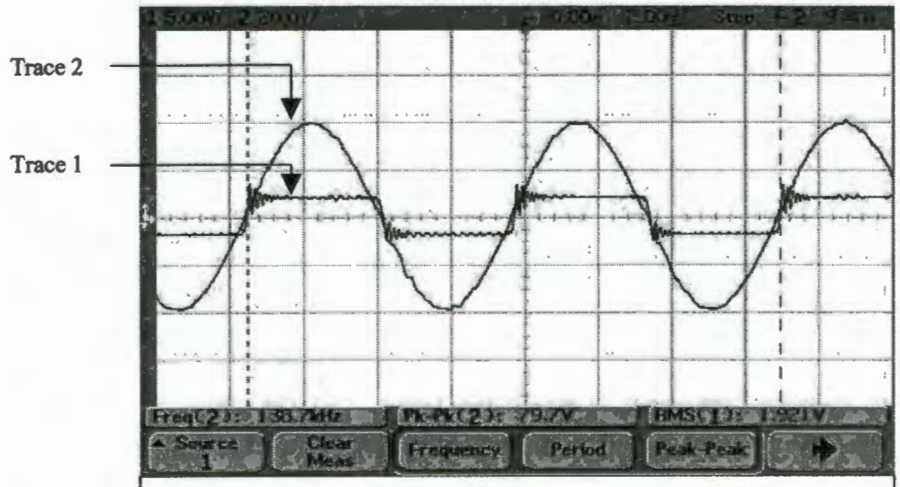

Figure 5.2: Load circuit energised at 2A RMS with a stainless-steel work-piece placed inside the induction heating coil, showing the inverter output current (trace 1) and voltage (trace 2) applied.

With a constant current of 2A RMS fed to the tank circuit, the loaded induction-heating coil was driven under closed-loop frequency control at its new resonant frequency of 138.7kHz. The peak voltage across the tank circuit for the loaded condition was measured to be approximately 39.85V peak. The drop in tank circuit voltage, as a result of the work-piece, is an indication that the coil to work-piece coupling efficiency is good. This is due to the reduction in tank circuit Q due to the presence of the work-piece, resulting in decrease in the tank circuit impedance. The tank capacitance was unchanged at 900nF. The procedure for extracting the load circuit components is provided in APPENDIX 1 D. The equivalent load circuit parameters determined for both the unloaded and stainless-steel loaded coil tests are shown in table 5.1.

No Load			**Stainless Steel**	
I_{DC}	2A		I_{DC}	2A
$V_{tank(peak)}$	196V		$V_{tank(peak)}$	39.85V
ω_o	728.85k rad/s		ω_o	871.48k rad/s
C_{total}	900nF		C_{total}	900nF
L_{total}	2.1uH		L_{total}	1.5uH
Z_p	77.78Ω		Z_p	16.29Ω
Q_{load}	55.02		Q_{load}	12.78
R_{total}	29.88mΩ		R_{total}	99.7mΩ

Table 5.1: Measurement results taken from the load circuit for the two conditions stated.

The measurement results in table 5.1 confirm the theory regarding the loading effect discussed in chapter 2. The presence of the work-piece in the coil increases the effective resistance R_{total}. This is also shown by the reduction in circuit Q and resonant impedance Z_p. The effect of work-piece loading on the coil inductance value is evident in the results above, and therefore results in a shift in resonant frequency from 116kHz (at no-load) to 138.7kHz (at stainless steel load). The measured value of no-load coil inductance agrees with the value calculated in APPENDIX 1 B using Wheeler's formula. Wheeler's formula however does not account for the loading effect of the work-piece in the induction-heating coil. This factor tends to yield a smaller inductance value (1.5uH) as compared to the loaded coil value shown in table 5.1 for a non-magnetic work-piece. The measured value of coil resistance is in agreement with the calculated value but not the measured and calculated values for work-piece resistance, which differ by 41mΩ. This can be attributed to inaccuracies due to certain simplifying assumptions made in the Baker model [11]. This difference however could be compensated for elsewhere in the process and still allowed the for target work-piece temperature to be reached with the specified power. The difference in work-piece resistance value, altered the resonant frequency, tank circuit Q, and the resonant impedance Zp as compared to the calculated values. The capacitance value closest to 630nF was 900nF, as the capacitor bank was constructed from

150nF capacitors placed in parallel. This factor altered the resonant frequency from the designed value as shown in the table above. These measurements provide a practical means of determining load circuit parameters and can be conducted on any parallel resonant induction-heating load. This will allow the designer to optimally match the load circuit to the source. From these measurements, the calculated coil to work-piece coupling efficiency at room temperature was 79.2% as shown in APPENDIX 1 B.

5.2 DC-AC INVERTER

A variable frequency MOSFET based current-fed inverter was successfully implemented for this research. Details of the inverter operation and performance characteristics are provided in the following section.

5.2.1 Operating waveforms at no-load

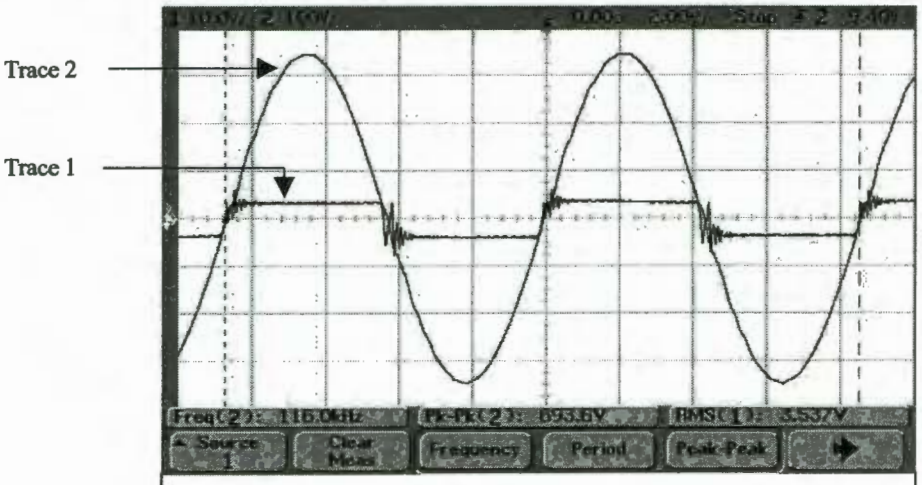

Figure 5.3: Inverter output voltage (trace 1) and output current (trace 2) under no-load conditions.

The inverter output voltage and current waveforms are shown in figure 5.3. The high tank circuit impedance (78Ω) yields a large tank voltage at no-load. The maximum tank circuit voltage under no-load is limited to 350Vpeak by setting the DC-DC converter duty cycle to a maximum of 75%. When the duty-cycle limit is reached it over-rides the current control, thereby maintaining a constant voltage across the tank circuit. This is done in order to limit the maximum voltage across the power MOSFET's in the inverter stage (which are rated at 500V). A compact circuit layout, minimizing parasitic elements, proved to be the key element in ensuring a clean

inverter output voltage free from over voltage transients. The critical layout path is between the inverter and the tank circuit capacitor. If this connecting path is not as short as possible, over voltage transients appear across the MOSFET's at the turn-off commutation period every half-cycle. Effective high frequency construction techniques therefore eliminated the need for any snubber components in the inverter stage. A block diagram of the test circuit is provided in APPENDIX 2 A.

5.2.2 Inverter gate drive waveforms

The gate control signals fed to the MOSFET's in the inverter stage are shown in figure 5.4. The switching rise and fall times of these control signals were adjusted (by delay networks on the MOSFET gate terminals) in order to provide an overlap period between commutations occurring every half-cycle of the inverter output. This commutation period is kept to a minimum to ensure maximum power delivery to the load. The delay network also performs a damping function which limits the over voltage ringing present on the MOSFET gate due to the pulse transformer leakage inductance. 1W-clamping zener diodes were also employed on the gate of each MOSFET for this purpose. A full schematic diagram of the gate-drive circuit is provided in APPENDIX 2 C.

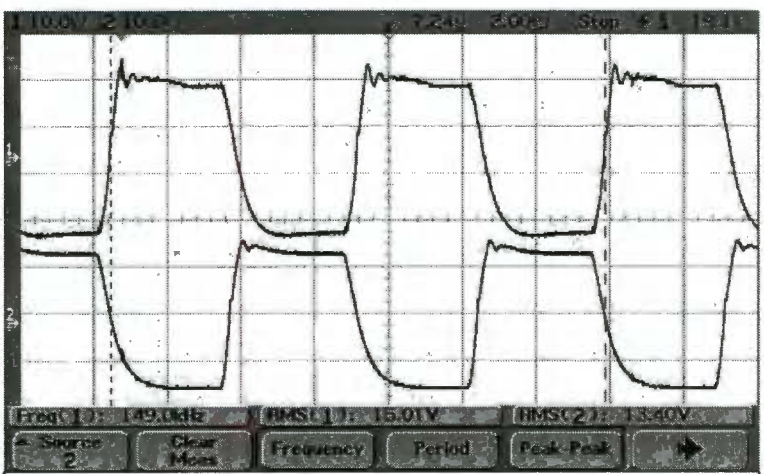

Figure 5. 4: Inverter gate-drive control signals fed from the high frequency pulse transformer circuitry.

5.2.3 Operating waveforms at full-load

The inverter was used to drive the tank circuit constructed, which contained the stainless steel work-piece mentioned in section 5.1. The inverter output voltage and current operating waveforms are shown in figure 5.5.

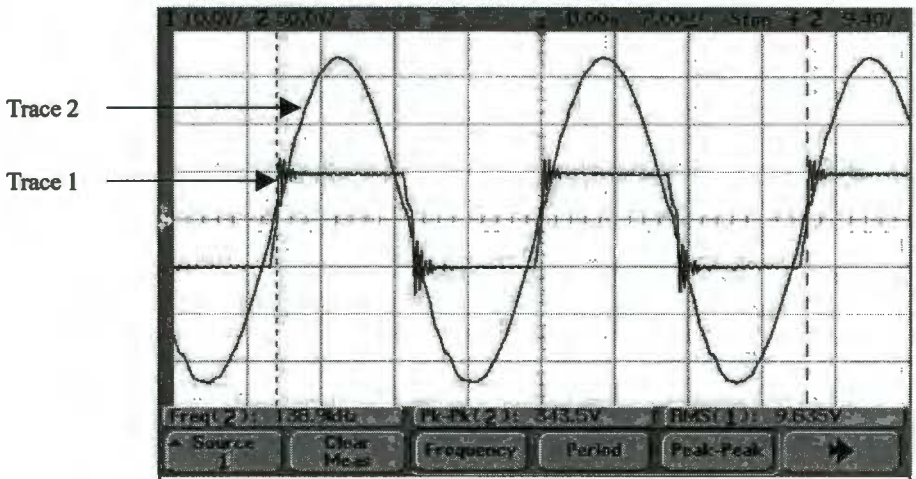

Figure 5. 4 The load circuit consists of a 9-turn, 1/8 inch, water-cooled copper coil and a stainless-steel work-piece. The work-piece is being heated to 1200°C by the power source. The figure shows the inverter output voltage (trace 2) and current (trace 1) at full power operating at approximately 139kHz.

The inverter output power was measured using a Fluke 99 high frequency scope meter and power analyser as shown in figure 5.6. This instrument has an operating bandwidth of 200MHz and a sampling rate of 2Gsamples/sec. The power delivered to the load at 138.9kHz was measured to be 1.18kW.

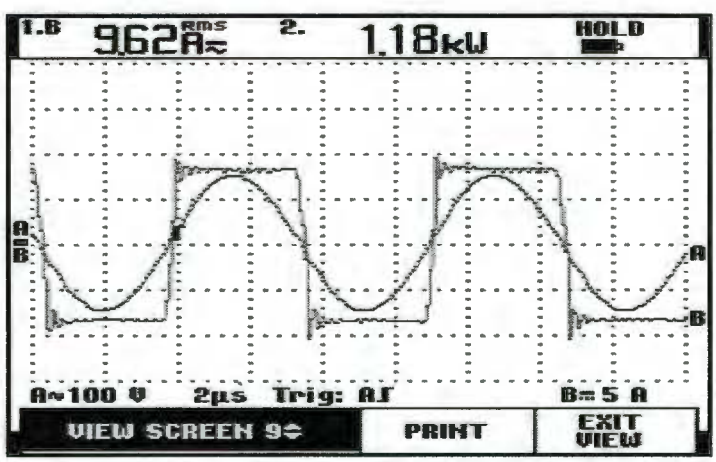

Figure 5.5: Inverter output power measured at 138.9kHz using a 200MHz, Fluke 99 scope meter and power analyser, showing the high frequency output voltage (trace A) and output current (trace B) being applied to the parallel resonant tank circuit.

5.2.4 MOSFET drain-source and gate-source voltage

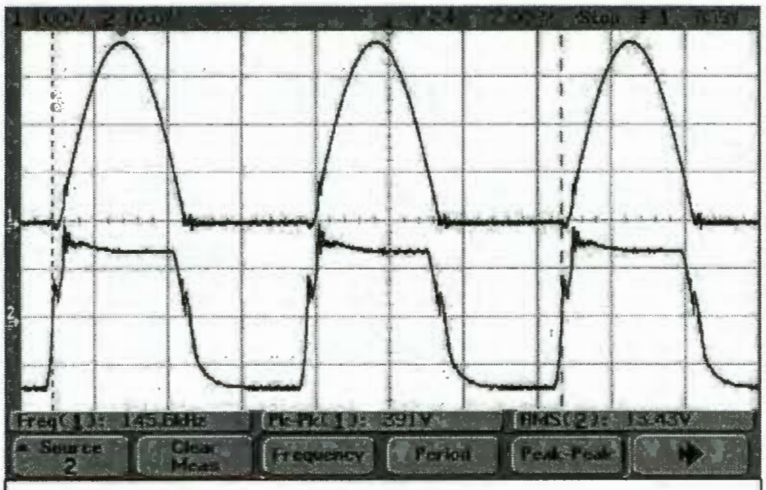

Figure 5.6: Power MOSFET gate control (Trace 2) and drain-source voltage (Trace 1) switching waveforms, showing operation free from over voltage transients without the use of any snubber circuitry.

The inverter power MOSFET switching waveforms at 145.6kHz are shown in figure 5.7. Trace 1 reveals the maximum voltage level of 391V being switched across the 500V power MOSFET. The zero-voltage switching (commutation) points on the MOSFET drain-source voltage can be seen in trace 1. The inverter always operates in this mode thereby optimizing performance and maximising efficiency and power throughput capability.

5.3 FREQUENCY CONTROL SYSTEM

The automatic frequency control system implemented for this research was tested over an operating frequency range varying from 108kHz to 175kHz. This was accomplished by employing different tank circuit parameters (coils, capacitors and work-pieces).

5.3.1 90° Phase-shifters

The inverter output voltage is transformed to a logic level and processed by main loop 1 which is phase locked at 90° to a MOSFET gate control signal which was used as a representative of the inverter output current. Both loops track the frequency of its input and maintain the 90° phase shift over the entire operating range (100kHz-200kHz). Figure 5.8 shows the loop 1 input and 90° phase shifted gate control signal on trace 1 and trace 2 respectively.

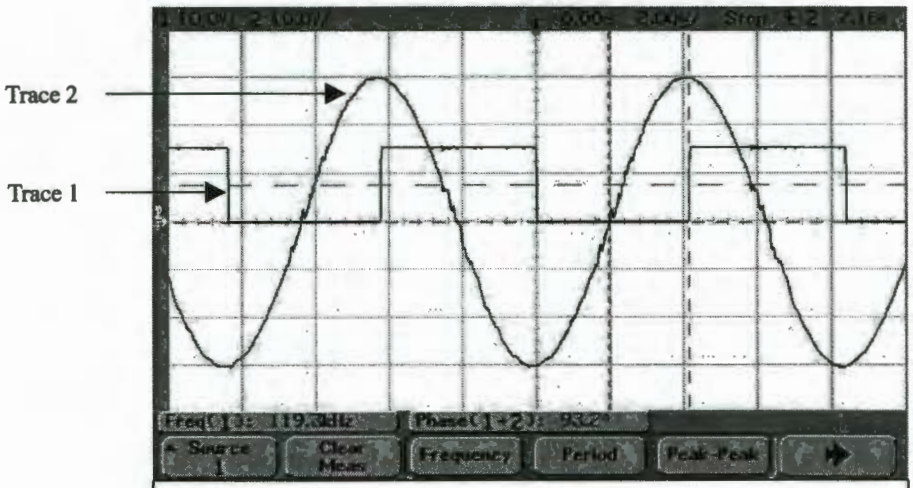

Figure 5.7: 90° phase-shifter phase-locked loop used to achieve phase locking in the automatic frequency control system, showing the inverter output voltage phase-locked to a 90° phase-shifted representation of the inverter gate control signal (which also represents the inverter output current).

Loop2, the ideal 90° phase-shifter phase-locked loop, reads in the MOSFET gate control signal and generates a 90° phase-shifted representative of its input at the resonant frequency of the tank circuit. Figure 5.9 shows the operation of the loop 2 90° phase-shifting phase-locked loop control circuit.

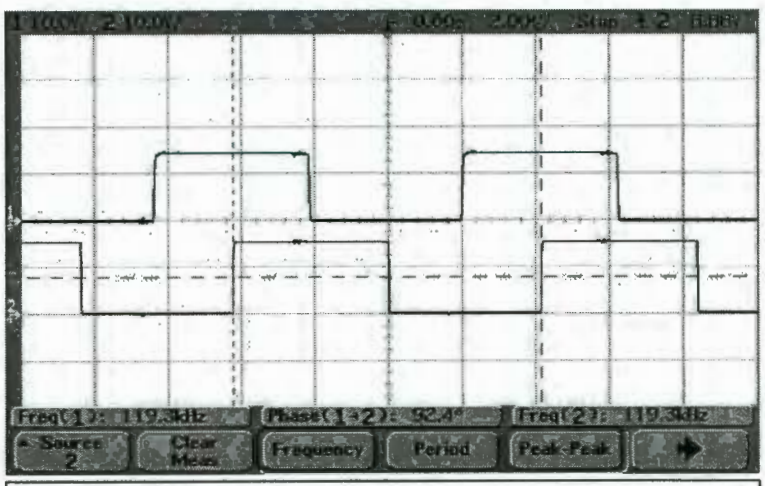

Figure 5.8: Loop2 phase-locked at 90° creating the necessary phase-shift required by loop1 to ensure operation at load resonance.

5.3.2 Operation at resonance

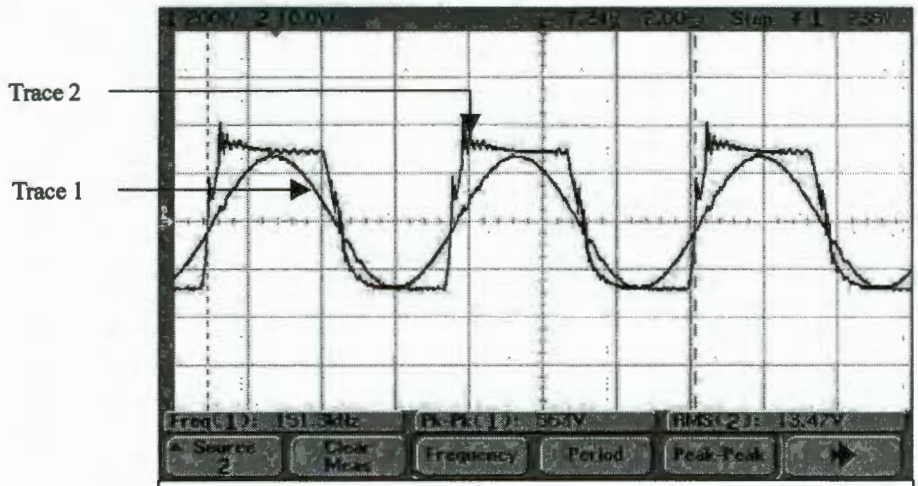

Figure 5.9: Operation at load resonance achieved by phase locking the gate control signal (trace 2) to the inverter output voltage (trace 1) across the tank circuit.

Operation at resonance is achieved by phase-locking a MOSFET gate control signal to the inverter output voltage as shown in figure 5.10. A phase delay is added to the gate control signal in order to compensate for the propagation delays in the MOSFET and driver circuitry. This delay is adjusted to provide a near zero phase delay between the actual inverter output voltage and current as shown in figures 5.6 and 5.7 above. The phase delayed gate control signal and the inverter output voltage are fed to the automatic frequency control circuit where the necessary processing (as explained above) is performed in order to achieve phase-lock at resonance. The frequency control system maintained operation at resonance over the tested frequency range of 100kHz to 170kHz as mentioned above.

A detailed schematic diagram of the actual frequency control system implemented for this research in provided in APPENDIX 2 D.

5.4 DC-DC CONVERTER

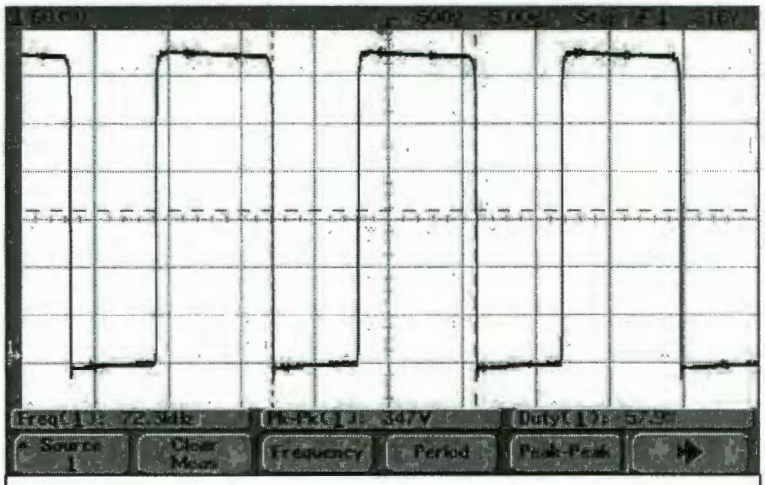

Figure 5. 10: Power MOSFET drain-source voltage of the DC-DC converter operating at a constant frequency of 72kHz.

The DC-DC converter was configured as a constant current source to provide a variable DC current of 0-10A to the inverter stage, which controls the power, delivered to the induction heating load circuit. The amount of voltage overshoot present in a system is a function of many variables such as the switch output capacitance, parasitic inductance and capacitance due to layout, current magnitude, and the device switching speed. Some of these parameters are difficult to estimate and can only be addressed once the converter has been constructed. The active switching elements in the converter employed two IRFP460 power MOSFET's connected in parallel. A compact layout was the first mechanism employed in this converter construction in order to prevent over voltage transients from appearing across the MOSFET's. The MOSFET dv/dt (slew rate) was controlled by selecting a suitable value gate resistor. The optimum gate resistor value, which provided fast switching transitions with minimal overshoot across the MOSFET drain-source was determined through a process of iterative tests. The implementation of these techniques therefore eliminated the need for any snubber circuit components in the DC-DC converter stage of the induction heating power supply.

The current feedback control signal was achieved by means of a 0.1Ω, 25W sense resistor situated in the ground return path of the DC-DC converter. Switching noise generated in the ground return path by the two power electronic converters was a

major problem in the design of this system. Switching currents generated noise spikes due to the charging and discharging of capacitances in the converter switches and passive components. This resulted in instability of the pulse-width modulator in the power controller circuitry, because the current feedback signal was buried in switching noise. Various attempts at solving this instability problem employing special filtering were all unsuccessful. The solution to this problem was realised by completely isolating the power control circuitry from the DC-DC converter. Isolation was achieved by employing an isolation amplifier between the sense resistor DC voltage feedback and the power control circuitry. The feedback input to the power control circuitry employed noise filtering, which eliminated the instability and resulted in the successful implementation of constant-current control.

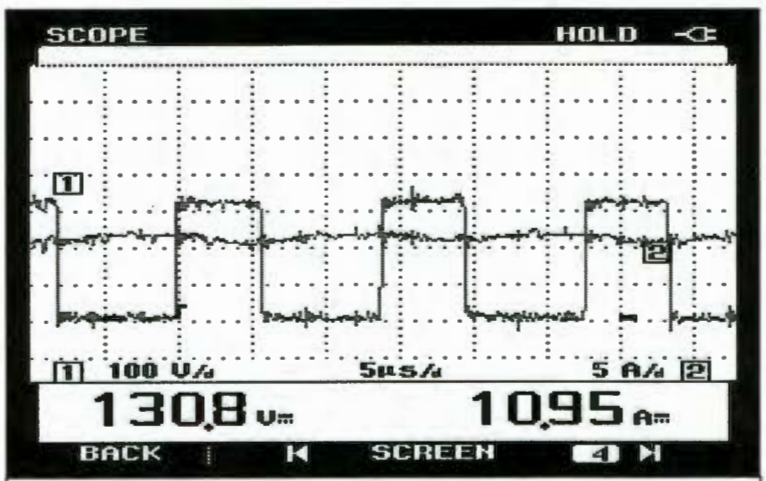

Figure 5.11: DC-DC converter operating at 1.43kW showing the inductor current (trace 2) and converter output voltage (trace 1) at an operating frequency of 72kHz.

Figure 5.12 shows the DC-DC converter operated at 1.43kW. As the load circuit impedance varies for different induction coils and work-pieces, so does the converter duty cycle in order to deliver the required current. The DC-DC converter output inductance (1mH) was sufficiently sized in order to minimise the output current ripple as shown in figure 5.12. The measured current ripple at 10A dc supplied to the inverter was 900mA.

Detailed schematic diagrams of the power control and DC-DC buck regulator circuits are provided in APPENDIX 2 B and APPENDIX 2 E.

5.5 PERFORMANCE TESTING

In order to validate the success of the system implemented, a series of performance tests were conducted on the induction heating power supply. The measurement results of these performance tests are then used evaluate the merits and shortcomings of the prototype system implemented for this research.

The load circuit discussed in section 5.1 using the 26mm diameter stainless-steel billet was used in a series of heating experiments. These experiments were conducted in order to verify the calculations performed in chapter 3. The experimental setup used to acquire the following measurements is shown in figure 5.13 below.

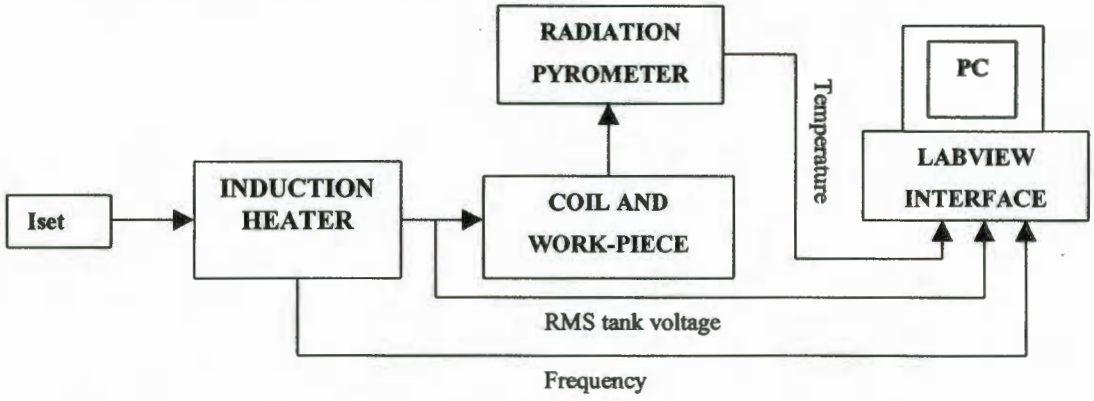

Figure 5. 12: Experimental setup used to obtain measurement results for this research. The user sets the reference current to the system at Iset and the RMS output voltage, frequency and temperature are recorded by the PC at 5 samples per second and written to a spreadsheet for post-processing.

The user determines the output current by adjusting the reference set-point (Iset) to the induction heating system. An Exergen infrared radiation pyrometer is used to measure the work-piece temperature. The pyrometer is emissivity compensated and its readings were verified by means of a type K thermocouple. The inverter output voltage and frequency are first sent to an intermediate processing circuit (not shown) where the necessary isolation and signal conditioning are performed. Load resonant frequency, RMS output voltage and work-piece temperature data are all recorded by the PC via a Labview interface data acquisition card. The data was written to a Microsoft Excel spreadsheet using a Labview user interface program, where it is stored for post-processing.

5.5.1 Heating cycle of stainless steel

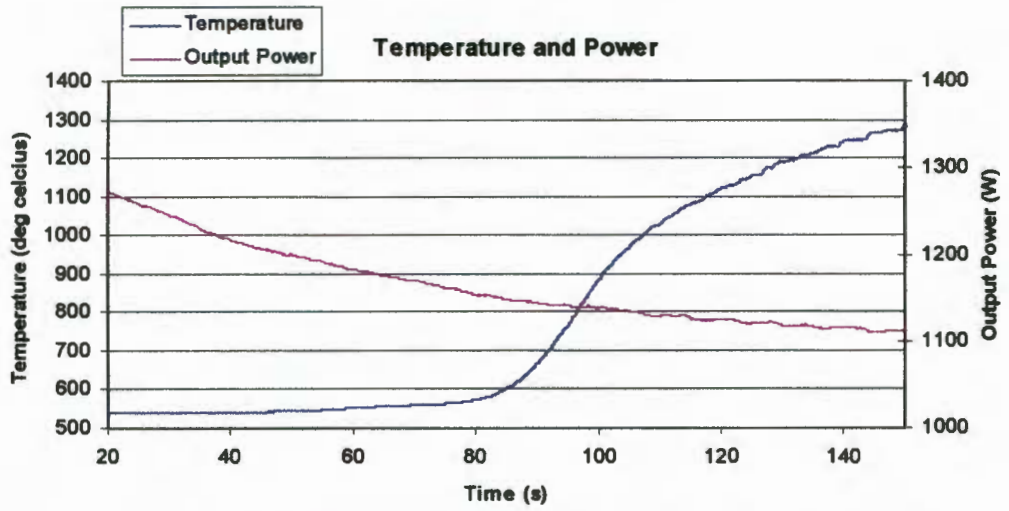

Figure 5.14: Heating cycle of the 26mm stainless steel work-piece. The power applied to the tank circuit varies due to the reduction of tank circuit impedance as the temperature increases.

Figure 5.14 shows the heating cycle of the 26mm stainless steel work-piece, induction-heated using the tank circuit configuration described in section 5.1. The radiation pyrometer has a limited measuring range, which for this experiment was between 500°C and 1400°C. With 1.35kW applied to the tank circuit at 138kHz (and a constant current of 10A) it is noted that as the work-piece temperature increases, the power to the tank circuit decreases. This effect is due to the increase in work-piece resistance with temperature, facilitating a reduction in tank circuit Q, which results in a decrease in tank circuit impedance. The reduction in power drawn does not significantly affect the heating rate since the coil to work-piece coupling efficiency has now also improved with temperature.

The target temperature of 1200°C was achieved in approximately 130 seconds compared to the calculated estimate of 145 seconds. The estimated time was longer than the actual time needed due to inaccuracies in the power calculations. The calculated value of 1.3kW needed was to maintain a work-piece temperature of 1200°C with the work-piece radiated power loss of 400W. This condition however does not apply at the temperatures leading up to 1200°C, which implies that less power is needed to heat the work-piece up to 1200°C, since the radiated power loss will be less. This inaccurate assumption however only constitutes a 10% difference

for this case, which still gives a reasonable approximation of the factors involved in this exercise.

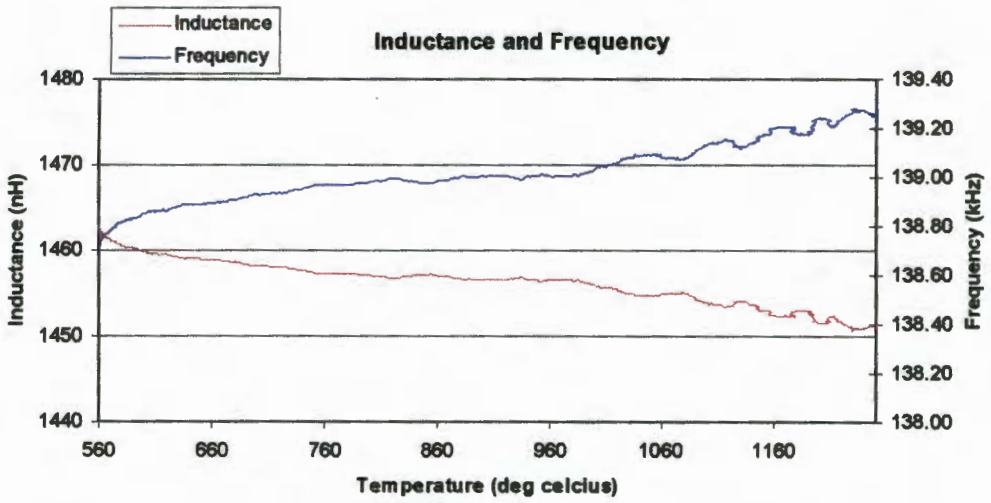

Figure 5. 15: Inductance and frequency versus temperature for the stainless-steel work-piece. It is noted that closed-loop frequency control makes it possible to measure the change in load circuit inductance during operation of a heating cycle. The trend lines of frequency and inductance are mirror images of each other showing the changes occurring in the tank circuit during heating. An increase in induced eddy-currents with temperature, results in the decrease in load circuit inductance

Figure 5.15 illustrates the load circuit inductance and resonant frequency for a heating cycle of the stainless steel work-piece. It is interesting to note here that the increase in tank circuit resonant frequency results from a corresponding decrease in load circuit inductance. This effect is caused by the increase in work-piece resistivity, which results in an increase in work-piece penetration depth (δ_{work}). This increase in work-piece penetration depth results in a stronger reaction flux caused by the induced eddy currents in the work-piece, which effectively decreases the load circuit inductance, hence giving the increase in tank circuit resonant frequency.

Operating this load circuit in open loop frequency control by setting the inverter driving frequency to 138.kHz at room temperature would result in the following:

- At 1200°C the new resonant frequency would be 139.3kHz resulting in a load phase angle of –28.2° as compared to closed loop operation at near 0°.
- This 600Hz deviation in the driving frequency under open-loop frequency control would result in 8.4% reduction in power delivered to the load.
- Operation at –28.2° load phase angle would also result in a loss of zero voltage switching in the inverter, thereby reducing its efficiency.

The effects described above will worsen for poorly coupled loads due the increase in load circuit quality factor, which reduces the circuit operating bandwidth. Open-loop frequency control for high Q load circuits would result in operation around the load circuit's 3dB operating point in response to deviations in operating frequency during a heating cycle. This would result in a loss of heating efficiency due to the rapid decrease in load circuit impedance when operating off resonance. A typical application of a high Q load circuit is found in melting precious metal such as platinum. The eddy currents need to be induced directly into the metal because no graphite susceptor (crucible lining) can be employed. Furthermore, the work-piece usually consists of platinum buttons or filings, which represent a poorly coupled load at room temperature. Typical load circuit Q's for this application range from 15 to 50 depending on the quantity of platinum required for melting.

Increasing the inverter output power supplied to the load and over designing semiconductors to handle the load mismatch usually compensates for this effect. The implementation of automatic frequency control therefore reduces the power required for a specific application by always tracking the optimum load operating point and also reduces the semiconductor power ratings by always ensuring zero-voltage switching during operation. These factors also tend to increase the power density of induction-heating generators due to a reduction in size and weight.

5.5.2 Dynamic frequency tracking capability

An experiment involving the heating of a mild-steel billet was performed in order to asses the system's ability to track dynamic changes in load resonant frequency. This is due to the material being ferromagnetic from room temperature up to a certain point, called the Curie temperature, where the material loses its magnetic properties. It occurs as a result of a rapid decrease in relative permeability around the Curie temperature. Many steel heating applications often require the metal to be heated past this Curie-transition temperature. This poses a special problem as mentioned in Chapter 2, in that the Curie-transition causes a substantial increase in skin depth, resulting in a reduction in heating power density.

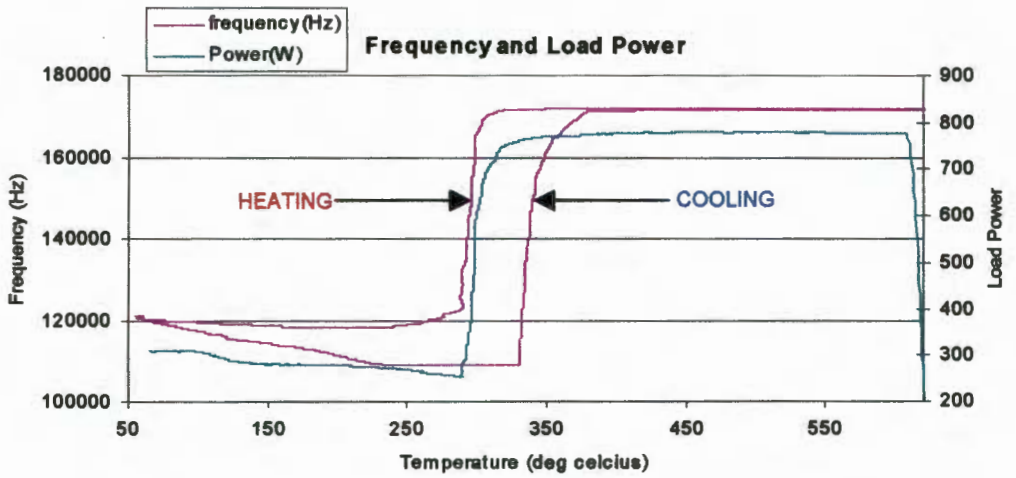

Figure 5. 16: Heating cycle of mild-steel billet showing the Curie transition which results in a rapid change in load characteristics.

A mild-steel work-piece with the same dimensions as the stainless steel (26mm x 35mm) was used for the experiment conducted in figure 5.16. With 10A RMS fed to the load the power at room temperature was approximately 270W. This was due to the low circuit Q of 2.92, which resulted in a tank circuit impedance of 4.75Ω at room temperature. At the beginning of the heating cycle (below Curie) the resonant frequency of the tank circuit starts at 121kHz decreasing slightly due to the increase in load inductance caused by the increase in work-piece resistance. This variation is caused by opposing magnetic fields created by the current induced in the work-piece causing a larger portion of the heating coil current to flow in the magnetising

inductance. This is opposite to the effect of load circuit inductance for non-magnetic materials, and above Curie temperature because of the relative permeability in magnetic materials, which tend to oppose the change in work-piece resistivity, maintaining a constant skin depth up to the Curie transition temperature. At this point the work-piece relative permeabilty reduces to 1, giving a substantial decrease in load circuit inductance resulting in a drastic change in load resonant frequency from 125kHz to 171kHz. This 46kHz change in resonant frequency also results in a rapid increase in load power demand from 270W to 770W. The increase in power demand is due to the increase in load circuit Q when the relative permeability falls, resulting in an increase in load circuit impedance from 4.75Ω to 19.7Ω.

This ability of an induction-heating power source to track load resonant frequency changes, now also finds an application in the heating of ferro-magnetic materials. With no frequency control present in the application above, the optimum load operating point would not be maintained, and heating above Curie temperature would require more power from the generator and also resulting in the loss of zero-voltage switching. In certain cases limitations in power source operating frequency would make heating of ferro-magnetic materials above the Curie temperature impossible. After heating the work-piece to 600°C the power was reduced to 20W and as the work-piece cooled and became re-magnetised, the automatic frequency control system tracked the load circuit resonant frequency, which is indicated by the cooling curve in figure 5.16.

The frequency control system tracks these transitions in load resonant frequency by virtue of the phase displacement between the load voltage and current presented to its inputs. The loop therefore operates by altering the driving frequency of the inverter in order to maintain a near zero phase displacement between the load voltage and current as described in chapter 3 resulting in the frequency variations presented in figure 5.16.

5.6 EFFICIENCY MEASUREMENTS

Measurements were performed in order to quantify the system efficiency and factors affecting it. A block diagram showing the system layout of the measurement points is shown in figure 5.17 below.

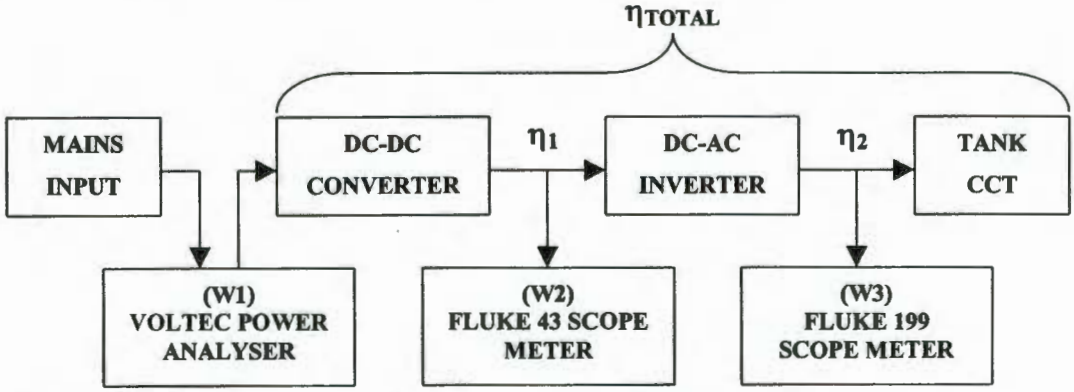

Figure 5.16: Layout of experimental setup used to perform efficiency measurements on the prototype induction furnace.

The system comprises an induction heating power source utilising three instruments configured as wattmeters in order to measure power. Wattmeter 1 (W1) comprised a Voltec single-phase power analyser, which was used to measure the system RMS input power. W2 comprised a Fluke 43 digital oscilloscope meter, which measured the DC-DC RMS output voltage and current. The current was measured using a hall-effect probe able to measure both DC and high frequency AC up to 200kHz. The power reading was obtained by multiplying the RMS voltage and current readings from the Fluke 43 scope meter. W3 comprised a Fluke 199, 200MHz digital oscilloscope meter, which measured the inverter output voltage and current, supplied to the load. The inverter output current was derived from a 100:1 ferrite core current transformer, which was terminated into a 100Ω resistor in order to provide a reading of 1V/A. The scope meter was then configured as a wattmeter and was used to display the inverter output power.

Three sets of power readings were taken over the entire range of input current (0-10A) at 0.5A intervals for each condition presented. The readings were averaged and used to provide the efficiency measurements given below.

5.6.1 System Efficiency vs. Power

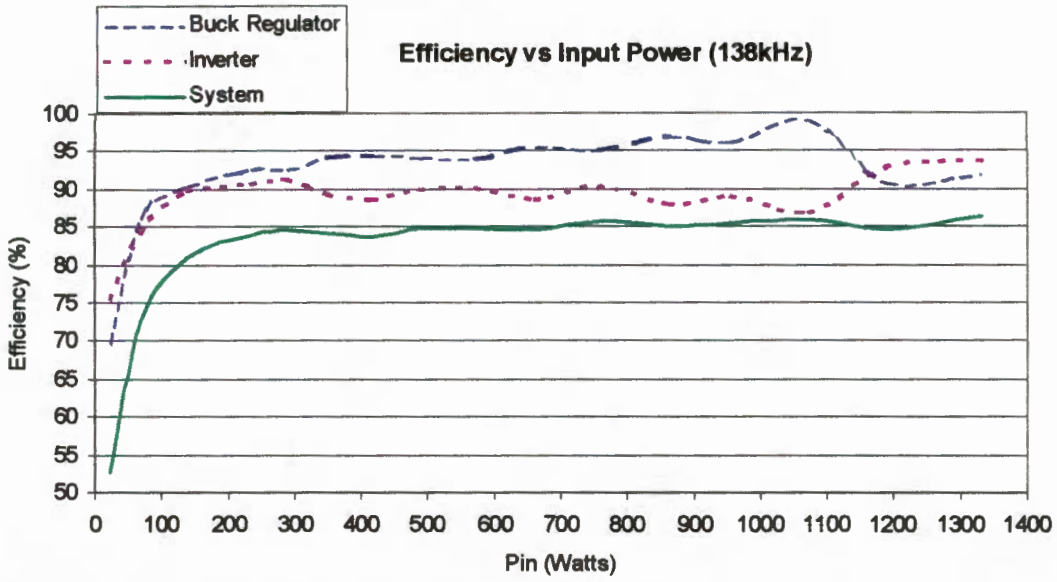

Figure 5. 18: Induction heating power supply efficiency measurements taking for the stainless-steel heating application.

Figure 5.18 illustrates efficiency measurements for the 26mm stainless steel work-piece presented above. Readings were taken at power levels ranging from 30W to 1.35kW at a load resonant frequency of 138kHz. At low power levels, the system efficiency is poor due to the switching losses being the dominant characteristic, making the ratio of power transferred to converter losses is low. As the power is increased this ratio becomes larger since the switching losses remain relatively constant. The conduction losses however do increase, but so does the power delivered to the load, yielding a maximum system efficiency of 86% at 1.3kW.

The inverter efficiency remains relatively constant due to reduction of switching loss facilitated by zero-voltage switching, and also the conduction losses increasing in proportion to the output power with an efficiency of 92% at 1.3kW. The DC-DC converter efficiency improves as the power increases, because of the duty cycle increasing, resulting in a larger power transfer to converter loss ratio achieving an efficiency of 90% at 1.3kW. The DC-DC converter efficiency is higher than the DC-AC inverter because two power MOSFET's were connected in parallel in order to implement the DC-DC converter switch, resulting in lower conduction losses than the in the inverter. Another reason for this result was because the inverter employed eight switching elements compared to the three in the DC-DC converter, which resulted in

ratio of power transferred, to conduction losses for the different loads, which explains why the highest efficiency was achieved at 150kHz.

5.6.3 Maximum Output Power

A maximum inverter output power of 2.3kW was achieved at 151kHz as shown in figure 5.20. The load consisted of a 36mm inner diameter, 6 turn, 3/16 inch, water-cooled induction-heating coil with a tank capacitance of 1.2uF. The loaded coil inductance was measured to be 0.91uH. The power MOSFET's in inverter and DC-DC converters settled at a case temperature of 46°C after running for 5 minutes. This was unfortunately the highest power level at which the inverter could be tested due to thermal limitations of the tank capacitor bank.

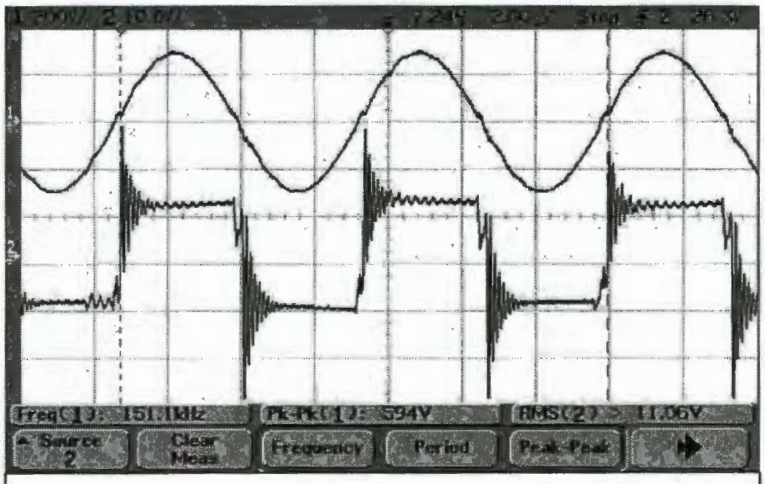

Figure 5. 19: Inverter output voltage and current at maximum tested power. The high frequency ringing on the output current (trace2) is the result of operation at elevated current and operating frequency

Trace 2 in figure 5.20 also reveals the effect of high frequency switching (151.1kHz) at elevated power levels. This can be seen in the increase in amplitude of the ringing currents on the inverter output. The ringing is caused by reverse-recovery effects of the series blocking diodes (HFA25TB60) in the inverter legs at elevated current levels.

CHAPTER 6

CONCLUSIONS AND RECOMMENDATIONS

6.1 CONCLUSIONS

A 2kW solid-state high frequency induction-heating system has been developed, which operates from a single-phase mains frequency supply. The unit has been successfully implemented and tested on different loads (work-pieces) at its rated power.

A global awareness into some of the applications and technology of induction-heating was provided which justified the validity and future applications of the research undertaken in this field of study. A method of determining the power required for a heating application was studied in Chapter 3, and compared to actual measurement results. The induction-heating load circuit has been studied in Chapter 2 and 3, highlighting some of the factors essential for efficient induction-heating load circuit design.

A resonant inverter topology was implemented, which utilised the load resonant nature in order to achieve a higher operating efficiency. An H-bridge current-fed inverter topology (directly driving the parallel resonant load) was implemented as the frequency conversion apparatus. Equations describing the inverter output voltage, current and power when driving the resonant load were developed in order to provide some insight into the operation of this power source topology. Implementation of the inverter gate-drive circuit was described and practical guidelines provided.

The implementation of the frequency control circuit gives the system automatic tracking capability over a frequency range extending from 80kHz to 200kHz whilst maintaining zero-voltage converter switching as well as maximum power transfer to the induction-heating load. Insight into the operation of the frequency control system was provided by a mathematical analysis of the load and frequency control circuits. The frequency control system's steady-state phase error response was also evaluated

using the mathematical model developed, by subjecting the system to two types of phase inputs (step and ramp), which occur in practice.

The high frequency DC-DC converter, implemented as the power control system was studied in the form of simulation analysis in Chapter 3. The induction-heating system implementation is described in detail in Chapter 4, with practical guidelines regarding layout and construction provided.

Experimental results assessing the performance of the induction-heating system implementation was presented in Chapter 5. Converter and control circuit operating waveforms were presented and discussed in order to verify the simulated and calculated relationships. Performance measurements on the induction-heating system were presented in order to assess the system's power output, operating efficiency and frequency tracking capability over its operating range.

The designed target for heating the 26mm stainless-steel billet was achieved with 1.35kW, achieving a target temperature of 1200°C in 130 seconds. The change in work-piece temperature resulted in a change in coil inductance (due to eddy current effects as a result of resistivity change), which caused a corresponding change in tank circuit resonant frequency as shown in Chapter 5. The system's frequency tracking capability was evaluated by heating a steel billet from room temperature, through its Curie point. This resulted in a drastic change in tank circuit resonant frequency, which was continuously tracked by the frequency control system. The system efficiency at 1.3kW and 138kHz was measured to be 86%. The resonant inverter achieved an efficiency of 92% under the operating conditions mentioned. The efficiency measurements however did not include drive and control circuit power losses, which were assumed to be negligible in comparison to the power delivered. Efficiency measurements at 150kHz and 172kHz were also conducted and were presented in Chapter 5. The maximum continuous rated output power tested with the current design was 2.3kW at 151kHz.

6.2 RECOMMENDATIONS FOR FUTURE WORK

From the present research, the following recommendations can be made:

- Finite element modeling of the load circuit can be performed, to more accurately approximate the circuit parameters as well as the loading effect on the inductance.
- Water-cooled RF tank capacitors should be employed in the parallel resonant circuit. These capacitors are designed for high frequencies and will be more stable at higher powers (>1.5kW).
- The induction-heating system can now be applied to other applications. An example would be to apply this technology to the melting of small quantities of precious metals such as gold, silver and platinum. The high frequency is needed to enable the efficient melting of fillings and cuttings, which are difficult to accomplish otherwise.
- Current controlled feedback is accomplished via a sense resistor, which resides in the ground return path of the DC-DC converter. At full power (10A) this constitutes a power loss of 10W, when using a sense resistor of 100mΩ, producing an output voltage of 1V. By using the CT output from the inverter as the current feedback sensor, one could eliminate the sense resistor power loss (especially at higher output powers), provide better noise immunity (higher signal to noise ratio), and also provide electrical isolation between the power and control circuits.
- The current design can also be easily scaled to higher powers (5kVA, 10kVA, etc.) using the same control and drive electronics. Higher rated power semiconductors would be needed as well as operation from a 3-phase supply.
- Application of the present frequency control system to a Voltage Fed Inverter driving a series resonant load, can be achieved by using the gate voltage locking technique explored in this research. For a VSI system, the inverter gate voltage will have to be phase-locked to the inverter output current using the same frequency control circuit.

- The frequency control system presented in this research can also be reconfigured to operation on a swept frequency inverter system. Here the inverter output power is controlled by varying the inverter driving frequency (for a series resonant load). This can be accomplished by offsetting phase operating point, anywhere from 0° - 90° of the frequency control circuit.

- Experimental results in Chapter 5 have shown that the change in load resonant frequency results from a change in induction coil inductance. The inductance however changes as a result of resistivity changes in the work-piece, and resistivity however changes with temperature. For a fixed work-piece (and using these relationships), the temperature of the work-piece can be indirectly predicted, based on the resonant frequency of the load circuit. This technique brings about a sensorless means of temperature measurement and thereby temperature control by means of frequency tracking.

REFERENCES

[1] L. Hobson, and D.W. Tebb, "Transistorized power supplies for induction", *Int. J. Electronics*, vol. 59, No. 5, June 1985, pp. 543-552.

[2] D. L. Loveless, "An Overview of Solid-State Power Supplies for Induction Heating," *Metal Production*, vol. 33, August 1995.

[3] D. L. Loveless, R. L. Cook and V. I. Rudnev, "Considering Nature and Parameters of Power Supplies for Efficient Induction Heat Treating," *Industrial Heating,* June 1995.

[4] M. Kamli, S. Yamamoto, and M. Abe, "A 50-150 kHz Half-Bridge Inverter for Induction Heating Applications," *IEEE Transactions on Industrial Electronics*, vol. 43, No. 1, February 1996, pp. 163-172.

[5] J. M. Ho and F. C. Juang, "A Practical PWM Inverter Control Circuitry for Induction Heating and Studying of the Performance under Load Variations", *Proc. IEEE Conf., International Symposium on Industrial Electronics,* vol. 1, July 1998, pp. 294-299.

[6] I de Vries, "High Power and High Frequency Class-DE Inverters", PhD Thesis, Department of Electrical Engineering, University of Cape Town, August 1999.

[7] I. Khan, J. Tapson and I. de Vries, "Automatic Frequency Control of an Induction Furnace", *Proc. IEEE Conf., Africon '99,* vol. 2, September 1999, pp. 913-916.

[8] I. Khan, J. Tapson and I. de Vries, "Frequency Control of a Current-Fed Inverter for Induction Heating", *Proc. IEEE Conf., ISIE'2000,* vol. 1, December 2000, pp. 343-346.

[9] D. Tebb, L. Hobson and W. Wilkinson, "A Current Fed MOSFET Inverter for Induction Heating Applications," *Proc. 20th Univ. Power Engineering Conf.,* April 1985, pp. 390-392.

[10] E. J. Davies, and P.G. Simpson, *Induction Heating Handbook,* Maidenhead, McGraw-Hill, 1979.

[11] E. J. Davies, *Conduction and Induction Heating,* Peter Peregrinus Ltd., UK, 1990.

[12] **www.ameritherm.com**

[13] C. Lang, "Hot Platinum, Novel platinum alloys and processing technology for jewellery manufacture", Innovation Fund Round 5 Proposal, August 2002.

[14] I Khan, J. Schedel, "Development of a low cost induction cooker", *Proc. Conf. on Domestic Uses of Energy,* vol. 1, Apr 2002, pp. 30-34.

[15] H. W. E. Koertzen, "Variable Load Induction Heating by Medium Frequency Power Electronic Converters", DEng. Thesis, Faculty of Engineering, Rand Afrikaans University, November 1994.

[16] AN9012, "Induction Heating System Topology Review", Power Device Division, Fairchild Semiconductor Corporation, July 2000.

[17] **www.cooktek.com**

[18] "Published Editorials for CIH", Cheltenham Induction Heating, October 2000.

[19] **www.cih-group.co.uk**

[20] **www.lepel.com**

[21] M. Nakaoka, "Electromagnetic Induction-Heated Fluid Energy Conversion Processing Appliance", US Pat. 5990465, November 1999.

[22] **www.transflux.co.nz**

[23] E.J. Dede, V. Esteve, J. Jordan, J. V. Gonzalez and E. Maset, "On the Design and Control Strategy of High Power, High Frequency Converters for Tube Welding Applications", *Proc. Power Conversion Conference,* April 1993, pp. 257-264.

[24] C. A. Tudbury, *Basics of Induction Heating*, vol. 1, New Rochelle, New York, 1960.

[25] V. I. Rudnev, R. L. Cook, D. L. Loveless and M. R. Black, *Induction Heat Treatment*, Marcel Dekker, Inc., New York, 1997.

[26] N. Mohan, T. M. Undeland and W. P. Robins, *Power Electronics: Converters, Applications and Design,* John Wiley & Sons Inc., 1989.

[27] H. Barber, *Electroheat*, London, Granada, 1983.

[28] P.C. Sen, *Principles of Electric Machines and Power Electronics,* John Wiley & Sons Inc., 1997.

[29] M. Thompson, "Inductance Calculation Techniques – Part I: Classical Methods", *Power Control and Intelligent Motion,* vol. 25, no. 12, December 1999, pp. 40-45.

[30] M. Thompson, "Inductance Calculation Techniques – Part II: Approximations and Handbook Methods", *Power Control and Intelligent Motion,* vol. 25, no. 12, December 1999, pp. 46-50.

[31] D. W. Tebb and L. Hobson, "Suppression of Drain-Source Ringing in 100kHz MOSFET Induction Heating Power Supply", *Electronics Letters*, vol. 22, No. 1, January 1986, pp. 7-8.

[32] R. L. Boylestad, *Introductory Circuit Analysis*, Macmillan, 1994.

[33] E.J. Dede, V. Esteve, J. Jordan, J. V. Gonzalez and E. Maset, "On the Design of High Power Current-Fed Inverters for Tube Welding Applications", *Proc. Int. Power Conversion Conf.,* June 1993, pp. 62-69.

[34] H. Akagi, T. Sawae and A. Nabae, "130kHz, 7.5kW Current Source Inverters Using Static Induction Transistors for Induction Heating Applications", *Proc. IEEE PESC.,* 1986, pp. 395-400.

[35] L. Hobson, D.W. Tebb and R. Christopher, "Microprocessor Control of a Transistorized Induction-Heating Power Supply", *Int. J. Electronics,* 1985, vol. 59, no. 6, pp. 735-745.

[36] E. J. Dede, J. V. Gonzalez, J. A. Linares, J. Jordan, D. Ramirez and P. Rueda, "25kW / 50kHz Generator for Induction Heating", *IEEE Trans. on Industrial Electronics,* June 1991, vol. 38, no. 3, pp. 203-209.

[37] S. Bottari, L. Malesani and P. Tenti, "High-Efficiency 200kHz Inverter for Induction Heating Applications", *Proc. IEEE Industry Applications Society Conf.,* 1985, pp. 308-316.

[38] K. Agbossou, J. L. Dion, S. Carignan, M. Abdelkrim and A. Cheriti, "Class D Amplifier for a Power Piezoelectric Load", *IEEE Trans. On Ultrasonics, Ferroelectrics and Frequency Control,* July 2000, vol. 47, no. 4, pp. 1036-1041.

[39] H. K. Sheikh, "Power Supply with Reduced Second Harmonic", US Pat. 6141227, October 2000.

[40] W. E. Frank and C. F. Der, "Solid State RF Generators for Induction Heating Applications", *Proc. IEEE Industry Applications Society Conf,* Oct 1982, pp. 939-944.

[41] T. Ferreira (verbal consultation), LH Power Electronics.

[42] F. M. Gardner, *PhaseLock Techniques,* John Wiley & Sons Inc., USA, 1967.

[43] P. Young, *Electronics Communication Techniques,* Englewood Cliffs, Macmillan, 1994.

[44] A. Veldhuizen, "Investigation into High Power Ultrasound for Industrial Applications", BTech Thesis, School of Electrical Engineering, Cape Technikon, November, 1998.

[45] D. H. Wolaver, *Phase-Locked Loop Circuit Design,* New Jersey, Prentice Hall, 1991.

[46] W. Egan, *Phase-Lock Basics,* John Wiley & Sons Inc., 1998.

[47] M. H. Rashid, *Power Electronics: Circuits, Devices and Applications,* 2nd Ed, Prentice-Hall Inc., 1993.

[48] J. Kassakian, M. F. Schlecht and G. C. Verghese, *Principles of Power Electronics,* Addison Wesley, 1992.

[49] D. W. Tebb and L. Hobson, "Design of Matching Circuitry for 100kHz MOSFET Induction Heating Power Supply", *IEEE Trans. on Industrial Electronics,* May 1987, vol. IE-34, no. 2, pp. 271-276.

[50] E. J. Dede, J. Jordan, V. Esteve, J. M. Espi and A. Ferreres, "Switching Modes and Short-circuit Considerations in Very High Frequency, Very High Power Resonant Inverters for Induction Heating Applications", *Proc. IEEE Power Conversion Conference,* May 1997, pp. 983-985.

[51] I. Khan, "Automatic Frequency Control of an Induction Furnace", MTech. Thesis, School of Electrical Engineering, Cape Technikon, December 2000.

[52] J. Tapson, "A Wide-Area Scanning Tunneling Microscope Configured for Metallurgical Research", PhD Thesis, Faculty of Engineering, University of Cape Town, July 1994.

[53] J. Davies, "Continuous Wave Mode-Locking for the Determination of the Acoustic Non-Linearity Parameter B/A", PhD Thesis, Faculty of Engineering, University of Cape Town, December 2001.

[54] J. Encinas, *Phase Locked Loops,* Chapman & Hall, 1993.

[55] G. Nash, "Phase-Locked Loop Design Fundamentals", *Application Note535, Motorola Inc,* 1994.

APPENDICES

APPENDIX 1 A:

Estimation of power required to through-heat a Stainless Steel Billet

Parameters: Taken from Basics of induction heating [24]:

Material	Stainless steel
Length	1.37in (35mm)
Diameter	1.02in (26mm)
Density	0.284 lb/in^3
Target T°	2192°F (1200°C)
Frequency	140kHz
Heat content	0.09kWh/lb
Thermal conductivity (K)	0.25W/in°F
Induction thermal factor (K_T)	0.0025
Radiation power loss density	0.093kW/in^2

Table A.1: Parameters needed for the calculation of power required to heat the stainless-steel billet test specimen.

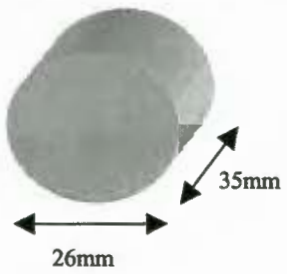

Fig.A.1: Physical dimensions of stainless-steel specimen.

The mass of the stainless steel billet to be heated can be calculated as follows:

$$Billet\,mass = \rho_{density} \times \frac{\pi \times diameter^2}{4} \times length = 0.305lb = 0.138kg$$

The heat content is used in commercial heating calculations to estimate the energy required to heat a material. Heat content takes into account the specific heat capacity of the metal, and is given at the target temperature (in this case, 1200°C).

$$Energy\ required = billet\,mass \times heat\,content = 0.0275kWh$$

Because this is a through heating application, the temperature difference between the surface and the center of the billet is small (200°F in this case). The power into billet is given by:

$$P_{BILLET} = (T_{surface} - T_{centre})K_T \times length = 685W$$

Time to heat the billet to the final temperature of 2192°F (1200°C) =

$$\frac{Energy\ required}{Power\ per\ unit\ length} \times 3600 = 145\text{sec}$$

The radiation power loss assuming a black body radiator (emissivity of 1) is =

Total power needed to heat the stainless steel billet = $P_{BILLET} + P_{RAD} = 1.085$kW.

$$P_{RAD} = P_{rad\ loss\ density} \times \pi \times l_{billet} \times diam_{billet} = 0.4kW$$

APPENDIX 1 B:

INDUCTION HEATING COIL DESIGN

Parameters: Taken from Induction heating Handbook [10]:

Material	Stainless steel
Resistivity @ 20°C	0.695uΩm
Resistivity @ 1200°C	1.2uΩm
Frequency	140kHz
Coil inner diameter	36mm
Coil Length	35mm
Coil turns	9
Coil resistivity	0.017uΩm
Coil space factor	0.9
Work-piece permeability	1

Table B.1: Parameters needed for the design of the induction-heating coil.

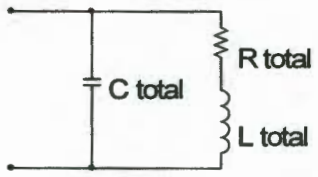

Fig.B1.2: Electrical equivalent circuit of induction heating load.

The skin depth δ in the work-piece at room temperature and 140kHz can be calculated

$$\delta_{work} = \sqrt{\frac{\rho_{work}}{\mu_o \mu_r \pi f}} = 1.12mm$$

by:

The equivalent circuit load resistance is comprised of $R_{total} = R_{coil} + R_{work} = 140.5m\Omega$. The coil efficiency gives an indication of the power required from the high frequency power source at the coil terminals, in order to deliver the calculated amount of 1.085kW to the stainless steel billet.

$$R_{work} = \frac{2\pi f \mu_o N^2}{l_{coil}} \times \left(\frac{2\mu_r A_{work}}{1.23 + \frac{d_{work}}{\delta_{work}}} \right) = 111.3m\Omega \quad R_{coil} = \frac{2\pi f \mu_o N^2}{l_{coil}} \times \left(\frac{k_r \pi d_{coil} \delta_{coil}}{2} \right) = 29.2m\Omega$$

The coil efficiency is dependent on geometry, frequency and the electrical conductivity of both the coil and work-piece. For the current application, the coil efficiency is lower at room temperature (79.2%) and increases with temperature. This is because the work-piece resistivity increases with temperature (increasing R_{work}) while the coil is water-cooled (maintaining a constant lower resistance at room temperature) Coil efficiency at 1200°C is given by:

$$\eta = \frac{R_{work}}{R_{work} + R_{coil}} = 79.2\% \qquad P_{tank} = \frac{P_{load}}{\eta} = 1.37kW$$

From the efficiency the input power required is estimated at 1.37kW. The inductance of the work-piece is significantly smaller that the inductance of the coil and for this analysis is assumed to be neglegable. The inductance of the unloaded coil is calculated using Wheelers formula based of the dimensions given in table B1:

$$L = \frac{(d_{coil} \times 1000)^2 \times N^2 \times 0.1}{4 \times 2.5 \times \left[\left(9 \times \frac{d_{coil} \times 1000}{2}\right) + (10 \times l_{coil} \times 1000)\right]} = 2.1uH$$

The total inductance calculated is 2.1uH and does not include the addition of stray inductance represented by connections between the coil and the inverter (which is kept to a minimum by compact circuit layout and assumed to be negligible in this case). The loading effect of the work-piece on the coil, changes its inductance as discussed in Chapter 3. The resonant capacitance of the tank circuit and the Q of the tank circuit are calculated at 140kHz:

$$C_{total} = \left(\frac{1}{2\pi f}\right)^2 \times \frac{1}{L} = 630nF \qquad Q_l = \frac{2\pi fL}{R_{total}} = 13.15 \qquad Z_{tank} = Q_l^2 R_{total} = 24.29\Omega$$

The impedance presented to the inverter at the resonant frequency is given by Z_{tank}. The power source can deliver a maximum current of $10A_{RMS}$ to the tank circuit. The estimated power delivered to the tank circuit is given by:

$$P_{tank} = I_{RMS}^2 \times Z_{tank} = 2430W \qquad V_{tank} = \frac{4 \cdot I_{DC} \cdot Z_{tank}}{\sqrt{2} \cdot \pi} = 218.69V$$

The RMS tank circuit voltage is used to calculate the kVAR rating of the tank capacitor. The RMS capacitor current rating is given by [26]:

$$kVAR_{CAP} = 2\pi fCV_{RMS}^2 = 26.5kVAR \qquad I_{cap} = Q_l \times I_{RMS} = 131.5A_{RMS}$$

APPENDIX 1 C:

PHASE-LOCKED LOOP ANALYSIS

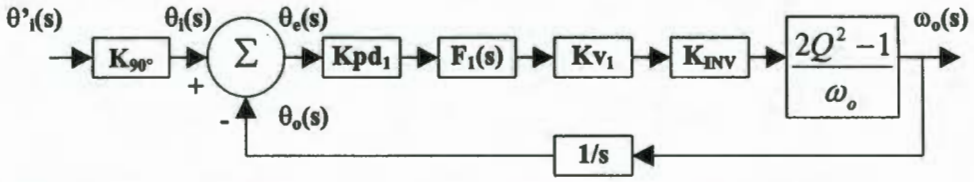

Fig.C.1: Loop model depicted in the frequency domain. Model consists of a main loop and a secondary loop. The secondary loop is given by $K_{90°}$ and is assumed to be an ideal phase shifting loop with much faster response time than the main loop.

The frequency control system comprises two-second order phase locked loops with active filters. The following analysis will assume that the 90° phase shifter loop The $K_{90°}$ (Loop2) has a much faster response time than the main loop (Loop1) and will be treated as ideal. A separate analysis will therefore be conducted on each loop.

Main Loop Analysis

$$Let: \quad K_{pd1}K_{v1}K_{INV}\left(\frac{2Q^2-1}{\omega_o}\right)=K_1$$

Determining the characteristic equation yields:

$$CE: \quad s^2+2\zeta\omega_n s+\omega_n^2=s^2+K_1\frac{\tau_2}{\tau_1}s+\frac{K_1}{\tau_1}=0$$

From the characteristic equation we can determine the following loop parameters:

$$\zeta=\frac{(K_1\tau_2+1)}{2\omega_n\tau_1} \qquad \omega_n=\sqrt{\frac{K_1}{\tau_1}}$$

Loop Components

- Phase detector

The type 1 Phase detector (XOR) has a linear operating range of 180 degrees as shown in figure 2.14. The phase detector gain for both loops are:

$$K_{pd1}=\frac{Vdd}{\pi}=\frac{15}{\pi}=4.77\,V/rad$$

- Loop filter

An active loop filter was used to provide optimum tracking and minimal static phase error. The loop filter consists of an integrator plus lead filter and its configuration is shown in figure 2A.2

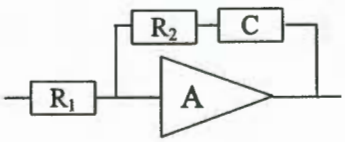

Fig.2A.2: Active integrator plus lead loop filter.

The loop filter transfer function is represented in the frequency domain by:

$$F_1(s) = \frac{(\tau_2 s + 1)}{\tau_1 s}$$

where:

$\tau_1 = R_1C$ and

$\tau_2 = R_2C$

The loop component values were found experimentally and the time constants for:

Loop1: τ_1 = 4.86us (R_1 =1.8kΩ ,C = 2.7nF); τ_2 = 5.94us (R_2 =2.2Ω,C=2.7nF).

Loop2: τ_1 = 23.5ns (R_1 =500Ω ,C = 47pF); τ_2 = 8.46us (R_2 =180kΩ,C=47pF).

- VCO

The transfer function of the VCO in the frequency domain is given by:

Ko =Kv/s (rad/s/V)

where

Kv = 2π ($f$max – $f$min)/Vdd-3.6V (rad/s/V)

- Feedback

The feedback loop usually contains a gain, Kn which represents a counter module of value 1/N where N is the dividing ratio of the counter.

1C.2 Transfer function

The open loop transfer function of a second order loop is given by:

$$GH(s) = \frac{K(\tau_2 s + 1)}{s(\tau_1 s + 1)}$$

where: K = A. Kϕ.Kv.Kn

The open loop transfer function yields a type-1 second order system, which should produce zero steady state phase error for a step phase input.

The characteristic equation for the loop is given by:

$$C.E: \quad s^2 + \frac{(K\tau_2 + 1)}{\tau_1} s + \frac{K}{\tau_1} = 0$$

This allows for the formulation of the expressions for ω_n and ζ :

$$\omega_n = \sqrt{\frac{K}{\tau_1}}$$

and

$$\zeta = \frac{(K\tau_2 + 1)}{2\omega_n \tau_1}$$

This allows for the design of a desired loop response. It is evident that ω_n can be controlled by adjusting the value of τ_1. It is also evident that the damping factor ζ can be controlled by adjusting τ_2.

APPENDIX 1 D:

MEASUREMENT PROCEDURE FOR DETERMINING LOAD CIRCUIT PARAMETERS

A combination of measurements and calculations yields the appropriate tank circuit components, which aids the designer in optimally matching the load to the source. The measurements and calculations are based on the model in figure 3A.1 below:

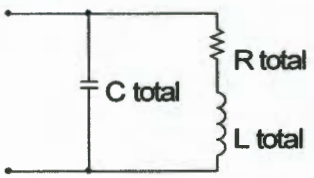

Fig.1D.1: Load circuit model

With the load circuit connected to the high frequency power source (operating in closed loop frequency and current control), set the reference current to a small value (such as 2A) and record the peak output voltage across the tank circuit ($V_{tank(peak)}$) as well as the resonant frequency (ω_o). With the tank circuit capacitance (C_{total}) known, from these two measurements we can now derive the values for the model in figure 1D.1.

The inductance of the tank circuit is given by:

$$L_{total} = \left(\frac{1}{\omega_o}\right)^2 \times \frac{1}{C_{total}} \quad [H]$$

The impedance of the tank circuit at resonance is given by:

$$Z_p = \frac{\pi \hat{V}_{tank(peak)}}{4 I_{DC}} \quad [\Omega]$$

We are now able to calculate the load circuit Quality factor (Q) which allows for the calculation of the last model parameter, R_{total}:

$$Q_{load} = Z_p \omega_o C \qquad R_{total} = \frac{\omega_o L_{total}}{Q_{load}} \quad [\Omega]$$

This procedure was conducted in order to determine the load circuit parameters for two cases namely; coil unloaded and coil loaded with stainless steel work-piece.

The 9-turn induction-heating coil was constructed using 1/8 inch annealed copper tubing. The coil had an inner diameter of 36mm and an axial length of 35mm. The resonant capacitor bank was constructed as described in Chapter 4.

No Load			**Stainless Steel**	
I_{DC}	2A		I_{DC}	2A
$V_{tank(peak)}$	195.7V		$V_{tank(peak)}$	39.85V
ω_o	729k rad/s		ω_o	871k rad/s
C_{total}	900nF		C_{total}	900nF
L_{total}	2.1uH		L_{total}	1.5uH
Z_p	77.784Ω		Z_P	16.29Ω
Q_{load}	55.02		Q_{load}	12.78
R_{total}	29.88mΩ		R_{total}	99.7mΩ

Table 1D.1: Measured load circuit parameters for two different loading conditions.

The measurement results in table 1D.1 confirm the theory regarding the loading effect discussed in chapter 3. The presence of the work-piece in the coil increases the effective resistance Rtotal. This is also given by the reduction in circuit Q and resonant impedance Z_p. The effect of work-piece loading on the coil inductance value is evident in the results above and therefore results in a shift in resonant frequency from 116kHz (at no-load) to 138.6kHz (at stainless steel load). The measured value of unloaded coil inductance is in agreement with the value calculated in APPENDIX 1 B using Wheeler's formula. The calculated value of coil resistance using the Baker model is in agreement with the measured value in Table 1D.1. The Baker model however does not yield accurate results for the calculation of work-piece resistance as compared above.

These measurements provide a practical means determining load parameters and can be conducted on any parallel resonant induction-heating load. This will allow the designer to optimally match the load circuit to the source.

APPENDIX 2 A:

BLOCK DIAGRAM 2kW INDUCTION HEATER

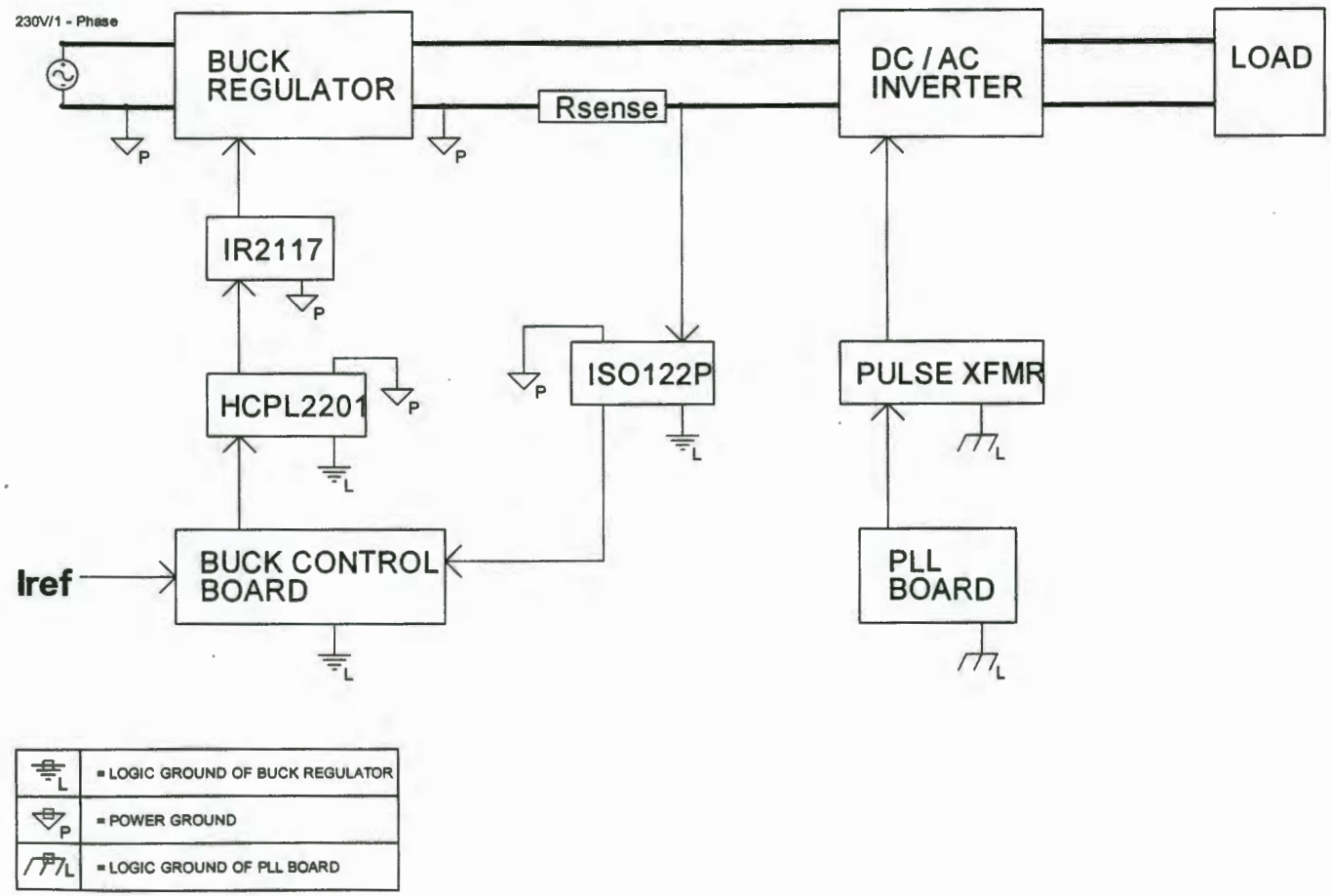

APPENDIX 2 B:

BUCK REGULATOR AND INVERTER LAYOUT

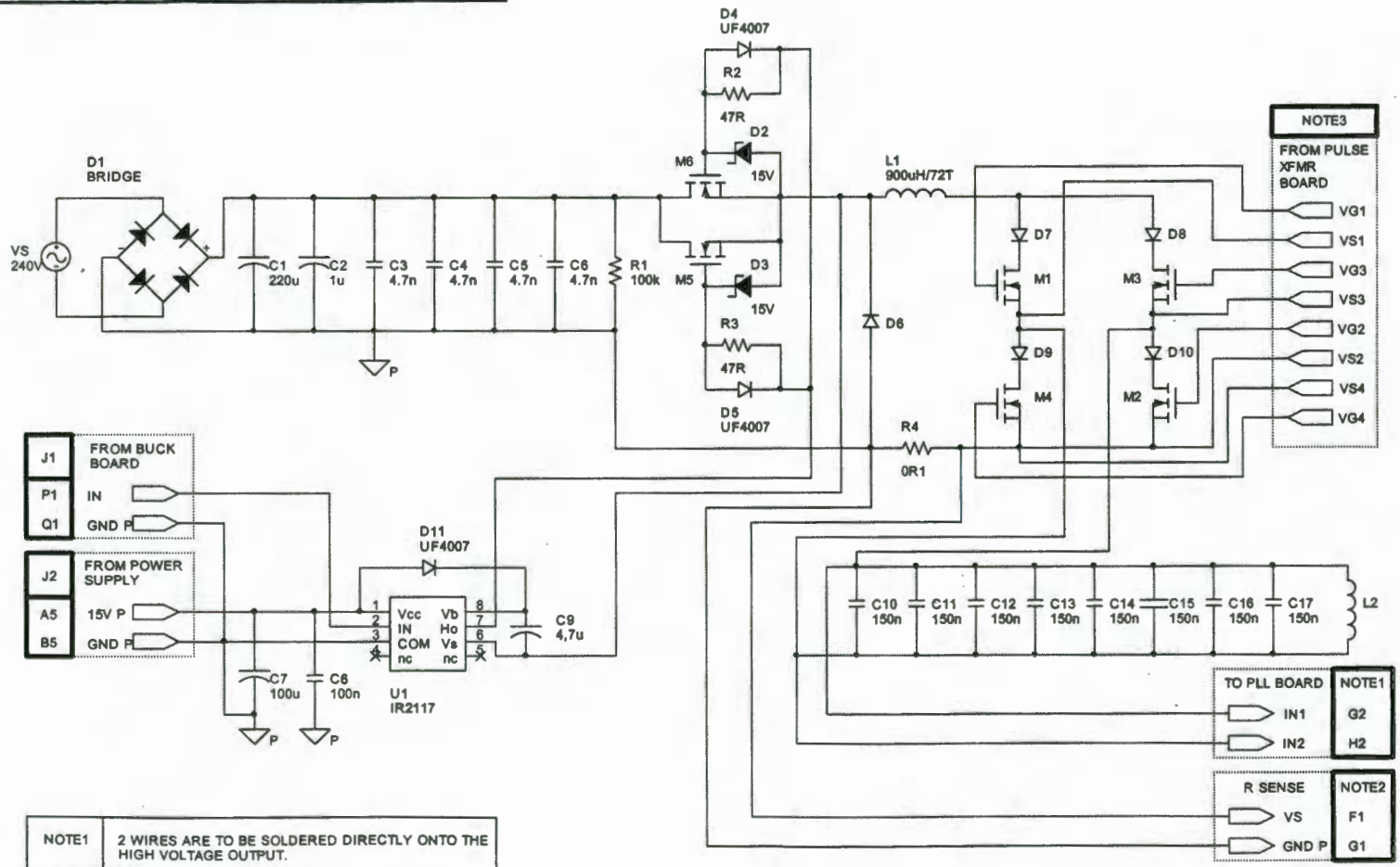

NOTE1	2 WIRES ARE TO BE SOLDERED DIRECTLY ONTO THE HIGH VOLTAGE OUTPUT.
NOTE2	2 WIRES ARE TO BE SOLDERED DIRCTLY ONTO THE SENSE RESISTERS LEADS
NOTE3	TWISTED LEADS CONNECTED DIRECTLY ONTO THE MOSFETS GATE AND SOURCE LEADS

APPENDIX 2 C:

INVERTER GATE-DRIVE CIRCUITRY

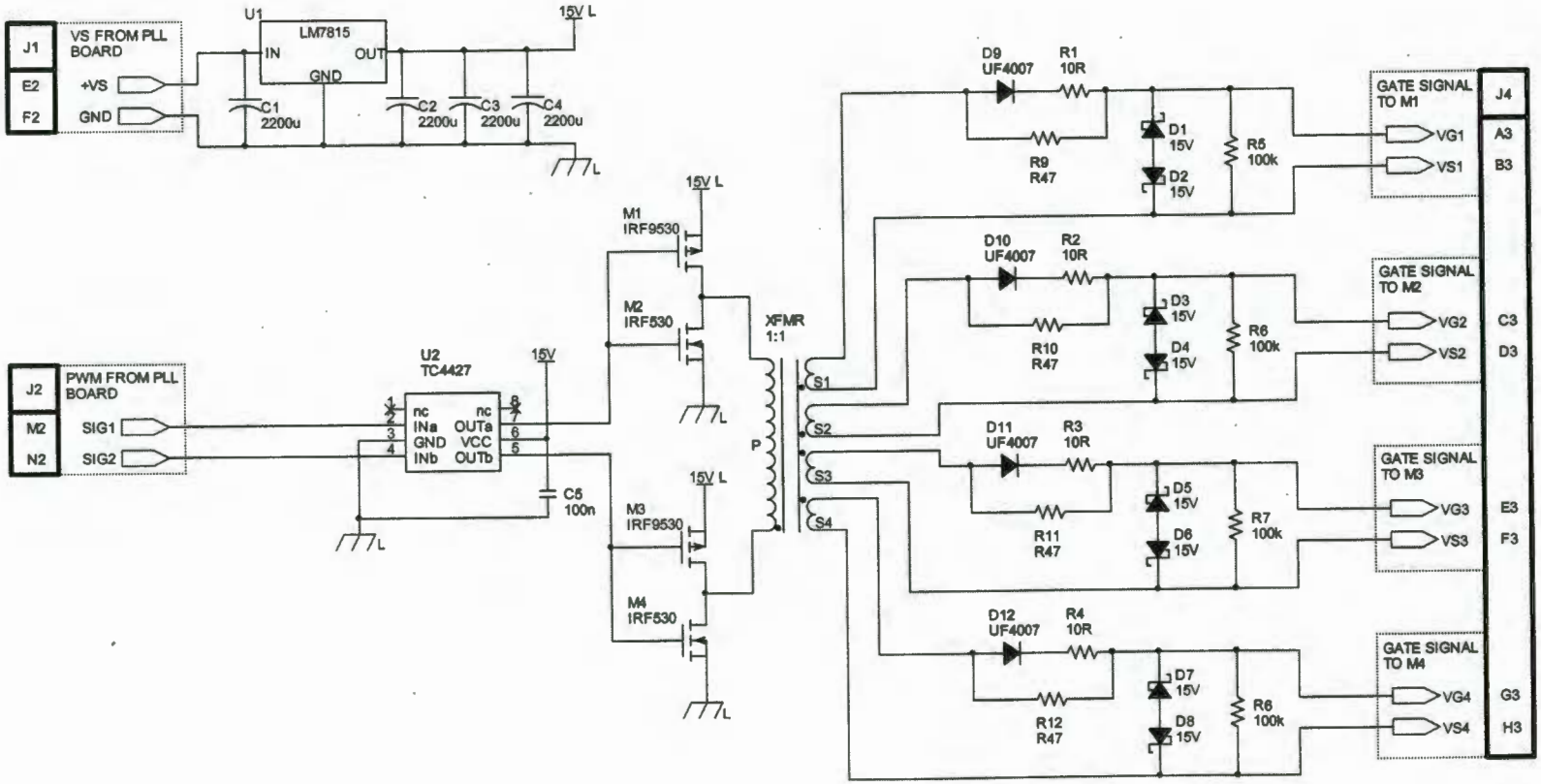

APPENDIX 2 D:

AUTOMATIC FREQUENCY CONTROL CIRCUIT

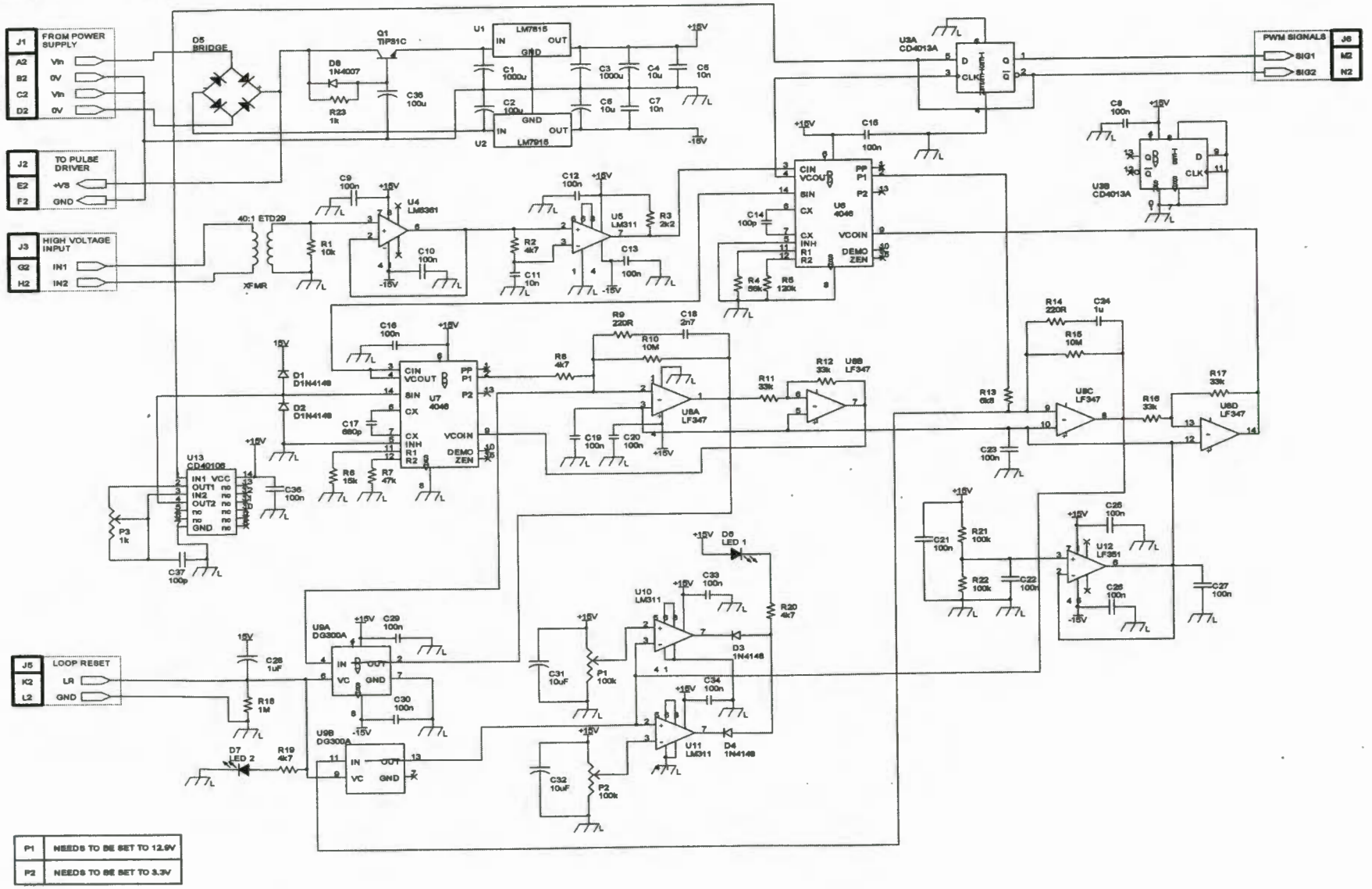

APPENDIX 2 E:

DC-DC POWER CONTROL CIRCUIT

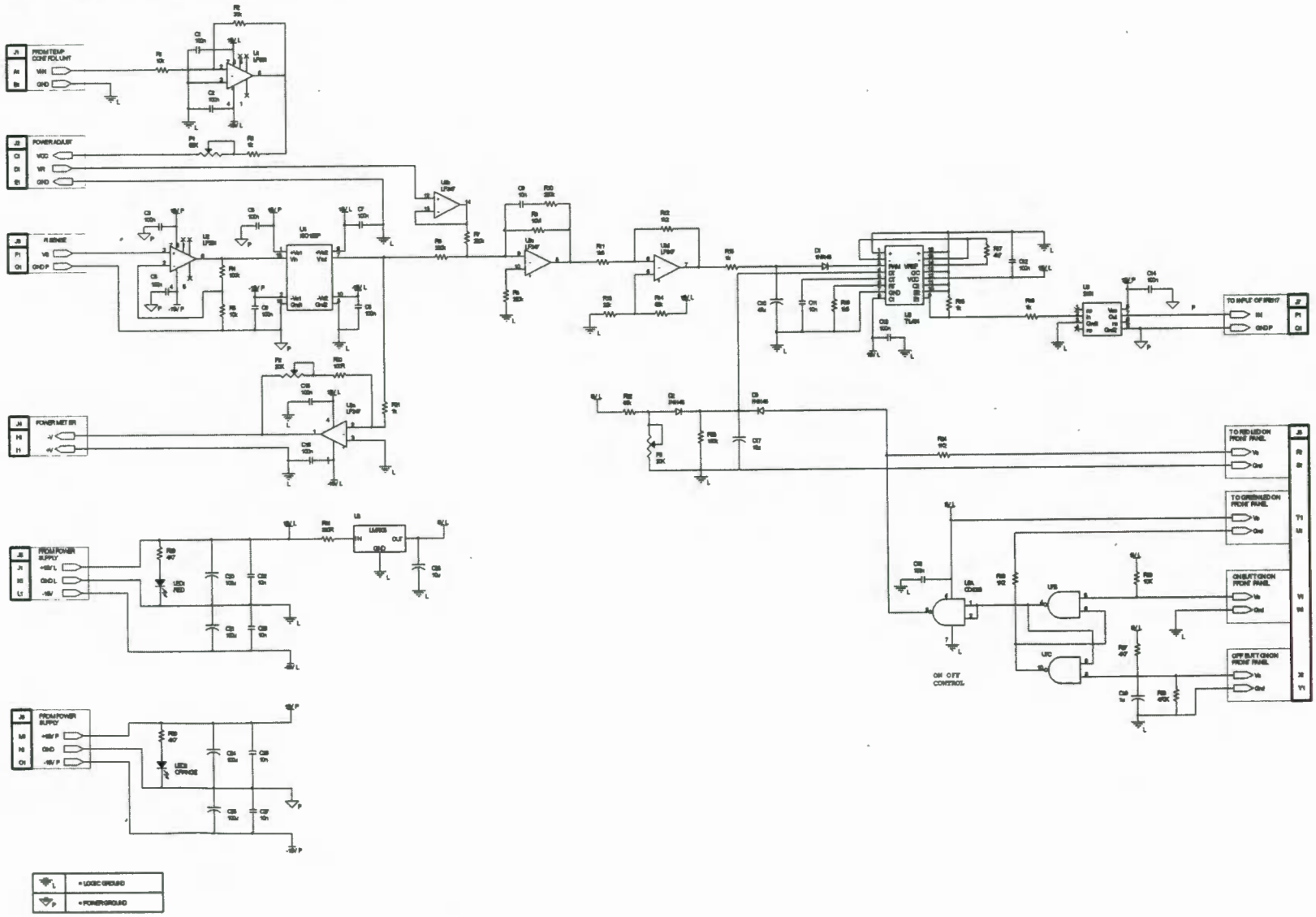

APPENDIX 2 F:

15V AUXILLIARY POWER SUPPLIES